University of Strathclyde

Department of Electronic and Electrical Engineering

Broadband Angle of Arrival Estimation Using Polynomial Matrix Decompositions

By

Mohamed Abubaker Alrmah

A thesis presented in fulfilment of the requirements for the degree
of
Doctor of Philosophy

September 2015

Declaration

This thesis is the result of the author's original research. It has been composed by the author and has not been previously submitted for examination which has lead to the award of a degree.

Acknowledgements

Through my PhD studies at the University of Strathclyde, I had the greatest privilege to work with kind and outstanding people without whom it would not be possible to finish this thesis. It is always easy to know whom to thank after finishing such big work, but it is truly hard for me to express my feeling of being grateful toward them in few words, mainly because the words are much less than the favour I have received. However, I am sure that all of the people who helped me know how grateful I am, with good thanking words or even without naming them.

I would like to begin with thanking my supervisor Dr Stephan Weiss for the opportunity to be his research student. His guidance and support throughout the research has been indispensable. His nice nature, valuable insights, clarity of thought, and comments have no doubt significantly improved this thesis. It has been an honour to work with Stephan through my research, and it has been an exceptional experience for me. I would like to express my most sincere gratitude for his taking the time to give me lots of useful feedback and comments on my papers. I will always be grateful for him.

Also I would like to thank my examiners Prof. Andreas Ahrens and Prof. John Soraghan for their constructive suggestions.

I would also like to thank my friends and the teaching staff in CeSIP centre with whom I enjoyed discussing problems and sharing ideas. I am especially thankful to all my colleagues in room R3.49 who no doubt made research life more interesting.

I would like to express my deepest gratitude to my family for their support. Special thanks to my mother, to the memory of my father, brothers and sisters for their constant support and prayers. I am so lucky and so proud to have such

a wonderful family.

Lastly, and most importantly, I would like to extend my sincerest thanks and appreciation to my wife and kids without their understanding, endless patience and encouragement it would have been impossible for me to finish this work.

Abstract

This thesis is concerned with the problem of broadband angle of arrival (AoA) estimation for sensor arrays. There is a rich theory of narrowband solutions to the AoA problem, which typically involves the covariance matrix of the received data and matrix factorisations such as the eigenvalue decomposition (EVD) to reach optimality in various senses. For broadband arrays, such as found in sonar, acoustics or other applications where signals do not fulfil the narrowband assumption, working with phase shifts between different signals — as sufficient in the narrowband case — does not suffice and explicit lags need to be taken into account. The required space-time covariance matrix of the data now has a lag dimension, and classical solutions such as those based on the EVD are no longer directly applicable.

There are a number of existing broadband AoA techniques, which are reviewed in this thesis. These include independent frequency bin processors, where the broadband problem is split into several narrowband ones, thus loosing coherence across bins. Coherent signal subspace methods effectively apply a pre-steering by focussing matrices in the assumed directions of existing sources, and sum the narrowband covariance matrices coherently. Subsequently, classical narrowband methods can be applied. A recent auto-focussing approach dispenses with the requirement of knowing the approximate direction of sources, and calculates the focussing matrices on a data-dependent fashion. A recent parametric covariance matrix approach for broadband AoA estimation is also reviewed, and it is shown that this can only detect a single — the strongest — source.

Based on a polynomial EVD (PEVD) factorisation of polynomial matrices such as created by a space-time covariance matrix emerging from a broadband problem, this thesis proposes an extension of the powerful high-resolution but

narrowband multiple signal classification (MUSIC) algorithm. While narrowband MUSIC is based on an EVD to identify signal and noise subspaces, the PEVD can extract polynomial subspaces. This also requires the definition of broadband steering vectors, which are used in the proposed polynomial MUSIC (P-MUSIC) method to scan the noise-only subspace. Two different P-MUSIC versions are proposed here: a spatio-spectral P-MUSIC (SSP-MUSIC) is capable to resolve sources with respect to the AoA and frequency range, and a spatial P-MUSIC (SP-MUSIC) extracts the AoA alone.

Broadband steering vectors are proposed as polynomial vectors containing fractional delay filters. For the implementation, a number of methods are reviewed and compared, including windowed sinc functions and Farrow structures. All these techniques show degraded performance as the frequency approaches half of the sampling rate. Therefore, this dissertation also proposes a highly accurate fractional delay filter implementation based on undecimated filter banks, whereby the subband signals are modulated to lower frequency ranges, where individual fractional delay filters can operate with high accuracy.

For the implementation of P-MUSIC, we demonstrate that the broadband steering vector accuracy is important. We also apply different iterative PEVD algorithms belonging to the families of second order sequential best rotation (SBR2) and sequential matrix diagonalisation (SMD) algorithms. We demonstrate the SMD familly, which offers a better diagonalisation of the space-time covariance matrix, is also capable of providing a more accurate subspace decomposition than SBR2. This is evidenced by a higher resolution that can be achieved if SP-MUSIC and SSP-MUSIC are based on SMD rather than SBR2.

The thesis concludes with an extensive set of simulations for both toy problems and realistic scenarios. This is to explain and highlight the operation of the P-MUSIC algorithms, but also compares their performance to other state-of-the-art broadband AoA methods. For the closest competitor, the auto-focussing approach, an analysis in a polynomial matrix framework is provided, which highlights similarities and differences to P-MUSIC. The simulations indicate that P-MUSIC is a powerful and robust extension of MUSIC to the broadband case.

Publications

- M. Alrmah, S. Weiss, and S. Lambotharan. An extension of the music algorithm to broadband scenarios using polynomial eigenvalue decomposition. In *19th European Signal Processing Conference*, Barcelona, Spain, August 2011, pp. 629–633.

- M. N. Hussin, M. Alrmah, and S. Weiss. Distributed Closed-Loop EO-STBC for a time-varying Relay Channel Based on Kalman Tracking. In *9th IMA International Conference on Mathematics in Signal Processing*, Birmingham, UK, December 2012.

- M. Alrmah, M. N. Hussin, S. Weiss, and S. Lambotharan. Comparison of Broadband Direction of Arrival Estimation Algorithms. In *9th IMA International Conference on Mathematics in Signal Processing,* Birmingham, UK, December 2012.

- M. Alrmah, S. Weiss and JG McWhirter. Implementation of Accurate Broadband Steering Vectors for Broadband Angle of Arrival Estimation. In *Intelligent Signal Processing (ISP) Conference,* London, UK, December 2013.

- M. Alrmah, S. Weiss, S Redif, S. Lambotharan and JG McWhirter. Angle of Arrival Estimation for Broadband Signals: A Comparison. In *Intelligent Signal Processing (ISP) Conference*, London, UK, December 2013.

- M. Alrmah and S. Weiss. Filter Bank Based Fractional Delay Filter Implementation for Widely Accurate Broadband Steering Vectors. In *5th IEEE International Workshop on Computational Advances in Multi-Sensor Adaptive Processing (CAMSAP)*, Saint Martin, December 2013

- S. Weiss, M. Alrmah, S. Lambotharan, JG. McWhirter and M. Kaveh. Broadband Angle of Arrival Estimation Methods in a Polynomial Matrix Decomposition Framework. In *5th IEEE International Workshop on Computational Advances in Multi-Sensor Adaptive Processing (CAMSAP)*, Saint Martin, December 2013

- M. Alrmah, J. Corr, A. Alzin, K. Thompson, and S. Weiss. Polynomial Subspace Decomposition for Broadband Angle of Arrival Estimation. In *Sensor Signal Processing for Defence (SSPD 2014)* , Edinburgh, UK, September 2014.

Dedication

Dedicated to my family & to the memory of my father

Contents

List of Figures

List of Tables

Acronyms

AF	Auto-focussing approach
AoA	Angle of Arrival
AWGN	Additive White Gaussian Noise
BSV	Broadband Steering Vector
CSD	Cross Power Spectral Density
CSSM	Coherent Signal Subspace Method
DFT	Discrete Fourier Transform
DSP	Digital Signal Processing
ESPRIT	Estimation of Signal Parameters via Rotational Invariance Technique
EVD	Eigenvalue Decomposition
FDF	Fractional Delay Filter
FFT	Fast Fourier Transform
FIR	Finite Impulse Response
IFB	Independent Frequency Bin
ISS	Incoherent Signal Subspace Approach
MIMO	Multi Input Multi Output
MSME-SMD	Multiple Shift Maximum Element Sequential Matrix Diagonalisation Algorithm
MUSIC	Multiple Signal Classification Algorithm
MVDR	Minimum Variance Distortionless Response
PEVD	Polynomial Matrix Eigenvalue Decomposition
P-MUSIC	Polynomial MUSIC Algorithm
PSCM	Parametrised Spatial Covariance Matrix Technique
PSD	Power Spectral Density

RSS	Rotational Signal Subspace Method
SBR2	Sequential Best Rotation Algorithm
SMD	Sequential Matrix Diagonalisation
SNR	Signal-to-Noise Ratio
SP-MUSIC	Spatial Polynomial MUSIC algorithm
SSP-MUSIC	Spatio-Spectral Polynomial MUSIC algorithm
ULA	Uniform Linear Array

List of Symbols

General Notation

a	Scalar quantity
$\mathbf{a}$	Vctor quantity
$\mathbf{A}$	Scalar matrix quantity
$a_{m,n}$	(m,n) element of a scalar matrix
$\mathbf{R}$	Autocorrelation matrix of the signal vector x, i.e.,$\mathcal{E}\{xx^{\mathrm{H}}\}$
$\mathbf{A}(z)$	Polynomial matrix (z-transform of $a[n]$)
$A_{m,n}(z)$	(m,n) entry of $\mathbf{A}(z)$
$\mathbf{A}(e^{j\Omega})$	PSD matrix (i.e. $A(z)\vert_{z=e^{j\Omega}}$)
$A_{m,n}(e^{j\Omega})$	(m,n) entry of a PSD matrix
$\mathbf{I}_{n\times n}$	$(n \times n)$ identity matrix

Relations and Operations

$(\cdot)^{\mathrm{T}}$	Transpose operation of a matrix or vector
$(\cdot)^{\mathrm{H}}$	Hermitian (conjugate transpose) operation.
$(\cdot)^*$	Complex conjugate operation
$\mathcal{E}\{\cdot\}$	Expectation operation
$\tilde{(\cdot)}$	Para-conjugation
$\bullet\!\!-\!\!\circ$	Transform pair, e.g., $\mathbf{A}(z)\bullet\!\!-\!\!\circ a[n]$
$*$	Convolution operator
$\vert\cdot\vert$	Magnitude operator
∇	Gradient operator

trace[·]	Operator that computs the sum of the diagonal elements of a matrix
diag[·]	Operator that takes the vector to a diagonal matrix
rank{**A**}	Rank of **A** (number of linearly independent rows)
$\|\cdot\|_{\mathrm{F}}$	Frobenius norm of a matrix

Sets and Spaces

$\mathbb{C}$	Set of complex number
$\mathbb{C}^{M\times N}$	Set of $M \times N$ matrices with complex entries
$\mathbb{C}^{M\times N}(z)$	Set of $M \times N$ matrices with complex polynomial entries
$\mathbb{R}$	Set of real number
$\mathbb{R}^{M\times N}$	Set of $M \times N$ matrices with real elements
$\mathbb{R}^{M\times N}(z)$	Set of $M \times N$ matrices with real polynomial entries

Principal Symbols

$\mathbf{a}_{\Omega,\vartheta}$	Narrowband steering vector
$\mathbf{a}_k[n]$	Broadband steering vector
c	Speed of the propagating waves
d	Distance between adjacent sensors
$f_{\mathbf{c}}$	Centre frequency
$f_{\mathbf{max}}$	Maximum frequency of a signal source
f_{s}	Sampling frequency
J	Number of subbands
K	Number of source signals
L	Number of frequency bins
L_P	Length of prototype filter
M	Number of sensors in an array
N	Total number of data samples (i.e. data length)
S_{BW}	Signal bandwidth
T_{s}	Sampling period
λ	Wavelength and also eigenvalue of covariance matrices
$\lambda_{\min}$	Minimum wavelength of a signal

ξ	Number of iterations for iterative PEVD algorithms
ω	Angular frequency
Ω	Normalised (angular) frequency
Δf	Ratio between a signal bandwidth and centre frequency
ϑ	Elevation angle of arrival
ϕ	Azimuth angle of arrival
σ	Variance
τ	Time delay (lag value)
$\Delta\tau_{0,m}$	Difference time delay between a signal received at a reference sensor 0 and the same signal received at sensor m

Chapter 1

Introduction

1.1 Background and Motivation

Sensor array signal processing has a growing number of important applications ranging from radar, mobile communications and acoustic systems to many other fields. Propagating signals carry information about the sources that generate them. Of particular important for the work in this thesis is source angle of arrival (AoA) estimation or direction finding, which needs to be estimated in many applications. For example, AoA is an important factor for target localisation in radar [1]. For wireless communications, AoA estimation can provide spatial diversity that allows multiuser scenarios [2]. In acoustic applications, AoA for microphone arrays can be used for speaker localisation [3] and source separation [4], which is required for televideo conferencing and concert halls applications [5, 6, 7].

The main principle of AoA estimation is to use the data received by a sensor array to estimate the angles of arrival of sources of interest. Moreover, AoA can be considered as a multiple input multiple output (MIMO) system with K input signals and M sensors, where it is usually assumed that the number of source

signals is less than the number of sensors, $K < M$, to guarantee the uniqueness of AoA estimation [8]. However, AoA algorithms are generally complex and their performance depends on many factors such as the number of source signals and their bandwidth, i.e., narrowband or broadband, and also the number of sensors in the array and their spacing [9].

Many methods and algorithms have been developed for determining the AoA of source signals received by the sensor array with a trade-off between accuracy and computations. Most high resolution AoA algorithms have been designed for narrowband signals, where the bandwidth of the source signal is relatively small compared to its centre frequency. For example, if the desired signal is narrowband, then the time delay arising from signal wave fronts travelling across the array at finite speed can be modelled by phase shifts, whereby these phase shifts depend only on the AoA. A powerful narrowband AoA estimation technique is the multiple signal classification (MUSIC) algorithm [10]. MUSIC is a high resolution subspace method that is based on the eigenvalue decomposition of the data covariance matrix, which provides the decomposition into two orthogonal subspaces, i.e., the signal-plus-noise and the noise only subspaces.

In contrast to the widely researched narrowband case, broadband signals present more complex problems, whereby first time delays rather than phase shifts need to be considered to distinguish spatially separated broadband sources. Secondly, the time delay (lag value) has to be taken into account when calculating the space-time covariance matrix for describing the broadband sensor array systems, which leads to the elements of the space-time covariance matrix containing the complete auto- or cross correlation sequences rather than just a single correlation coefficient. This results in its corresponding cross-spectral density (CSD) matrix forming a polynomial matrix. As a result, MUSIC or any powerful narrowband AoA estimation methods are not directly applicable to the broadband

case.

Recently a number of efforts to derive broadband algorithms for direction of arrival estimation problems have been pursued. Most existing broadband AoA estimation techniques bypass the broadband AoA problems in favour of narrowband AoA processing, whereby firstly the broadband sensor data is decomposed into multiple narrowband signals of various frequencies by means of a discrete Fourier transform (DFT). Thereafter, narrowband AoA algorithms can be applied to the different narrowband signals incoherently or coherently to obtain accurate broadband AoA estimates. The incoherent based approachesin [11, 12, 13] process the narrowband problems individually and then combine the results. The coherent based methods [14, 15, 16, 17] by contrast are based on the idea of cohering the different frequencies into a single "common" frequency model describing the whole broadband signal for which narrowband high resolution AoA based method can then be used to estimate the sources' angles.

Other broadband AoA estimation techniques include [18], where a frequency domain approach leads to a decoupling of source parameters such as frequency and angle of arrival, over which estimation is performed. A wideband time domain approach reported in [19] is based on a Markov chain Monte-Carlo method. While [18, 19] are broadband approaches, they are unrelated to subspace methods or specifically the MUSIC algorithm. The contributions in [20, 21] introduce a parameterised spatial covariance matrix, which depends on the AoA and subsequently the relative time delay between array elements. Based on this description, a number of algebraic techniques including a broadband MUSIC algorithm have been derived [22, 23, 24]. A broadband method that does not perform the subband decomposition is proposed in [25]. This method builds on a low-rank signal model which relies on polynomial spline approximation of the source signals, however, requires inverse problems consisting of very large matrices.

Since the space-time covariance matrix for broadband signals is a polynomial matrix, it can no longer be diagonalised using the eigenvalue decomposition (EVD). Instead a polynomial matrix EVD (PEVD) technique is required. The PEVD is a generalisation of the EVD to polynomial matrices and can be calculated using iterative techniques [27, 28, 29]. This decomposition has found applications in the design of broadband precoding and equalisation of MIMO systems [30, 31], subband coding [32], filter bank-based channel coding [33], and other problems.

The motivation of this thesis is to develop reliable broadband AoA estimation methods using polynomial matrix techniques, which can locate broadband sources to enhance e.g. the performance of wideband wireless communication systems. Important performance metrics for candidate algorithms will be their resolution, robustness, and computational complexity.

1.2 Thesis Contributions

This thesis comprises the following novel contributions in the area of broadband angle of arrival estimation.

- **Broadband steering vectors** [34, 35, 36]

  To model the time delays that arise from signal wavefronts travelling across a sensor array, the design of broadband steering vectors (BSV) based on fractional delay filters (FDF) is proposed. Different existing FDF designs are compared w.r.t. to their accuracy and complexity. Motivated by the need of highly accurate BSVs for applications such as broadband AoA estimation, a new FDF design based on undecimated filter banks is proposed. Unlike standard fractional delay filters, which break down at frequencies close to half of the sampling rate, this new design offers very accurate group

delays across the entire spectrum. If high accuracy is required, the filter bank approach can also offer computational advantages.

- **Polynomial MUSIC algorithm** [34]

  A new novel broadband AoA estimation technique, referred to as polynomial MUSIC (P-MUSIC) has been proposed, which resolves either AoA alone or in combination with the frequency range over which sources are active. P-MUSIC is based on the broadband subspace decomposition afforded by the PEVD techniques, whereby the sequential best rotation (SBR2) algorithm is firstly adopted for calculating the PEVD. Performance of the P-MUSIC algorithm is demonstrated for different simulation scenarios.

- **An improved P-MUSIC algorithm** [37]

  Enhanced resolution of the proposed algorithms P-MUSIC has been achieved by utilising iterative PEVD algorithms that have recently evolved from the original SBR2 algorithm, in form of a new family of sequential matrix decomposition (SMD) algorithms [28, 29]. SMD provides a higher level of diagonalisation than SBR2 which leads to a better identification of the relevant signal subspace. The improved performance of the new P-MUSIC over the original one is demonstrated in simulations for different scenarios.

- **Comparison of broadband angle of arrival approaches** [38, 39]

  The proposed P-MUSIC algorithm has been compared to other broadband AoA techniques, including independent frequency bin, auto-focussing, broadband beamforming and a parametric covariance methods, under an extensive set of tests and benchmarks. Simulation results highlight the benefits of the proposed algorithms compared to these state-of-the-art AoA estimation techniques.

- **Broadband AoA estimation methods in a PEVD framework** [40]

The recently proposed auto-focussing (AF) approach [41] for broadband AoA estimation is analysed in the framework of polynomial space-time covariance matrices and their PEVD. This leads to comparisons to the proposed P-MUSIC algorithms. The analysis is complemented with numerical simulations. Simulation results show that AF is falsely claimed to belong to the coherent signal subspace (CSS) [14] family of algorithms. While the proposed algorithms perform similarly to AF if exact knowledge of the sources' spectral parameters is given, they do not require this a priori information and can outperform AF if spectra are unknown.

1.3 Thesis Organisation

In the following, a brief overview of the remaining chapters in this thesis is presented.

Chapter 2 introduces the fundamentals of propagating wave fields, and describes the sensor array signal model for broadband and narrowband scenarios. The concept of AoA estimation is presented, followed by an overview of narrowband AoA techniques, particularly the high resolution narrowband MUSIC signal subspace based method. Finally, at the end of this chapter, broadband AoA estimation approaches are reviewed.

Chapter 3 presents the idea of a BSV for broadband sensor array applications and describes its implementation using fractional delay filters. It also presents a review of the state-of-the-arts FDFs, which includes the windowed sinc functions [42, 43] and the Farrow structure [44]. The common feature of these FDF implementations, poor performance at frequencies of around half of the sampling rate, is discussed and demonstrated in simulations. A new FDF scheme based on a filter bank approach is proposed. The new technique aims to approach the ideal fractional delay over the entire bandwidth. The computational complexity

of the various FDF schemes is then evaluated. Simulation results are presented, highlighting the benefits of the proposed filter bank approach in comparison with windowed sinc functions and Farrow structures. The simulation results show that the proposed scheme is an accurate tool when compared to these state-of-the-art FDF schemes [35, 36].

Chapter 4 proposes a novel broadband AoA estimation polynomial MUSIC (P-MUSIC) algorithm [34]. P-MUSIC is an extension of the powerful narrowband MUSIC algorithm for broadband AoA problems. We start by presenting the broadband (polynomial) subspace estimation afforded by a PEVD. The concept of the PEVD and its calculation using iterative methods are introduced. Two iterative algorithms for implementing the PEVD, i.e., the SBR2 and MSME-SMD algorithms will be reviewed in this chapter. These algorithms can be viewed as a generalisation of the EVD to polynomial matrices, and can be used to obtain broadband (polynomial) subspace decompositions. Based on the calculated polynomial noise-only subspace and the definition of the BSVs introduced in Chapter 3, a new broadband AoA estimation technique known as polynomial MUSIC (P-MUSIC) algorithm is proposed. P-MUSIC was originally based on the SBR2 algorithm. A comparison between the P-MUSIC and an independent frequency bin (IFB) approach, whereby a narrowband MUSIC algorithm is independently applied in every frequency bin, is outlined through simulations. The results show that the proposed method is powerful and very robust when compared to IFB schemes. The impact of the BSV implementation methods on the accuracy of the P-MUSIC algorithm is evaluated and demonstrated through simulations. Moreover, to further enhance the performance of the P-MUSIC algorithms, the recently proposed MSME-SMD algorithm is used to estimate the polynomial noise-only subspace, instead of using the SBR2 algorithm. Simulation results are presented, highlighting the potential performance improvements using

MSME-SMD algorithm when compared to SBR2.

Chapter 5 consists of two parts. The first part addresses links between the proposed P-MUSIC algorithms and the recently proposed AF approach for broadband AoA estimation, that aims to highlight the similarities by analysing the AF in the framework of polynomial matrix decompositions. The analysis is complemented with numerical simulations. In the second part, a comprehensive comparison between the P-MUSIC algorithms proposed in this thesis and others broadband AoA methods for different scenarios are considered in simulations. The results show that the proposed scheme is a powerful tool when compared with other AoA algorithms.

Chapter 6 includes a summary and conclusions, along with suggestion for potential future work.

Chapter 2

Angle of Arrival (AoA) Estimation

For array signal processing, the most common applications include estimating and tracking signals and determining their parameters such as the number of contributing sources, their locations, or the angles from which they illuminate the array. The angle of arrival (AoA) of signal sources is one of the most important parameters to be estimated in many applications such as radar, sonar, air traffic control and wireless communication [1]. Furthermore, knowing the AoA, this information can be used to localise the signal sources via beamforming, by placing high gains in the direction of desired AoAs or by steering nulls in the direction of interferers. Depending on the bandwidth of the desired signal, the direction finding can be classified either into narrowband or broadband techniques. AoA estimation for broadband signals will be considered in this thesis with the aim to design and implement high performance broadband direction finding algorithm.

The organisation of this chapter is as follows. Sec. 2.1 begins with an introduction for wave propagation in space. In Sec. 2.2, a description of a spatio-temporal signal model that will be used in this thesis is presented and followed by a defin-

ition of a signal model for both narrowband and broadband scenarios. Then the concept of AoA estimation and its classification from the signal bandwidth perspective is reviewed in Sec. 2.3. In Sec. 2.4, various narrowband AoA estimation methods are introduced, particularly MUSIC signal subspace based method is considered with more details, followed by broadband AoA estimation techniques in Sec. 2.5, before conclusions are drawn in Sec. 2.6.

2.1 Propagation of Wave Fields

This section will describe the wave propagation in three dimensions and identify the space-time signal model that will be considered in this thesis. A wave field propagates in both time and space. The spatial quantities generally expanded over all three space dimensions are denoted by Cartesian coordinates $(x; y; z)$ or by spherical coordinates (r, ϑ, ϕ). In spherical coordinates, r is the radius, ϕ is the azimuth angle $\phi \in [0,\ 2\pi]$ and ϑ is the elevation angle $\vartheta \in [-\frac{\pi}{2},\ \frac{\pi}{2}]$. The relationship between the Cartesian and the spherical coordinates is shown in Fig. 2.1. The space-time signals can be expressed as $s(\mathbf{r}, t)$ or $s(x, y, z, t)$ where $\mathbf{r}$ is the spatial location vector $\mathbf{r} = (x, y, z)$, and t denotes continuous time.

Assuming that $s(\mathbf{r}, t)$ relates to a source signal impinging onto a sensor array from far-field such that the signal propagates with a planar wavefront. In addition, the propagation medium is assumed to be homogeneous and lossless. Homogeneous means a constant propagation speed throughout space and time, and a lossless environment implies that there is no amplitude attenuation for signals due to propagation. Generally, the signal can be represented by the wave equation [45, 46], such as

$$\nabla^2 s(\mathbf{r}, t) = \frac{1}{c^2} \frac{\partial^2 s(\mathbf{r}, t)}{\partial t^2} \quad , \tag{2.1}$$

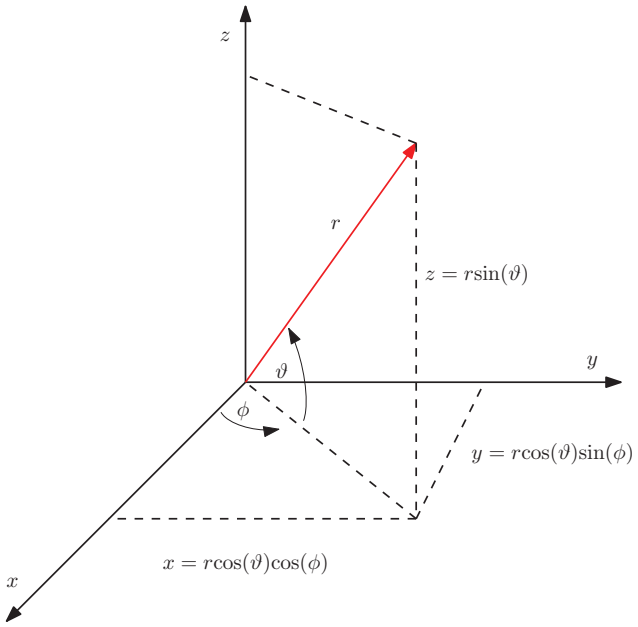

Figure 2.1: 3-dimensional coordinate system with Cartesian coordinates $(x; y; z)$ and spherical coordinates (r, ϑ, ϕ).

where ∇^2 is the Laplacian operator and c is the propagation speed in the medium.

A possible solution of the wave equation (2.1) is generally assumed to be a complex exponential and given by

$$s(\mathbf{r}, t) = A \exp(j(\omega t - \mathbf{k}^{\mathrm{T}}\mathbf{r})) \quad , \tag{2.2}$$

whereby A is a complex constant, ω is the angular (temporal) frequency, and $(\cdot)^{\mathrm{T}}$ denotes the transpose operation. The vector $\mathbf{k} = [k_x, k_y, k_z]^{\mathrm{T}}$ is referred to the wavenumber vector of the source wavefront [45] which points to the direction of propagation and is defined as

$$|\mathbf{k}| = \frac{\omega}{c} = \frac{2\pi}{\lambda} \quad , \tag{2.3}$$

where λ is the wavelength of the complex exponential signal. In addition, $\mathbf{k}$ depends on the elevation ϑ and azimuth ϕ angles, and can be expressed by

$$\mathbf{k} = \frac{\omega}{c} \begin{bmatrix} k_x \\ k_y \\ k_z \end{bmatrix} = \frac{\omega}{c} \begin{bmatrix} \cos(\vartheta)\cos(\phi) \\ \cos(\vartheta)\sin(\phi) \\ \sin(\vartheta) \end{bmatrix} \quad , \tag{2.4}$$

where these angles, ϑ and ϕ, define the direction of arrival. Moreover, the wavenumber vector $\mathbf{k}$ can be interpreted as the spatial frequency of a signal analogously to the (temporal) angular frequency ω. In addition, it is important to point out that $\mathbf{k}$ refers to a monochromatic planar wave, i.e. spatial and temporal frequencies are coupled and cannot be chosen independently.

Furthermore, for the discrete-variable representation of signals, spatio-temporal sampling for the continuous time signal is required for array processing. In order to permit perfect reconstruction and prevent temporal aliasing of a temporally sampled signal, i.e., such that there is no loss of information, the sampling frequency f_s is higher than twice the maximum frequency component f_max in the signal, i.e., $f_s \geq 2\, f_\mathrm{max}$. In addition, the sensor array samples the incoming signals spatially, where the distance d between adjacent sensors has to be less than half the smallest wavelength λ_min present in the signal, i.e., $d \leq \lambda_\mathrm{min}/2$ in order to avoid spatial aliasing problem. If signals are not correctly sampled by the sensor array, then sources from different directions can have the same steering vectors which leads to ambiguity w.r.t. AoA.

For simplicity, linear uniform arrays are to be considered throughout this thesis, where the sensors are placed on a straight line with equal spacing d between sensors. The sensors are assumed to have identical characteristics and to be omnidirectional, having the same sensitivity for all frequencies of interest and to all directions. In the case of linear arrays when the sensor array is arranged along

the z-axis, the AoA is uniquely distinguished by elevation angles but there is an ambiguity w.r.t. azimuth angles.

2.2 Signal Model

There are many ways to classify signals. The category relevant to this thesis relates to a signal's bandwidth. According to [47], a signal can be considered broadband, if the fractional signal bandwidth, Δf defined as the ratio between the signal bandwidth S_{BW} and the centre frequency f_c, i.e. $\Delta f = \frac{S_{BW}}{f_c}$, is higher than a specific threshold (typically 0.025). A signal with a fractional bandwidth below this threshold may be considered narrowband. In [27, 28] another distinction between narrowband and broadband signals is outlined, whereby a situation is broadband, if explicit delays need to be modelled, requiring tap delay lines rather than just phase shifts modelled by complex multipliers.

A uniform linear array (ULA) is the particular structure used for this thesis, which consist of M equally spaced sensors lying along the z-axis, the inter sensor spacing d should not exceed half a wavelength ($d \leq \lambda_{\min}/2$) to avoid spatial aliasing, where $\lambda_{\min}$ is the wavelength corresponding to the highest frequency component for any signal impinging onto the sensor array. The sensors are assumed to have the same characteristics and also they are isotropic (omnidirectional). A signal source can illuminate a sensor array from an angle $\vartheta \in [-\frac{\pi}{2}, \frac{\pi}{2}]$.

Assume K far-field sources $s_k[n]$, $k = 1 \dots K$, illuminating the sensor array, with the sensor data collected in a vector $\mathbf{x}[n] \in \mathbb{C}^M$. As the contribution from the kth source arrives at a reference point in the array it is delayed by $\Delta\tau_{k,m}$, $m = 1 \dots M-1$, to reach each sensor in the array, the propagation delay incurred as the wavefront travels across the sensors at a finite speed as shown in Fig. 2.2. This model only considers the relative delay between signals at the sensors which is dependent on the sources angle of arrival ϑ, but neglects any attenuation in the

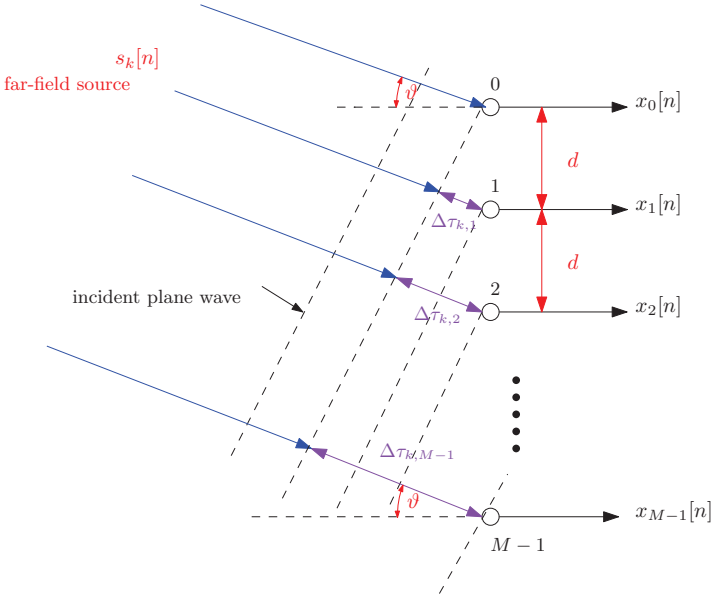

Figure 2.2: M elements uniform linear array antenna.

medium. Note that it is generally assumed that the number of sensors is greater than the number of sources, i.e. $M > K$, to guarantee the uniqueness of the AoA estimation.

2.2.1 Broadband Signal Model

We assume that the source signals that imping on the array are broadband signals, such that the received data vector $\mathbf{x}[n]$ as depicted in Fig. 2.2 can be expressed by,

$$\begin{aligned} \mathbf{x}[n] &= \sum_{k=1}^{K} \mathbf{s}_k[n] + \mathbf{v}[n] \\ &= \sum_{k=1}^{K} \mathbf{a}_k[n] * s_k[n] + \mathbf{v}[n] \quad , \end{aligned} \tag{2.5}$$

where $s_k[n]$ is the kth source signal, $\mathbf{a}_k[n]$ the corresponding broadband steering vector, and $*$ denotes the convolution operator, which thereby forms the contribution of the kth source to the array. The vector $\mathbf{v}[n]$ is the additive noise.

The vector $\mathbf{s}_k[n]$ in (2.5) describes the contribution from the kth source to $\mathbf{x}[n]$. Taking the first sensor signal on the top as shown in Fig. 2.2 as reference, the relative delays of the remaining sensor signals can be characterised as

$$\mathbf{s}_k[n] = \begin{bmatrix} s_k[n] \\ s_k[n - \Delta\tau_{k,1}] \\ \vdots \\ s_k[n - \Delta\tau_{k,M-1}] \end{bmatrix} = \mathbf{a}_k[n] * s_k[n] \quad , \tag{2.6}$$

where $\Delta\tau_{k,m}$ denotes the time that the signal takes to propagate from the reference point to the mth sensor and being a function of AoA ϑ. It can be seen that spatially sampling a propagating planar wave in a lossless homogeneous medium (neglecting attenuation) results in delayed versions of the original source signals.

2.2.2 Narrowband Signal Model

If the propagating signals are narrowband, i.e., $s_k[n] = e^{j\Omega n}$, where Ω is the normalised angular frequency, the time delays $\Delta\tau_{k,m}$ in (2.6) collapse to simple phase shifts, and (2.6) becomes

$$\mathbf{s}_k[n] = \begin{bmatrix} 1 \\ e^{-j\Omega\Delta\tau_{k,1}} \\ \vdots \\ e^{-j\Omega\Delta\tau_{k,M-1}} \end{bmatrix} e^{j\Omega n} = \mathbf{a}_{\Omega,\vartheta}\, e^{j\Omega n} \quad , \tag{2.7}$$

where $\mathbf{a}_{\Omega,\vartheta}$ is termed the narrowband steering vector and characterises the phase shifts of the kth waveform incurred at the different sensors. The dependency of $\Delta\tau_{k,m}$ in (2.7) as a function of the source's AoA, ϑ, can be obtained using the planar wave assumption.

Example. We derive the steering vector of a linear equidistant array with critical sensor spacing $d = \frac{\lambda_{\min}}{2} = \frac{c}{2f_{\max}} = \frac{c}{f_\mathrm{s}}$, based on the propagation speed c in the medium and critical sampling $f_\mathrm{s} = 2f_{\max}$. A source illuminates the array with a complex exponential $x_0(t) = e^{j\omega t}$ from an angle ϑ measured against broadside as depicted in Fig. 2.2. Once sampled with a sampling period T_s with discrete time index n such that $t = nT_\mathrm{s} = \frac{n}{f_\mathrm{s}}$, leads to the reference signal $x_0[n] = e^{j\Omega n}$ with normalised angular sampling rate $\Omega = \omega/f_\mathrm{s}$ and versions delayed by $\Delta\tau_m = m\frac{d\sin(\vartheta)}{c}, m = 0 \ldots M-1$. Then the narrowband steering vector can be written as

$$\mathbf{a}_{\Omega,\vartheta} = \begin{bmatrix} 1 \\ e^{-j\Omega\sin(\vartheta)} \\ \vdots \\ e^{-j(M-1)\Omega\sin(\vartheta)} \end{bmatrix} \quad . \tag{2.8}$$

As can clearly be seen from (2.8), the steering vector is dependent on the source's AoA ϑ.

As a specific case of (2.5), for a narrowband scenario with K narrowband sources the steering vectors are characterised by pairs $\{\Omega_k, \vartheta_k\}$. Then the received signal is a superposition of the K source signals and hence the array vector is given by

$$\mathbf{x}[n] = \sum_{k=1}^{K} \mathbf{a}_{\Omega_k,\vartheta_k}\mathbf{s}_k[n] + \mathbf{v}[n] \quad , \tag{2.9}$$

where ϑ_k, Ω_k are the AoA and normalised frequency of the kth source, $s_k[n]$ is the signal corresponding to the kth source, and $\mathbf{v}[n]$ is independent and identically distributed additive white Gaussian noise, such that $\mathcal{E}\left\{\mathbf{v}[n]\mathbf{v}^\mathrm{H}[n-\tau]\right\} = \delta[\tau]\sigma_v^2\mathbf{I}$.

The following section will describe the angle of arrival (AoA) estimation and its classification.

2.3 Classification of AoA Estimation Methods

AoA estimation is a principle feature for sensor array processing. High resolution AoA estimation has attracted significant attention in the past few decades due to its importance in many applications such as radar, sonar, air traffic control, acoustic detection and wireless communication. Depending on the spectrum (bandwidth) of the impinging signals, AoA estimation techniques can be classified as either narrowband or broadband, as shown in Fig. 2.3, where the latter will be the focus of this thesis. Moreover, the former also can be categorised into traditional techniques, i.e. beamforming [48, 49] and Capon's minimum variance (MVDR) method [50] or to signal subspace based methods such as multiple signal classification (MUSIC) algorithm [10] and the estimation of signal parameters via rotational invariance (ESPRIT) technique [51]. On the other hand, the broadband AoA estimation methods may also be classified into whether a narrowband decomposition for the broadband signals is applied or not. Splitting a broadband signal into several narrowband signals using a filter bank, narrowband direction finding techniques can be applied to the resulting subband signals. The methods in [11, 12, 13,14, 41] use this narrowband decomposition**,** while the methods in [19, 20, 21] do not. Most AoA estimation techniques are designed for narrowband signals, which are generally simpler and less complex compared with broadband techniques. These two categories will be discussed next.

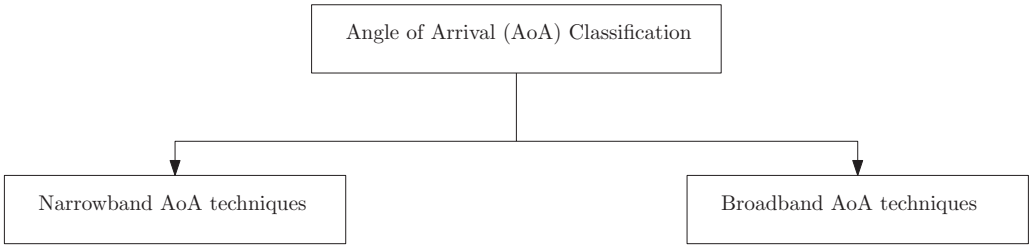

Figure 2.3: Classification of AoA estimation methods based on the signal bandwidth.

2.4 Review of Narrowband AoA Estimation

In this section, we briefly review the most important narrowband AoA estimation algorithms, whereby we focus on standard and superresolution approaches. In Sec. 2.4.1, we start by reviewing the most basic narrowband AoA estimation technique, known as the delay and sum beamformer [49]. The idea behind beamforming also is applied to Capon's minimum variance distortionless response (MVDR) technique [50]. Sec. 2.4.2 introduces signal subspace based methods, in particular the MUSIC algorithm [10] will be described in more details.

2.4.1 Beamforming

The basic idea of the beamforming is to steer the array's gain towards a source of interest, thus separating signals arriving from different directions. Moreover, the beamformer can also be used for AoA estimation by steering the sensor array in one direction at a time and computing the output power. Peak power is then assumed to be corresponding to the source's AoA.

Delay-and-sum is the simplest implementation of the beamformer. In this technique the sensor outputs in $\mathbf{x}[n]$ as shown in Fig. 2.4 are phase-shifted by complex valued coefficient w_m, $m = 0...M-1$, in a vector $\mathbf{w}$ to create constructive

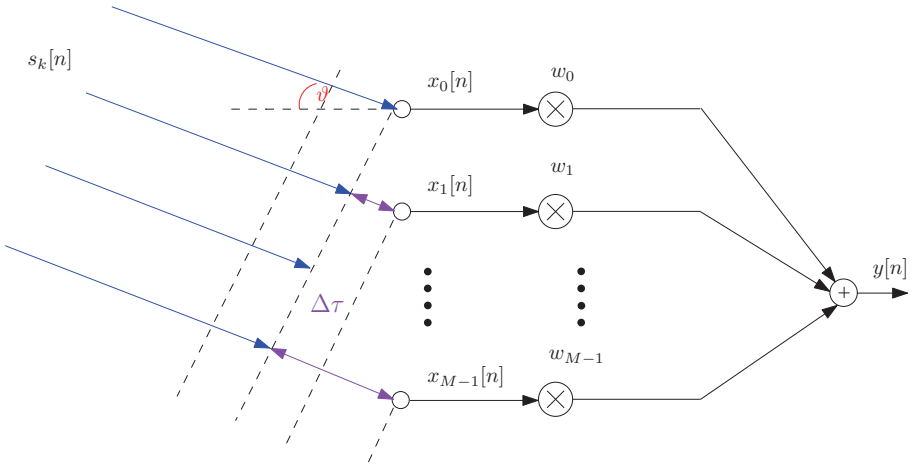

Figure 2.4: A general structure for beamforming.

interference at the output $y[n]$

$$y[n] = \mathbf{w}^{\mathrm{H}}\mathbf{x}[n] \quad . \tag{2.10}$$

The coefficients w_m, $m = 0, 1, \ldots, (M-1)$, are the beamforming weights. To steer the sensor array in a specific direction ϑ, the beamforming weights $\mathbf{w}$ can be calculated as [49]

$$\mathbf{w}(\vartheta) = \frac{1}{M}\,\mathbf{a}_{\Omega,\vartheta} \quad , \tag{2.11}$$

where $\mathbf{a}_{\Omega,\vartheta}$ is the narrowband steering vector as defined in (2.8). It is clear that the beamforming weights $\mathbf{w}$ are independent of the actual received waveforms data. By using the weight vector in (2.11), we can rewrite (2.10) as

$$y[n] = (\frac{1}{M}\,\mathbf{a}_{\Omega,\vartheta})^{\mathrm{H}}\mathbf{x}[n] \quad . \tag{2.12}$$

The sources AoA's can be obtained by computing the total mean output power

of the array's output in (2.12),

$$\begin{aligned} S_{\text{Beamformer}}(\vartheta) &= \mathcal{E}\left\{|y[n]|^2\right\} \\ &= \frac{\mathbf{a}_{\Omega,\vartheta}^{\text{H}}\,\mathbf{R}\,\mathbf{a}_{\Omega,\vartheta}}{M^2} \quad , \end{aligned} \tag{2.13}$$

where $\mathbf{R} = \mathcal{E}\left\{\mathbf{x}[n]\,\mathbf{x}^{\text{H}}[n]\right\}$ is the data covariance matrix. The highest peaks of $S_{\text{Beamformer}}(\vartheta)$ are corresponding to the directions of sources. The performance of this approach is dependent on the beamwidth of the mainlobe, which is inversely proportional to the array's aperture and proportional to the narrowband operating frequency [50], and may require a large number of sensors to achieve high resolution.

The MVDR [50] beamformer is an enhancement over the simple delay-and-sum approach. In this technique, the beamformer weights $\mathbf{w}$ are obtained by minimising the output power $\mathcal{E}\left\{|y[n]|^2\right\}$ subject to unity constraint in the look direction such as

$$\min_{\mathbf{w}} \mathcal{E}\left\{|y[n]|^2\right\} \qquad \text{subject to} \quad \mathbf{a}_{\Omega,\vartheta}^{\text{H}}\mathbf{w} = 1 \quad . \tag{2.14}$$

The constraint $\mathbf{a}_{\Omega,\vartheta}^{\text{H}}\mathbf{w} = 1$ ensures that the desired signal coming from AoA ϑ passes the beamformer's output undistorted. While MVDR is minimising the output power, it reduces the power contributions from directions other than the look direction as much as possible. This is in contrast to the delay-and-sum beamformer, where structured interference from directions other than the look direction can leak through the delay-and-sum beamformer's sidelobes, and therefore distort the estimated power that is received from a particular AoA. The Lagrange method can be used to solve the constraint problem in (2.14), resulting in

$$\mathbf{w}_{\text{MVDR}} = \frac{\mathbf{R}^{-1}\mathbf{a}_{\Omega,\vartheta}}{(\mathbf{a}_{\Omega,\vartheta}^{\text{H}}\mathbf{R}^{-1}\mathbf{a}_{\Omega,\vartheta})} \quad . \tag{2.15}$$

The MVDR beamformer can be used for AoA estimation by computing the power spectrum

$$S_{\mathrm{MVDR}}(\vartheta) = \mathcal{E}\left\{|y[n]|^2\right\} = (\mathbf{a}_{\Omega,\vartheta}^{\mathrm{H}}\mathbf{R}^{-1}\mathbf{a}_{\Omega,\vartheta})^{-1} \quad . \tag{2.16}$$

The AoA estimates are obtained by determining the peaks in the $S_{\mathrm{MVDR}}(\vartheta)$.

2.4.2 Subspace-based Methods

Subspace based methods are high resolution AoA estimation techniques. Instead of directly processing the received data as in the beamforming technique, this approach is based on the eigenvalue decomposition (EVD) of the covariance matrix of the sensor outputs, in order to identify and separate the signal-plus-noise and noise-only subspaces. A search using either the noise-only subspace or the signal-plus-noise subspace is performed over all possible AoAs to determine the angles of target sources. Amongst signal subspace methods, the multiple signal classification (MUSIC) algorithm [10] is one of the most popular techniques. MUSIC is a high resolution technique that can estimate the AoA of closely spaced signals. MUSIC does not only estimate the AoA of sources, but can also be used for spectrum estimation, or for determining the number of the incoming signals and other signal-related parameters [52, 53].

There are a numerous subspace-based methods in addition to MUSIC such as Root MUSIC [54] and beamspace MUSIC [55]. ESPRIT [51] is another signal subspace method which does not require the array steering vector to be known. While its computation complexity and storage requirements are lower than MUSIC, however, MUSIC is more accurate, stable and has better resolution than ESPRIT [56]. Moreover, all subspace-based techniques are using a common process for finding both the signal-plus-noise and noise-only subspaces before computing signals AoAs. In this section the MUSIC algorithm is considered in more detail, since the proposed method in this thesis is a generalisation of MUSIC for broad-

band AoA problems and will be presented in Chapter 4.

Narrowband MUSIC.

Referring to the narrowband data model presented in Sec. 2.2.2, we consider K independent narrowband sources $s_k[n]$ characterised by a pair $\{\Omega_k, \vartheta_k\}$ that are impinging on the array antenna with M sensors. The received sampled data vector $\mathbf{x}[n]$ can be expressed as

$$\mathbf{x}[n] = \sum_{k=1}^{K} \mathbf{a}_{\Omega_k,\vartheta_k} s_k[n] + \mathbf{v}[n] \quad , \tag{2.17}$$

where $\mathbf{a}_{\Omega_k,\vartheta_k}$ is the steering vector for the kth source with normalised angular frequency Ω_k, and angle of arrival ϑ_k, and $\mathbf{v}[n]$ is independent and identically distributed white Gaussian noise and is assumed uncorrelated with the source signals. MUSIC requires the spatial covariance matrix and being narrowband, only correlations for lag zero need to be considered, such that the covariance matrix $\mathbf{R} \in \mathbb{C}^{\mathrm{M}\times\mathrm{M}}$ can be calculated as

$$\mathbf{R} = \mathcal{E}\left\{\mathbf{x}[n]\,\mathbf{x}^{\mathrm{H}}[n]\right\} \quad , \tag{2.18}$$

where $\mathcal{E}\{\cdot\}$ is the expectation operator and $(\cdot)^{\mathrm{H}}$ indicates the Hermitian operation, i.e., complex conjugate transpose. This covariance matrix entirely describes the data as modelled in (2.17). In a real application, the data is acquired over a data window of N samples, and can be assembled into a data matrix

$$\mathbf{X}_n = [\mathbf{x}[n-N+1] \ldots \mathbf{x}[n-1]\,\mathbf{x}[n]] \quad . \tag{2.19}$$

Therefore, the estimated covariance matrix can be obtained using a simple averaging such as

$$\hat{\mathbf{R}}_n \approx \frac{1}{N}\mathbf{X}_n\mathbf{X}_n^{\mathrm{H}} \quad . \tag{2.20}$$

While below the analysis is continued with $\mathbf{R}$, an appropriate estimation of this covariance matrix according to (2.20) with a sufficiently large N is assumed.

In the case of K independent narrowband sources of power σ_k^2, $k \in (1, K)$, and uncorrelated white the noise with a variance σ_v^2, $\mathbf{R}$ can also be expressed as [57]

$$\mathbf{R} = \sum_{k=1}^{K} \sigma_k^2 \mathbf{a}_{\Omega,\vartheta_k} \mathbf{a}_{\Omega,\vartheta_k}^{\mathrm{H}} + \sigma_v^2 \mathbf{I} = \mathbf{A}(\Omega, \vartheta) \mathbf{R}_s \mathbf{A}^{\mathrm{H}}(\Omega, \vartheta) + \mathbf{R}_v \quad , \tag{2.21}$$

where $\mathbf{R}_s = \mathcal{E}\left\{\mathbf{s}[n]\mathbf{s}^{\mathrm{H}}[n]\right\}$, $\mathbf{R}_v = \sigma_v^2 \mathbf{I}$ are denoting the sources and the noise covariance matrices respectively, and $\mathbf{s}[n]$ is a vector of source signals of dimension K. The matrix $\mathbf{A}(\Omega, \vartheta) \in \mathbb{C}^{M \times K}$ contains in its columns the steering vectors for the K sources

$$\mathbf{A}(\Omega, \vartheta) = [\mathbf{a}_{\Omega_1,\vartheta_1}\, \mathbf{a}_{\Omega_2,\vartheta_2}\, \ldots\, \mathbf{a}_{\Omega_k,\vartheta_k}] \quad . \tag{2.22}$$

Since the covariance matrix $\mathbf{R}$ is a Hermitian matrix, i.e., $\mathbf{R} = \mathbf{R}^{\mathrm{H}}$, this matrix can be decomposed using the eigenvalue decomposition (EVD) to yield

$$\mathbf{R} = \mathbf{Q} \mathbf{\Lambda} \mathbf{Q}^{\mathrm{H}} \quad , \tag{2.23}$$

where $\mathbf{Q}$ is a unitary matrix, i.e. $\mathbf{Q}\mathbf{Q}^{\mathrm{H}} = \mathbf{I}$, that contains the eigenvectors in its columns $\mathbf{Q} = [\mathbf{q}_0\, \mathbf{q}_1 \ldots\, \mathbf{q}_{M-1}]$, and $\mathbf{\Lambda}$ is a diagonal matrix containing the real non-negative eigenvalues on its diagonal,

$$\mathbf{\Lambda} = \mathrm{diag}[\lambda_0, \cdots, \lambda_K, \cdots, \lambda_{M-1}] \quad . \tag{2.24}$$

The eigenvalues λ in $\mathbf{\Lambda}$ can be split into two parts, i.e., a noise floor $\lambda_m \approx \sigma_v^2$, $m \geq K$, and a signal part with eigenvalues λ_m, $m < K$ above the noise threshold. This allows identification of the signal-plus-noise and noise-only subspaces. Thus, the data is known to contain K linearly independent sources which lie in the signal-

plus-noise subspace spanned by the columns of $\mathbf{Q}_s$, while $\mathbf{Q}_s^{\perp}$ spans the noise-only subspace,

$$\begin{aligned}\mathbf{R} &= [\mathbf{Q}_s\,\mathbf{Q}_s^{\perp}]\begin{bmatrix}\mathbf{\Lambda}_s & \mathbf{0}\\ \mathbf{0} & \mathbf{\Lambda}_n\end{bmatrix}\begin{bmatrix}\mathbf{Q}_s^{\mathrm{H}}\\ \mathbf{Q}_s^{\perp,\mathrm{H}}\end{bmatrix},\\ &= [\mathbf{Q}_s\,\mathbf{Q}_s^{\perp}]\left[\begin{array}{ccc|c}\lambda_0+\sigma_v^2 & \cdots & & 0\\ \vdots & \ddots & \vdots & 0\\ & \cdots & \lambda_{K-1}+\sigma_v^2 & 0\\ \hline & \cdots & & \sigma_v^2\,\mathbf{I}_{M-K}\end{array}\right]\begin{bmatrix}\mathbf{Q}_s^{\mathrm{H}}\\ \mathbf{Q}_s^{\perp,\mathrm{H}}\end{bmatrix},\end{aligned} \tag{2.25}$$

When trying to estimate the angle of sources contributed to $\mathbf{R}$, a potential idea is to investigate the signal-plus-noise subspace $\mathbf{Q}_s$. However, since $\mathbf{Q}$ is unitary, scanning $\mathbf{Q}_s$ with steering vectors for maxima is likely to extract the steering vector of only the strongest source correctly; otherwise the results will contain orthonormalised basis vectors of the signal subspace in $\mathbf{Q}_s$, which will likely not match the directions of weaker sources.

Therefore, the idea of the MUSIC algorithm is to scan the noise-only subspace $\mathbf{Q}_s^{\perp}$, which is spanned by eigenvectors corresponding to the $(M-K)$ eigenvalues close to the noise floor, $\mathbf{\Lambda}_n \approx \sigma_v^2\mathbf{I}$. The eigenvectors of the noise-only subspace are orthogonal to the steering vectors of sources that contribute to $\mathbf{R}$ and will define the signal-plus-noise subspace $\mathbf{Q}_s$. Based on this orthogonality the vector $\mathbf{Q}_s^{\perp,\mathrm{H}}\mathbf{a}_{\Omega,\vartheta}$ has to be close to the origin for $\mathbf{a}_{\Omega,\vartheta}$ to be a steering vector of a contributing source. The MUSIC algorithm therefore calculates the inverse of the squared Euclidean norm of this vector as the MUSIC spectrum $S_{\mathrm{MUSIC}}(\vartheta)$ such as

$$S_{\mathrm{MUSIC}}(\vartheta) = \frac{1}{\mathbf{a}_{\Omega,\vartheta}^{\mathrm{H}}\mathbf{Q}_{\mathrm{s}}^{\perp}\mathbf{Q}_s^{\perp,\mathrm{H}}\mathbf{a}_{\Omega,\vartheta}} \quad . \tag{2.26}$$

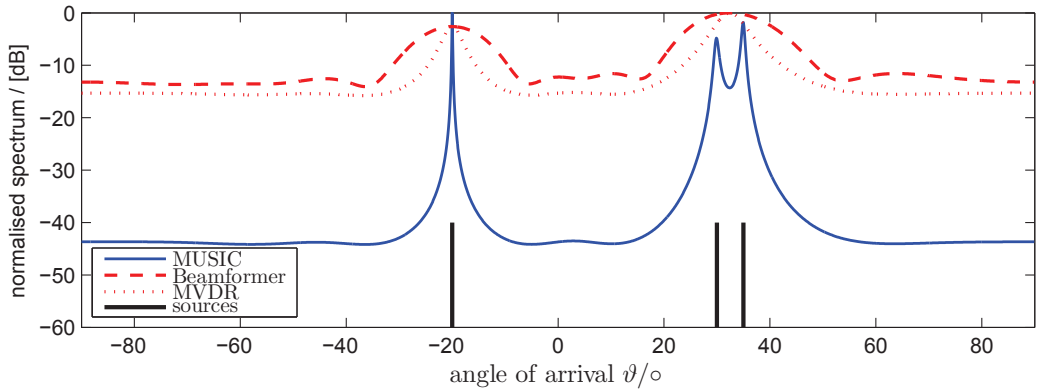

Figure 2.5: Comparison of (i) MUSIC, (ii) beamformer and (iii) Capon's minimum variance method for a scenario with three sources located at angles $[-20°, 30°, 35°]$.

The K largest peaks of (2.26) corresponding to the direction of arrival for the sources of interest as proposed by [10]. Fig. 2.5 shows a comparison between the resolution performance of MUSIC, beamforming and Capon's minimum variance method, for a scenario with three uncorrelated narrowband sources of equal power at an SNR of 10dB. The sources illuminate a sensor array with $M = 8$ elements from directions $-20°, 30°$ and $35°$ respectively. As can be seen clearly from Fig. 2.5, MUSIC is able to distinguish between the three signals whereby three sharp peaks are presented at angles,$-20°, 30°$ and $35°$ where the target sources are actually located. Note that the closely space angles of $30°$ and $35°$ can be resolved. MVDR provides better resolution than the beamforming for the source located at $-20°$, while both MVDR and beamformer fail to differentiate between the two closely signals. This demonstrates that MUSIC can provide higher resolution of detecting and separating the AoAs of multiple sources than the beamforming and Capon approaches.

However, the performance of the MUSIC algorithm degrades in coherent or highly correlated signals [58] which arises e.g. through multipath propagation in the medium. Several algorithms have been developed in order to overcome

this problem such as maximum likelihood [59], spatial smoothing [60, 61] and methods based on the fourth order cumulants [62]. In the spatial smoothing technique the sensor array is divided into multiple overlapping subarrays. The correlation matrix of each subarray is being estimated from its sampled data. Then the final correlation matrix is given as the average of all subarray correlation matrices. As a result, the final correlation matrix has structurally the same form as the covariance matrix for uncoherent signals [61]. Hence, the subspace-based techniques can be applied to this smoothed correlation matrix to estimate the AoA of the correlated sources. In the following section, a brief review of broadband AoA estimation algorithms is provided.

2.5 Review of Broadband AoA Estimation Techniques

If the source of interest is a broadband signal, then powerful narrowband AoA methods such as the MUSIC algorithm are not directly applicable. Recently, a number of efforts to derive broadband algorithms for AoA estimation have been pursued. Most of the existing broadband AoA methods are based on the idea of transforming the broadband AoA problem to yield one or several narrowband problems. Generally, broadband signals can be decomposed (split) into several frequency bins, either by using a discrete Fourier transformer (DFT) or via band-pass filtering methods, which then can be processed independently (incoherent) or coherently by narrowband direction finding techniques, e.g, the high resolution signal subspace MUSIC algorithm. In the incoherent broadband AoA estimation methods, narrowband AoA techniques are applied separately for each frequency bin to estimate the source's AoAs. Coherent techniques are based on the idea of cohering the different frequencies into a single frequency to which narrowband

AoA techniques can then be applied. The new approach proposed in this thesis, the polynomial MUSIC algorithm [34], is free from such assumptions and instead it implements a generalisation of the MUSIC algorithm to broadband problems; it will be introduced in Chapter 4 of this thesis. The next subsections provide a review of various broadband AoA estimation techniques. In particular, we will be concentrating on methods that are based on subspace decompositions.

2.5.1 Independent Frequency Bin Processing

The basic idea of the independent frequency bin (IFB) approach is to split the broadband signal into a number of L independent frequency bins Ω_l, $l = 1 \dots L$, by means of a DFT. The decomposition into frequency bins is assumed to yield narrowband signals, and each bin is processed independently by narrowband AoA techniques such as the MUSIC algorithm.

Assuming that K spectrally overlapping independent broadband sources illuminate the sensor array and contribute to $\mathbf{x}[n]$ as defined in (2.5). The IFB approach decomposes $\mathbf{x}[n]$ into different frequency bins using a DFT to yield

$$\mathbf{X}(e^{j\Omega_l}) = \mathbf{A}_{\vartheta_k}(e^{j\Omega_l})\mathbf{S}(e^{j\Omega_l}) + \mathbf{V}(e^{j\Omega_l}) \quad , \tag{2.27}$$

where $l = 1, \dots, L$ denotes the number of frequency bins, and $\mathbf{S}(e^{j\Omega_l}) \in \mathbb{C}^K$, $\mathbf{V}(e^{j\Omega_l}) \in \mathbb{C}^M$ are the lth DFT coefficients of the source signal and the noise respectively. The matrix $\mathbf{A}_{\vartheta_k}(e^{j\Omega_l}) \in \mathbb{C}^{M\times K}$ is a frequency dependent steering vector matrix

$$\mathbf{A}_{\vartheta_k}(e^{j\Omega_l}) = [\mathbf{a}_{\Omega_l,\vartheta_1}\ \mathbf{a}_{\Omega_l,\vartheta_2}\ \dots\ \mathbf{a}_{\Omega_l,\vartheta_K}] \quad , \tag{2.28}$$

containing in its columns the narrowband steering vectors $\mathbf{a}_{\Omega_l,\vartheta_k}$ at frequency Ω_l for different AoAs ϑ_k.

The covariance matrix for the lth frequency bin of the data model in (2.27)

can be calculated as

$$\begin{aligned}\mathbf{R}(e^{j\Omega_l}) &= \mathcal{E}\left\{\mathbf{X}(e^{j\Omega_l})\,\mathbf{X}^{\mathrm{H}}(e^{j\Omega_l})\right\} \\ &= \mathbf{A}_{\vartheta_k}(e^{j\Omega_l})\mathbf{R}_{\mathbf{s}}(e^{j\Omega_l})\mathbf{A}^{\mathrm{H}}_{\vartheta_k}(e^{j\Omega_l}) + \sigma_v^2(e^{j\Omega_l})\mathbf{I} \quad , \end{aligned} \tag{2.29}$$

where $\mathbf{R}_{\mathbf{s}}(e^{j\Omega_l}) = \mathcal{E}\left\{\mathbf{S}(e^{j\Omega_l})\mathbf{S}^{\mathbf{H}}(e^{j\Omega_l})\right\} \in \mathbb{C}^{K\times K}$ is the diagonal source covariance matrix containing the power spectral density values in the $l$the frequency bin of the K sources along its diagonal. .

Finally, the original narrowband MUSIC algorithm [10] can be applied to each $\mathbf{R}(e^{j\Omega_l})$ with $l = 1, \ldots, L$, by probing its noise-only subspace $\mathbf{Q}_n(e^{j^{\Omega_l}})$ with a set of narrowband steering vectors as defined in (2.8). The broadband IFB-MUSIC estimator is given by

$$S_{\mathrm{IFB}}(\Omega_l, \vartheta) = \frac{1}{\mathbf{a}^{\mathrm{H}}_{\Omega_l,\vartheta}\mathbf{Q}_n(e^{j^{\Omega_l}})\mathbf{Q}^{\mathrm{H}}_n(e^{j^{\Omega_l}})\mathbf{a}_{\mathbf{\Omega_l},\vartheta}} \quad . \tag{2.30}$$

The performance of this approach is highly dependent on the location of the source frequencies with respect to the bin frequencies of the IFB processor, i.e. if the signal frequencies coincide within frequency bins, the IFB will provide a very accurate estimation for the sources' AoAs and their frequency range. On the other hand, when the signal of interest does not sit exactly on a bin frequency then the IFB technique is likely to result in a very poor performance [34].

An approach similar to IFB is the incoherent signal subspace (ISS) method [11, 12]. In this technique, in addition to processing each frequency band separately and estimating the sources' AoAs, the final estimate of the sources' angle of arrival is obtained by averaging individual results. The ISS-MUSIC spectrum

can be defined as

$$\begin{aligned} S_{\mathrm{ISS}}(\vartheta) &= \frac{1}{L}\sum_{l=1}^{L} S_{\mathrm{IFB}}(\Omega_l, \vartheta) \\ &= \frac{1}{L}\sum_{l=1}^{L} \frac{1}{\mathbf{a}^{\mathrm{H}}_{\Omega_l,\vartheta}\mathbf{Q}_n(e^{j\Omega_l})\mathbf{Q}^{\mathrm{H}}_n(e^{j\Omega_l})\mathbf{a}_{\mathbf{\Omega_l},\vartheta}} \quad . \end{aligned} \tag{2.31}$$

The performance of the ISS method can degrade if the signal-to-noise ratio (SNR) is low or the decomposed narrowband signals are correlated, i.e., the assumption of the independence between all frequency bins is violated. Additionally, since the final AoA estimate is the average of the results obtained from all frequency bins, even few false estimates may lead to a degraded performance of the final estimate [14].

2.5.2 Coherent Signal Subspace Approach

A fundamental feature of coherent signal subspace (CSS) method [14, 63, 64] is that it coherently combines narrowband covariance matrices at different frequency bins covering the entire band occupied by the sources into a single general (common) covariance matrix. In CSS, instead of processing each frequency bin individually using a narrowband AoA technique (as is done in the IFB approach) the covariance matrices are calculated in a number of frequency bins, and then coherently combined such that their signal subspaces align into one single scalar-valued correlation matrix that is a representative of the broadband signal, to which narrowband high resolution AoA techniques such as MUSIC are applicable. The coherence across different frequency bins is created by a frequency-dependent and unitary focussing matrix $\mathbf{T}(e^{j\Omega})$, which transforms the correlation matrices for all frequency bins into one common correlation matrix at one focussing frequency.

Assuming $\mathbf{R}(e^{j\Omega_l})$ is the covariance matrix for $\mathbf{X}(e^{j\Omega_l})$, with $l = 1, \ldots, L$ bin frequencies, the CSS common covariance matrix is given by

$$\mathbf{R}_{coh} = \sum_{l=1}^{L} \alpha_l \mathbf{T}(e^{j\Omega_l}) \mathbf{R}(e^{j\Omega_l}) \mathbf{T}^{\mathbf{H}}(e^{j\Omega_l}) \quad , \tag{2.32}$$

where α_l is a weighting for maximum ratio combination of its coherently rotated contributions. The basic assumption of CSS is that the designed focussing matrix $\mathbf{T}(e^{j\Omega_l})$ is used to transform the steering vector matrix $\mathbf{A}_{\vartheta_f}(e^{j\Omega_l})$ with focussing angles ϑ_f at frequency Ω_l into another steering matrix $\mathbf{A}_{\vartheta_f}(e^{j\Omega_0})$ at a reference frequency Ω_0, such that

$$\mathbf{T}(e^{j\Omega_l}) \mathbf{A}_{\vartheta_f}(e^{j\Omega_l}) = \mathbf{A}_{\vartheta_f}(e^{j\Omega_0}) \quad , \tag{2.33}$$

where ϑ_f is a set of focussing angles based on a pre-estimation or approximate knowledge of the signal of interest's AoAs. Therefore, the coherent covariance matrix in (2.32) can be calculated based on the assumption in (2.33) to yield [14]

$$\begin{aligned} \mathbf{R}_{\text{coh}} &= \sum_{l} \mathbf{T}(e^{j\Omega_l}) \{ \mathbf{A}_{\vartheta_f}(e^{j\Omega_l}) \mathbf{R}_{\mathbf{s}}(e^{j\Omega_l}) \mathbf{A}^{\text{H}}_{\vartheta_f}(e^{j\Omega_l}) + \sigma_v^2 \mathbf{I} \} \mathbf{T}^{\text{H}}(e^{j\Omega_l}) \\ &= \mathbf{A}_{\vartheta_f}(e^{j\Omega_0}) \{ \sum_{l} \mathbf{R}_{\mathbf{s}}(e^{j\Omega_l}) \} \mathbf{A}^{\text{H}}_{\vartheta_f}(e^{j\Omega_0}) + \sigma_v^2 \sum_{l} \mathbf{T}(e^{j\Omega_l}) \mathbf{T}^{\text{H}}(e^{j\Omega_l}) \end{aligned} \tag{2.34}$$

which has approximately the same structure as the narrowband covariance matrix at a reference frequency Ω_0. As a result, any narrowband AoA estimation technique can be applied to $\mathbf{R}_{\text{coh}}$. The calculation of focussing matrices can be based on approximate knowledge of the signals of interest's angles of arrival (AoA), or obtained numerically by a best fit of a rotated $\mathbf{T}(e^{j\Omega_l})$ to a reference $\mathbf{T}(e^{j\Omega_0})$, whereby the rotation forms the focussing matrix. In the rotational signal subspace (RSS) method [64], the focussing matrix is required to be unitary in order to preserve the SNR before and after the focussing. The focussing matrix is

constructed based on minimising the Frobenius norm of the mismatches between steering vectors, such that

$$\min_{\mathbf{T}(e^{j\Omega_l})} ||\mathbf{A}_{\vartheta_f}(e^{j\Omega_0}) - \mathbf{T}(e^{j\Omega_l})\mathbf{A}_{\vartheta_f}(e^{j\Omega_l})||_{\mathrm{F}} \quad , \tag{2.35}$$

subject to $\mathbf{T}^{\mathrm{H}}(e^{j\Omega_l})\mathbf{T}(e^{j\Omega_l}) = \mathbf{I}$. The solution for (2.35) is given by [51]

$$\mathbf{T}(e^{j\Omega_l}) = \mathbf{Q}(e^{j\Omega_l})\mathbf{U}^{\mathrm{H}}(e^{j\Omega_l}) \quad , \tag{2.36}$$

where the columns of $\mathbf{Q}(e^{j\Omega_l})$ and $\mathbf{U}(e^{j\Omega_l})$ are the left and right singular vectors of $\mathbf{A}_{\vartheta_f}(e^{j\Omega_0})\mathbf{A}^{\mathrm{H}}_{\vartheta_f}(e^{j\Omega_l})$.

Finally, the MUSIC spectrum for CSS is given by

$$S_{CSS}(\vartheta) = \frac{1}{\mathbf{a}^H_{\vartheta}(e^{j\Omega_0})\mathbf{Q}_{n,coh}\mathbf{Q}^H_{n,coh}\mathbf{a}_{\vartheta}(e^{j\Omega_0})} \quad , \tag{2.37}$$

where $\mathbf{Q}_{n,\mathrm{coh}}$ denotes the noise-only subspace of $\mathbf{R}_{\mathrm{coh}}$ and $\mathbf{a}_{\vartheta}(e^{j\Omega_0})$ is the steering vector at the reference frequency Ω_0.

This technique provides better performance than the IFB and ISS methods as by using the frequency smoothing (averaging0 technique in (2.32), CSS can deal with coherent sources [14]**.** However, CSS is highly dependent on the focussing angle to construct the focussing matrix. Furthermore, the focussing angles should be close to the true AoAs in order to provide a good estimation. A poor estimate of these factors may lead to poor results of this approach.

2.5.3 Auto-focussing Approach

The auto-focussing (AF) technique [41] is similar to the CSS method in the sense that it uses a focussing matrix for cohering the various frequencies. The difference with respect to CSS is that the focussing matrix is constructed in a fully

data dependent manner, directly from the array's space-time covariance matrix without the requirement for explicit knowledge of approximate AoAs.

AF calculates, based on a reference frequency Ω_0, an EVD of the appropriate frequency-bin covariance matrix $\mathbf{R}(e^{j\Omega_0})$,

$$\mathbf{R}(e^{j\Omega_0}) = \mathbf{Q}_0\mathbf{\Lambda}_0\mathbf{Q}_0^{\mathrm{H}} \quad . \tag{2.38}$$

Together with the modal matrix extracted for frequency bin l, $l = 1...L$, the auto-focussing matrix is constructed according to

$$\mathbf{T}_{\mathrm{AF}}(e^{j\Omega_l}) = \frac{1}{\sqrt{L}}\mathbf{Q}_0\mathbf{Q}^{\mathrm{H}}(e^{j\Omega_l}) \quad , \tag{2.39}$$

where L is the number of frequency bins, and $\mathbf{Q}(e^{j\Omega_l})$ is a unitary matrix containing in its columns the eigenvectors of the autocorrelation matrix $\mathbf{R}(e^{j\Omega_l})$ at the lth frequency bin. The AF coherent covariance matrix is calculated similar to (2.32),

$$\mathbf{R}_{\mathrm{AF}} = \sum_{l=1}^{L}\mathbf{T}_{\mathrm{AF}}(e^{j\Omega_l})\mathbf{R}(e^{j\Omega_l})\mathbf{T}_{\mathrm{AF}}^{\mathrm{H}}(e^{j\Omega_l}) \quad , \tag{2.40}$$

and can be diagonalised by $\mathbf{Q}_0$ to provide

$$\mathbf{\Lambda}_{\mathrm{AF}} = \mathbf{Q}_0^{\mathrm{H}}\mathbf{R}_{\mathrm{AF}}\mathbf{Q}_0 = \mathrm{diag}\{\lambda_1\,\lambda_2\,\ldots\,\lambda_M\} \quad , \tag{2.41}$$

with λ_m, $m = 1\,...\,M$ the eigenvalues of $\mathbf{R}_{\mathrm{AF}}$ in (2.40). If the eigenvalues in $\mathbf{R}_{\mathrm{AF}}$ reveal K linearly independent sources, then the last $M-K$ columns of $\mathbf{Q}_0 = \left[\mathbf{Q}_{0,s}\mathbf{Q}_{0,s}^{\perp}\right]$ contained in $\mathbf{Q}_{0,s}^{\perp} \in \mathbb{C}^{M\times(M-K)}$ span the noise-only subspace of the AF covariance matrix.

Similar to the CSS approach, the narrowband MUSIC algorithm [10] can be applied to $\mathbf{R}_{\mathrm{AF}}$ by probing its noise-only subspace $\mathbf{Q}_{0,s}^{\perp}$ with a set of narrowband steering vectors $\mathbf{a}_\vartheta(e^{j\Omega_0})$ at the reference frequency Ω_0. Therefore, the AF ap-

proach estimates the signal's directions as the peaks of the AF spatial spectrum estimate given by

$$\begin{aligned} S_{\mathrm{AF}}(\vartheta) &= ||\mathbf{Q}_{0,s}^{\perp}\mathbf{a}_{\vartheta}(e^{j\Omega_0})||_2^{-2} \\ &= \frac{1}{\mathbf{a}_{\vartheta}^{\mathrm{H}}(e^{j\Omega_0})\mathbf{Q}_{0,s}^{\perp,\mathrm{H}}\mathbf{Q}_{0,s}^{\perp}\mathbf{a}_{\vartheta}(e^{j\Omega_0})} \quad , \end{aligned} \tag{2.42}$$

Although the AF approach does not require focussing angles compared with CSS method, its performance does depend on the selected focusing (reference) frequency.

2.5.4 Parametrised Spatial Covariance Matrix Approach

The parametrised spatial covariance (PSC) matrix [20, 21] is a different approach for broadband AoA estimation. Unlike the previously mentioned broadband AoA methods, where the broadband approach is bypassed in favour of narrowband AoA processing, PSC is based on testing the zero-lag coherence of a spatial correlation matrix calculated from appropriately pre-steered array data. Knowing the array configuration, a broadband steering vector can be defined for a specific AoA represented by elevation angle ϑ, and pre-steering can be accomplished by a matched broadband steering vector. As such the PSC matrix depends on the angle of arrival ϑ.

Assuming a linear array, the PSC approach delays every sensor output signal $\mathbf{x}[n]$ by $\Delta\tau_m(\vartheta)$ to yield an output data vector $\mathbf{y}_{\vartheta}[n]$, such that

$$\mathbf{y}_{\vartheta}[n] = \begin{bmatrix} x[n-\Delta\tau_0(\vartheta)] \\ x[n-\Delta\tau_1(\vartheta)] \\ \vdots \\ x[n-\Delta\tau_{M-1}(\vartheta)] \end{bmatrix} = \mathbf{\Gamma}_{\vartheta}[n] * \mathbf{x}[n] \quad , \tag{2.43}$$

where the time delay $\Delta\tau_m(\vartheta)$ is calculated according to Sec. 2.2, and the diagonal pre-steering system is given by [21]

$$\mathbf{\Gamma}_\vartheta[n] = \text{diag}\{\delta[n - \Delta\tau_0(\vartheta)]\ \delta[n - \Delta\tau_1(\vartheta)]\ \ldots\ \delta[n - \Delta\tau_{M-1}(\vartheta)\} \quad . \tag{2.44}$$

The PSC matrix of the pre-steered data $\mathbf{y}_\vartheta[n]$ is given by

$$\mathbf{R}_\vartheta = \mathcal{E}\left\{\mathbf{y}_\vartheta[n]\,\mathbf{y}_\vartheta^{\text{H}}[n]\right\} \quad . \tag{2.45}$$

The proposed method then evaluates the maximum eigenvalue of $\mathbf{R}_\vartheta$ in (2.45) using an EVD for a range of angles ϑ, with the best match indicated by ϑ_{opt} ,

$$\vartheta_{\text{opt}} = \underset{\vartheta}{\text{argmax}}\{\max_i \lambda_i(\mathbf{R}_\vartheta)\} \quad , \tag{2.46}$$

with $\lambda_i(\mathbf{R}_\vartheta)$ denoting the ith eigenvalue of $\mathbf{R}_\vartheta$. The drawback of this method is that it can only resolve a single source. In a scenario with multiple source signals, only the strongest source can be estimated.

2.5.5 Other Broadband AoA Estimation Methods

Other broadband AoA estimation methods based on sparse signal representation are presented in [65, 66 , 67], whereby the idea to recover the spatial distribution of the incident signals by directly representing the array output by an over-complete dictionary under sparsity constraint. In [65] the broadband covariance matrix sparse representation method is presented which forms a new measurement vector by aligning the lower left triangular elements of the array output covariance matrix and reconstructs this vector to realise wideband AoA estimation. However, it relies on some prior information such as signal modulation types and the preestimated signal power spectrum which leads to a degradation in per-

formance when the incident signals arises from different types of modulations or have different signal power spectra.

The method in [66] firstly performs a subband decomposition of the broadband signal and then uses a sparse representation model of the joint narrowband array covariance data in the frequency domain to enforce joint sparsity in the concatenated covariance matrix at all frequencies. Thereafter, based on the greed matching pursuit algorithm [68], the AoA is estimated by joint processing of the array covariance data at different frequency bins. A similar technique in [67], extends an existing narrowband covariance fitting method by additionally introducing group sparsity regularisation. That jointly fits the powers of the signals using overcomplete dictionaries of the AoAs, into the estimated covariance matrices for all narrowband signals, and appropriately chooses the regularisation constants for both the individual sparsity and the group sparsity. The AoAs are estimated by finding the directions that contain most of the power. However, this approach requires additional estimation of the number of directions of arrival and has much higher complexity than the CSS method [67].

2.6 Conclusion

This chapter has provided a basic introduction to the principles of propagating wavefields, followed by a definition for narrowband and broadband signals for a space-time model of the system used in this work. Thereafter, the fundamental concept of angle of arrival (AoA) estimation was introduced with a classification of AoA based on the signal bandwidth. Narrowband AoA estimation approaches were then reviewed. In particular, the narrowband MUSIC algorithm has been considered in more detail due to its ability to achieve high angular resolution for narrowband AoA applications compared with other narrowband techniques such as standard delay-sum beamformer and Capon's minimum variance tech-

nique. Simulation results show the accuracy of the MUSIC algorithm compared with beamformer and MVDR methods for narrowband AoA applications. However, MUSIC or any narrowband AoA techniques are not directly applicable for broadband AoA problems. Therefore various existing broadband AoA estimation techniques have been overviewed.

The next chapter will define the broadband steering vector and its implementation using a fractional delay filter. In addition, a new method for implementing a fractional delay filter based on a filter bank approach will be presented. This method is able to achieve high accuracy across the entire bandwidth compared with the state-of-the-art of the fractional delay techniques which perform best only at low frequencies.

Chapter 3

Broadband Steering Vector Implementation

For broadband array signal processing applications, the time delays arising from signal wave fronts travelling across an array at finite speed cannot be represented by phase shifts as in the narrowband case but require to be addressed as lags. Since these delays are normally not integer multiples of the sampling interval, fractional delay filters need to be used [20, 34]. With broadband sensor array applications potentially operating across several octaves, the implementation accuracy of such fractional delay is crucial to the accuracy of broadband angle of arrival estimation or the performance of any other subsequent processing [69].

Therefore, this chapter provides an overview of various fractional delay filter designs that can be used to implement accurate broadband steering vector requirements for applications such as broadband AoA estimation. In particular, we reviews windowed sinc methods and the Farrow structure approach. A common feature across these techniques is their rapidly decreasing performance as half of the sampling rate is approached. Therefore, we propose a filter bank based approach, which operates standard fractional delay filters on a series of

frequency-shifted subband signals, such that they appear in the filter's lowpass region, where the above fractional delay techniques can perform very accurately.

The organisation of this chapter is as follows. Sec. 3.1 motivates the requirement of highly accurate fractional delay filters by reviewing the construction of broadband steering vectors. Then, different approaches for designing fractional delay filters are reviewed in Sec. 3.2. After that, the proposed method based on the filter bank approach is introduced and outlined in Sec. 3.3. The complexity of various fractional delay filter implementation methods is then analysed and compared in Sec. 3.4. Simulation results are provided in Sec. 3.5 to demonstrate the performance of the proposed approach, which is benchmarked against windowed sinc methods and the Farrow structure, before conclusions are drawn in Sec. 3.6.

3.1 Broadband Steering Vector

This section defines the concept of a broadband steering vector, which characterises a broadband signal when it illuminates a sensor array from an angle of arrival ϑ. For this, an $M-$element array of omnidirectional sensors located at positions $\mathbf{r}_m$, $m = 1 \dots M$ collects a signal vector $\mathbf{x}(t) \in \mathbb{C}^M$, with the continuous time variable t. If a far field source illuminates the array such that the signal at the origin $\mathbf{r} = \underline{\mathbf{0}}$ is $s(t)$ and we neglect attenuation, then

$$\mathbf{x}(t) = \begin{bmatrix} s(t-T_1) \\ s(t-T_2) \\ \vdots \\ s(t-T_M) \end{bmatrix} = \begin{bmatrix} \delta(t-T_1) \\ \delta(t-T_2) \\ \vdots \\ \delta(t-T_M) \end{bmatrix} * s(t) \tag{3.1}$$

where $*$ denotes convolution. For the delays $T_m = \frac{1}{c}\mathbf{k}^T\mathbf{r}_m$, $m = 1...M$, $\mathbf{k}$ is the normal vector of the source's wave front, and $\mathbf{k}/c$ is known as the slowness vector of the source. Sampling $\mathbf{x}(t)$ with a sampling period T_s yields $\mathbf{x}[n]$, with discrete

time index n such that $t = nT_s$. The assumption is a perfectly bandlimited signal $s(t)$, such that the interpolation function underlying the sampling process is a sinc. With

$$\mathbf{x}[n] = \begin{bmatrix} \delta[n-\tau_1] \\ \delta[t-\tau_2] \\ \vdots \\ \delta[t-\tau_M] \end{bmatrix} * s[n] = \mathbf{a}[n] * s[n] \tag{3.2}$$

and normalised delays $\tau_m = T_m/T_s$, the ideal fractional delays $\delta[n-\tau_m]$ can be defined as

$$\delta[n-\tau] = \begin{cases} \frac{sin(\pi(n-\tau))}{\pi(n-\tau)} & , \quad n \neq \tau \\ 1 & , \quad n = \tau \end{cases} \tag{3.3}$$

and are now sinc functions which not necessarily remain sampled in the sinc's zero crossing, and therefore generally possess infinite support. The quantity $\mathbf{a}[n]$ in (3.2) is referred to as broadband steering vector, and consists of a number of different fractional delays of the type in (3.3).

A signal model for a scenario with K independent far field broadband sources $s_k[n]$, $k = 1 \ldots K$, each characterised by a broadband steering vector $\mathbf{a}_k[n]$, therefore becomes

$$\mathbf{x}[n] = \sum_{k=1}^{K} \sum_{\nu=-\infty}^{\infty} \mathbf{a}_k[\nu] s_k[n-\nu] + \mathbf{v}[n] \tag{3.4}$$

with $\mathbf{v}[n]$ representing spatially and temporally uncorrelated noise with covariance $\mathcal{E}\{\mathbf{v}[n]\mathbf{v}^H[n]\} = \sigma_v^2\mathbf{I}$. To capture information contained in the data vector $\mathbf{x}[n]$ requires a space-time covariance matrix $\mathbf{R}[\nu] = \mathcal{E}\{\mathbf{x}[n]\mathbf{x}^H[n-\nu]\}$with lag parameter ν. Its Fourier pair, the cross-spectral density matrix $\mathbf{R}(z) = \sum_\nu \mathbf{R}[\nu]z^{-\nu}$ or short $\mathbf{R}[n] \circ\!\!-\!\!\bullet \mathbf{R}(z)$,

$$\mathbf{R}(z) = \sum_{k=1}^{K} \mathbf{a}(z)\mathbf{a}^H(z^{-1})S_k(z) + \sigma_\nu^2\mathbf{I} \tag{3.5}$$

with $S_k(z)$ being the power spectral density of the lth source, forms a polynomial matrix. In the next section, a brief review of fractional delay filter design and implementation methods are provided.

3.2 Review of Fractional Delay Filters

A fractional delay filter (FDF) can be defined as a device which delays the discrete signal by a fraction of the sampling period. In this section, we brief review various implementation methods for fractional delay filters that can be used for implementation of broadband steering vector. However, for more details the reader is referred to [43].

3.2.1 Ideal Delay

The ideal fractional delay can be defined as

$$f_{\text{ideal}}[n] = \delta[n - \tau] \quad . \tag{3.6}$$

With the Fourier pair $\delta[n] \circ\!\!-\!\!\bullet 1$ and the Fourier transform's time delay property, a Fourier transform of the fractional delay yields

$$F_{\text{ideal}}(e^{j\Omega}) = 1 \cdot e^{-j\Omega\tau} \quad . \tag{3.7}$$

The desired frequency response for the ideal delay is a complex-valued function that specifies both the magnitude and the phase response respectively, such as

$$|F_{\text{ideal}}(e^{j\Omega})| = 1 \quad \text{for all } \Omega$$

$$\arg\{F_{\text{ideal}}(e^{j\Omega})\} = \Theta_{\text{ideal}}(\Omega) = -\tau\Omega.$$

Therefore the group delay of the ideal fractional delay can be calculated as

$$\gamma_{\text{ideal}} = -\frac{\partial(\Theta_{\text{ideal}}(\Omega))}{\partial\Omega} = -\frac{\partial}{\partial\Omega}(-\Omega\tau) = \tau \quad . \tag{3.8}$$

which is a constant in the entire frequency band.

Based on this ideal delay, an error metric for an arbitrary fractional delay filter approximation $f[n]$ can be defined as

$$S_{ee}(e^{j\Omega}) = |F_{\text{ideal}}(e^{j\Omega}) - F(e^{j\Omega})|^2, \tag{3.9}$$

with $F(e^{j\Omega})\bullet\!\!-\!\!\circ f[n]$, such that $S_{ee}(e^{j\Omega})$ is a quadratic error type metric for the approximation of $f_{\text{ideal}}[n]$ by $f[n]$.

3.2.2 Windowed Sinc Methods

For most cases, the incurred delays τ are not integer multiples of the sampling period. Therefore, the ideal fractional delay in (3.6) cannot be reduced to a single impulse, unlike the one shown in Fig. 3.1(a) where the delay is an integer value. Instead, when sampling off the regular — i.e. integer valued — sampling grid the impulse response is possessing infinite support and represents a shifted and sampled version of the sinc function as indicated in Fig. 3.1(b). In addition, the ideal fractional delay response is not only infinitely long but also non-causal [70] which makes it impossible to implement in real time applications. Therefore, a window function $w_N[n]$ and time delay τ have to be applied to create a causal filter of length $2N$, such that

$$f[n] = f_{\text{ideal}}[n - \tau - N] \cdot w_N[n - \tau - N] \quad . \tag{3.10}$$

Below, a number of different methods of selecting the window $w_N[n]$ will be explored.

3.2.2.1 Rectangular Window

In order to implement an approximation to ideal fractional delay filter in (3.6), in the simplest case a rectangular window with $w_{N,\text{rect}}[n] = p_N[n]$ performs a truncation to the sinc function according to

$$p_N[n] = \begin{cases} 1 & , \quad |n| \leq N \\ 0 & , \quad |n| > N \end{cases} \quad . \tag{3.11}$$

The resulting discrete prolate spheroidal sequence $f[n] = f_{\text{ideal}}[n - \tau - N] \cdot p_N[n]$ [71] provides an approximation of $f_{\text{ideal}}[n]$ that generally demonstrates increasing accuracy with N at lower frequencies. However, independent from N, the performance degrades due Gibbs phenomena as the Nyquist frequency is approached [72], which compared to an ideal delay system causes ripple in the group delay and an increasingly poor approximation with increasing frequency. This leads to a restricted accuracy of the fractional delay filter [43, 72], and a limitation of its application to lowpass-type signals. This Gibbs phenomenon results in a deterioration of the magnitude response close to half the sampling frequency. In addition, the group delay response suffers similar deterioration.

The limitation of the rectangular window for a filter length of $N = 21$, when modelling the delays previously illustrated in the example for Fig. 3.1 is shown in Fig. 3.2. The magnitude and the group delay responses in Fig. 3.2(a) and Fig. 3.2(b) respectively indicate that oscillation (the Gibbs phenomenon) occurs at higher frequency ranges. In order to overcome these problems, tapered window methods have been proposed and will be considered next.

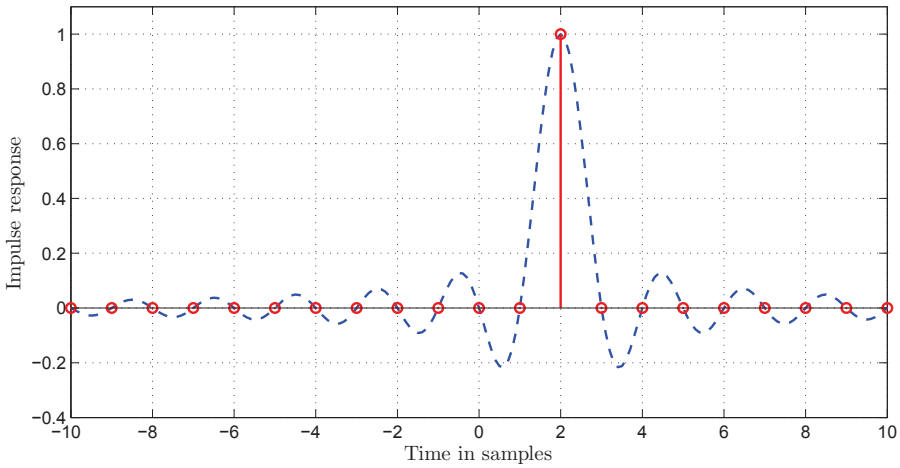

(a)

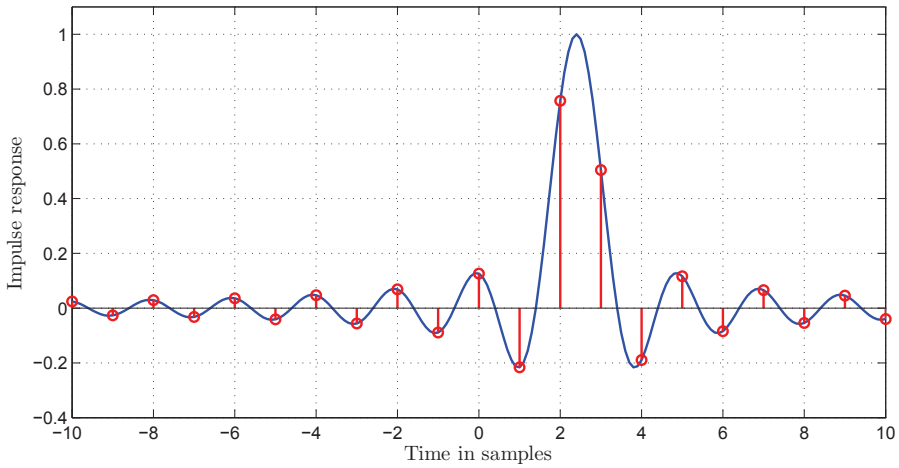

(b)

Figure 3.1: Impulse response of a fractional delay filter with (a) integer delay $\tau = 2$ and (b) fractional delay $\tau = 2.4$.

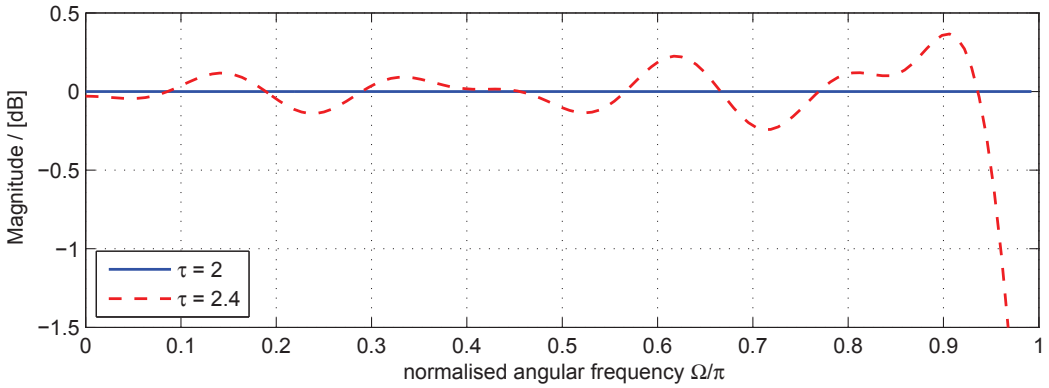

(a)

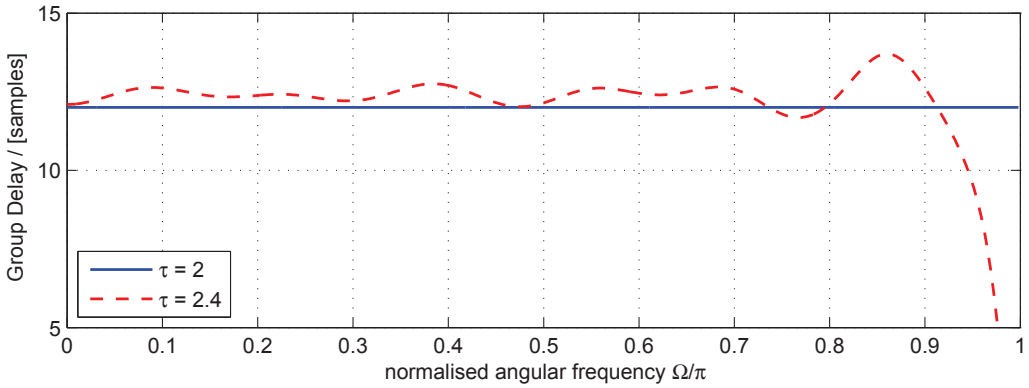

(b)

Figure 3.2: (a) The magnitude and (b) group delay response for integer delay $\tau = 2$ and fractional delay $\tau = 2.4$.

3.2.2.2 Tapered (Hann & Hamming) Windows

To enhance the performance of fractional delay filters, tapered windows instead of rectangular have been proposed for the truncation of the sinc [70, 73]. Examples for such windows include a Hann window [74, 75]

$$w_{N,\text{Hann}}[n] = (0.5 - 0.5\cos(\frac{\pi n}{2N}))p_N[n]. \tag{3.12}$$

or a Hamming window [75]

$$w_{N,\text{Hamming}}[n] = (0.54 - 0.46\ \cos(\frac{\pi n}{2N}))p_N[n]. \tag{3.13}$$

By using such windowing techniques, the ripple in the frequency response can be reduced; it also leads to a reduced group delay ripple compared with the rectangular window, but will result in a wider transition band of the filter, as depicted in Figs. 3.3(a) and (b) for a fractional delay of $\tau = 2.4$. However, both windowed sinc methods still perform best at low frequencies, and degrade significantly in higher frequency ranges.

3.2.3 Farrow Structure

The Farrow structure [44, 76] is a polynomial-based interpolation between input samples generating fractional delay filters. Fig. 3.4 depicts the structure of the Farrow filter which is consisting of $P + 1$ sections of N_Fth-order FIR filters with constant coefficients $c_{p,k}, p = 1 \ldots P, k = 0 \ldots N_F$. The fractional delay parameter τ is multiplied and accumulated to the outputs of the FIR subfilters. The coefficients of the Farrow structure can be determined from the interpolation filter based on Lagrange's or B-spline polynomial interpolation time domain methods [77, 78, 79], can be optimised directly in the frequency domain [43, 80]. The transfer function of the Farrow structure is given by

$$F(z, \tau) \quad = \quad \sum_{p=0}^{P} C_k(z)\tau^k \quad . \tag{3.14}$$

where $\tau \in [0, 1]$ is the desired fractional delay, P is the degree of the polynomials

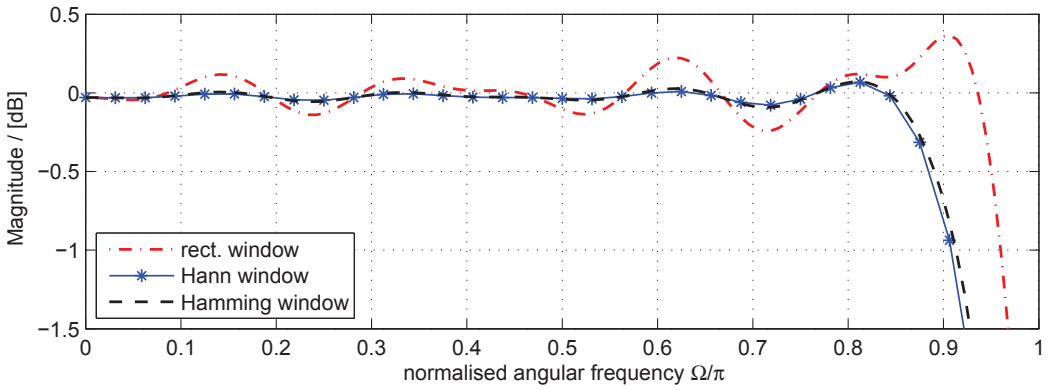

(a)

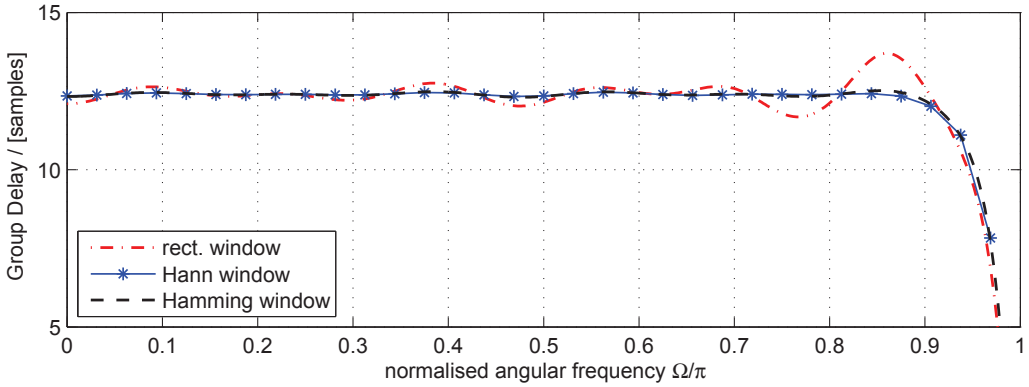

(b)

Figure 3.3: (a) The magnitude and (b) group delay response for tapered (Hann & Hamming) window and rectangular window for fractional delay $\tau = 2.4$.

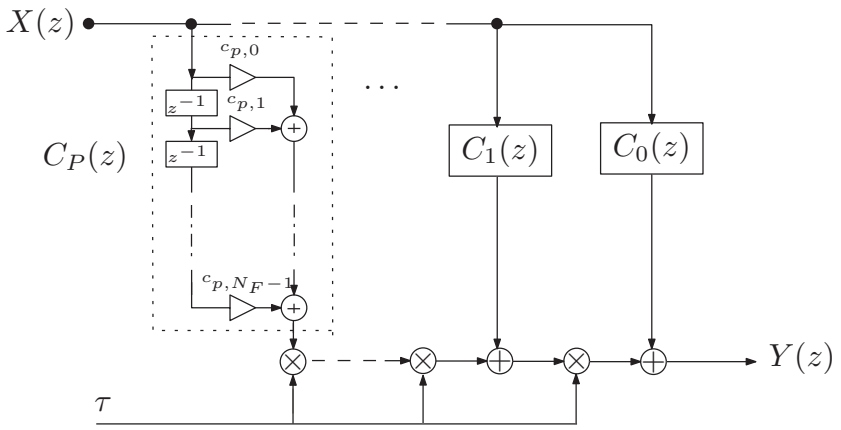

Figure 3.4: Farrow structure with $P+1$ subsystems of order N_F approximating a fractional delay τ between input $X(z)$ and output $Y(z)$.

and $C_k(z)$ are the transfer functions of the FIR subfilters and given by

$$C_k(z) = \sum_{k=0}^{N_F-1} c_{p,k}\, z^{-n} \tag{3.15}$$

with $c_{p,k}$ are the coefficients for the $P+1$ FIR subfilters.

The main feature of the Farrow structure is that the coefficients of the FIR subfilters are fixed for a given filter structure order and the only changeable parameter is the fractional delay τ. As a result, the Farrow structure can be implemented as a variable fractional delay with constant coefficients. The magnitude response of the Farrow filter is flat at low frequencies only, thus limiting its applicability to broadband problems that do not extend beyond lowpass-type signals.

3.3 Filter Bank Approach

Filter banks have been used in the context of fractional delays previously, since subband processing can shorten the long impulse responses found when sampling

a sinc off the zero-crossings [81]. Exploiting the high accuracy of various fractional delay filters reviewed in Sec. 3.2.2 for lowpass signals only, in this section we will discuss proposed solutions for fractional delay filters suitable for broadband signals. A filter bank based structure is proposed as an implementation framework for fractional delay filters for constructing accurate time delays in the low frequency range of every subband.

3.3.1 Idea

Filter banks decompose a fullband input signal into a number of different frequency bands; if the analysis filter bank is sufficiently frequency-selective, then processing can be performed in each band individually. Due to the reduced bandwidth, the subband signals generally can be downsampled, leading to a reduced cost for any processing to be performed on the subband signals. Thereafter, a fullband output signal can be reconstructed by combining the processed subband signals using a synthesis filter bank.

For the FDF implementation, we exploit the band limitation not to downsample subband signals; instead we keep the subband signals oversampled and their bandlimited, but modulate each of them to a lowpass characteristic; thus applying a fractional delay filter to lowpass signals only, accuracy is guaranteed. Thereafter, demodulation can restore the original band position, followed by a synthesis filter bank for reconstruction of a fractionally delayed fullband signal.

3.3.2 Filter Bank Characteristic

The proposed filter bank based fractional delay filter structure is illustrated in Fig. 3.5. In this structure, the input signal $x[n]$ is split into J different frequency bands or subbands $x_j[n], \quad j = 0, \ldots, J-1$, using an analysis filter bank with

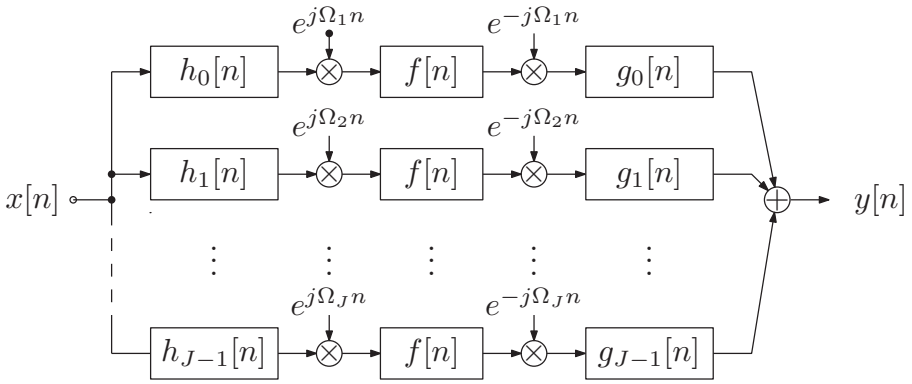

Figure 3.5: Proposed subband-based fractional delay filter with analysis filter bank stage with analysis filters $h_j[n] \circ\!\!-\!\!\bullet H_j(z)$, a modulation stage, the fractional delay filters $f[n]$, a demodulation stage, followed by a synthesis filter bank with synthesis filters $g_j[n] \circ\!\!-\!\!\bullet G_j(z)$.

filters $H_j(z)$, $j = 0...J-1$,

$$x_j[n] = h_j[n] * x[n] \quad \longleftrightarrow \quad X_j(z) = H_j(z)X(z), \tag{3.16}$$

Undecimated, the subband signals $x_j[n]$ then are modulated or frequency shifted by Ω_j such that the fractional delay filters are applied to lowpass signals

$$v_j[n] = x_j[n]e^{j\Omega_j n} \quad , \tag{3.17}$$

in every branch, where Ω_j is the normalised angular centre frequency

$$\Omega_j = \frac{(2j-1)\pi}{J} \quad , \tag{3.18}$$

which translates every subband in frequency to sit symmetrically around $\Omega = 0$.

Subsequently each modulated subband signal $v_j[n]$ is processed separately using a fractional delay filters $f[n]$ (e.g. tapered Hann window or Farrow FDF)

to reconstruct the accurate time delays

$$u_j[n] = f[n] * v_j[n], \quad \longleftrightarrow \quad U_j(z) = F(z)V_j(z), \tag{3.19}$$

Then the demodulation process is performed for the subband filter outputs $u_j[n]$ to return them to their original spectral position by

$$y_j[n] = u_j[n]e^{-j\Omega_j n} \quad . \tag{3.20}$$

Finally, a fullband output signal $y[n]$ can be reconstructed by combining the demodulated subband signals $y_j[n]$ using the synthesis filter bank $G_J(z)$,

$$y[n] = \sum_{j=0}^{J-1} g_j[n] * y_j[n] \quad \longleftrightarrow \quad Y(z) = \sum_{j=0}^{J-1} G_j(z)Y_j(z) \quad . \tag{3.21}$$

For memory and computational simplicity, the analysis filter can be derived from a prototype lowpass filter by means of a modulating transform. We here use a generalised discrete Fourier transform (GDFT) modulated filter bank, which offers advantages over other modulations in terms of subband uniformity and the ability to implement a near perfect paraunitary system, where the synthesis filters $G_j(z)$ can be derived by time reversal from the analysis filters [82]. The prototype filter can be designed using a least-squares approach [82], whereby the reconstruction error of the filter bank is a design criterion that is optimised. Therefore, depending on the quality of the prototype filter, and therefore its length and complexity, different levels of reconstruction errors can be achieved for the filter bank.

3.4 Complexity Consideration

Before assessing and comparing the accuracy of various fractional delay filter methods and the proposed filter bank approach as discussed in Sec. 3.2 and Sec. 3.3 respectively, this section will analyse the computational complexity of these approaches.

The straightforward windowed sinc functions with length N requires

$$C_{\text{Window}} = 2N \quad , \tag{3.22}$$

multiply accumulates (MACs), which is independent of the particular window function such as rectangular or Hann window, as the coefficients can be saved readily multiplied onto sinc values.

The Farrow structure with its polynomial order W and filter length N_F consumes

$$C_{\text{Farrow}} = N_F(P+1) + P \quad , \tag{3.23}$$

MACs per sampling period, which can be substantial if $N_F \approx N$.

Finally, the computational complexity for the filter bank approach in its most efficient implementation based on a modulated filter bank in polyphase implementation [83], requires

$$C_{\text{F-Bank}} = 2L_p + 4J\log_2(J) \quad , \tag{3.24}$$

MACs per filter bank and sampling period, where L_p is the order of filter bank's prototype filter and J is the number of subbands. For the proposed approach, 2 filter bank operations and a total of J fractional delay filter implementations

according to Fig. 2.5 therefore lead to

$$C_{\text{Proposed}} = 2C_{\text{F-Bank}} + J \cdot C \quad , \tag{3.25}$$

whereby C takes on the value in (3.22) or (3.23), depending on which fractional delay scheme is integrated into the proposed architecture.

Considering (3.22), (3.23) and (3.25), it is clear that the filter bank based approach is significantly more expensive compared to a direct implementation. Therefore, the performance analysis in the next section will have to demonstrate if the computational cost that needs to be afforded for the proposed approach is worthwhile.

3.5 Simulation and Results

In this section, we present simulation results for comparing the error metric of different implementation methods for FDF introduced in this chapter. In addition, the complexity of these techniques forms a useful benchmark to which the computational cost of the proposed method can be compared.

3.5.1 Performance Metrics

For the windowed approaches, Fig. 3.6 provides some preliminary results on the maximisation of the error $S_{ee}(e^{j\Omega})$ over the fractional delay as a variable. The rectangular window performs worst, and improvements can be made at no cost through the use of tapered windows. As an alternative to the Hann window, we also show a Hamming window, which however performs slightly worse than its competitor. The approximation error for a truncated sinc function with $N = 41$ is shown in Fig. 3.7, where a maximum error is reached for a fractional delay of $\tau = \frac{1}{2}$ and frequencies approaching half the sampling rate.

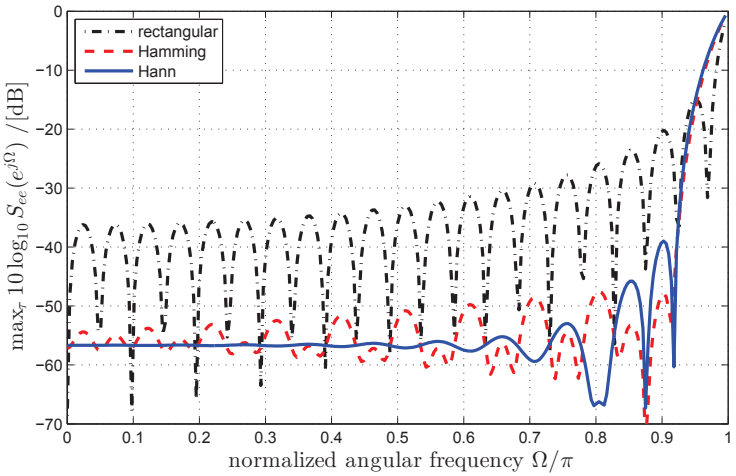

Figure 3.6: Approximation error $S_{ee}(e^{j\Omega})$ maximised over fractional delay τ , and dependent on normalised angular frequency Ω.

The degradation towards half the sampling rate is shared by both Hann and Hamming windowed sinc functions, which are shown in Figs. 3.8 and 3.9 respectively, also with window length of $N = 41$.

Figs. 3.10 and 3.11 show the performance of the Farrow structure with polynomial orders $P = 3$ and $P = 9$. From these figures, it can be seen that while the Farrow structure does not perform well for higher frequencies, it significantly exceeds both the rectangular and the tapered windowed sinc approaches at lower frequency range, in addition its performance can be increased for higher polynomial order, whereby tapered windowing such as with the Hann window offers advantages over the rectangular window at no cost.

For the proposed filter bank approach to a fractional delay implementation, Fig. 3.12 shows the combination of a $J = 16$ channel filter bank with prototype filter length $L_p = 448$ and an $P = 3$ order Farrow structure to implement the fractional delay in the frequency-shifted subbands. As can be seen from the results in Fig. 3.12, the error is uniformly low with a maximum error $S_{ee}(e^{j\Omega})$ of -55dB

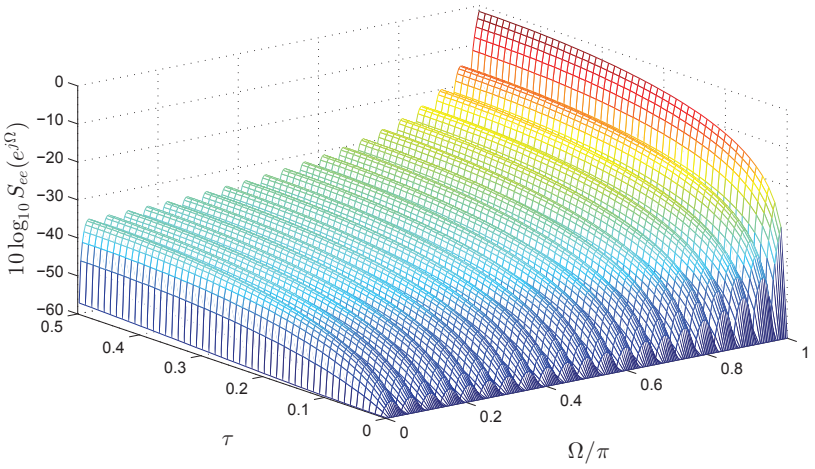

Figure 3.7: Approximation error for truncated sinc function with $N = 41$.

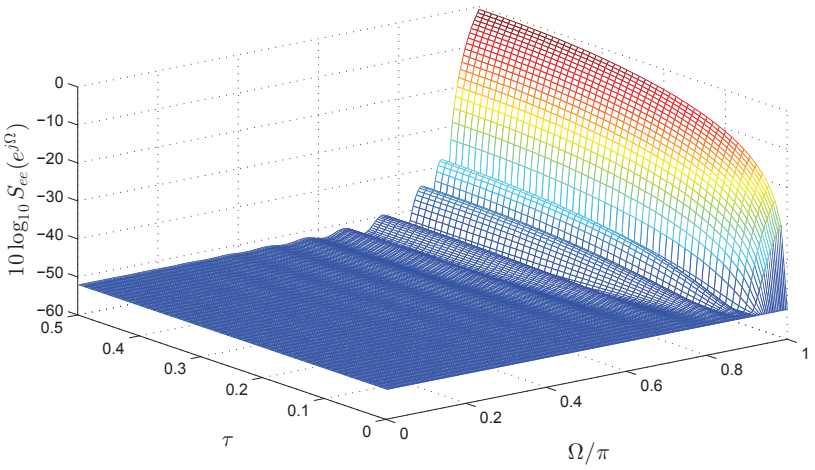

Figure 3.8: Approximation error for Hann windowed sinc function with $N = 41$.

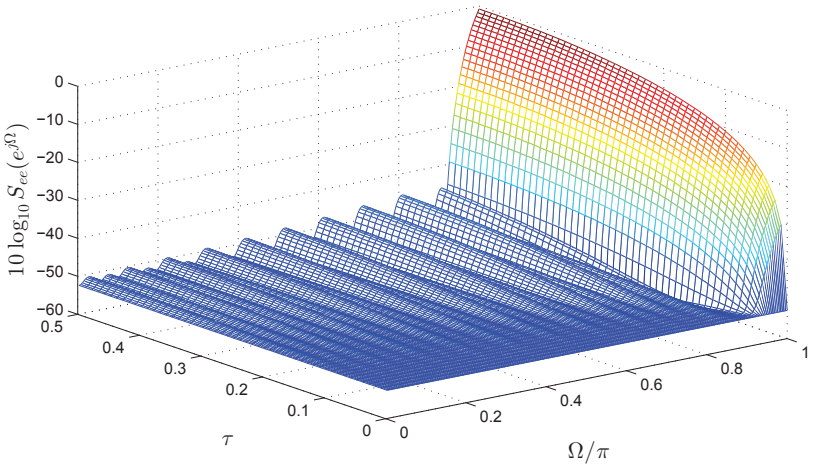

Figure 3.9: Approximation error for Hamming windowed sinc function with $N = 41$.

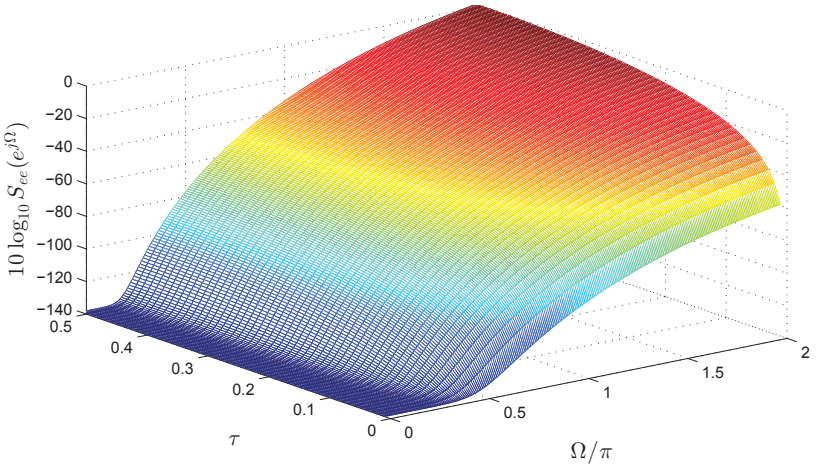

Figure 3.10: Approximation error for Farrow structure with polynomial order $P = 3$.

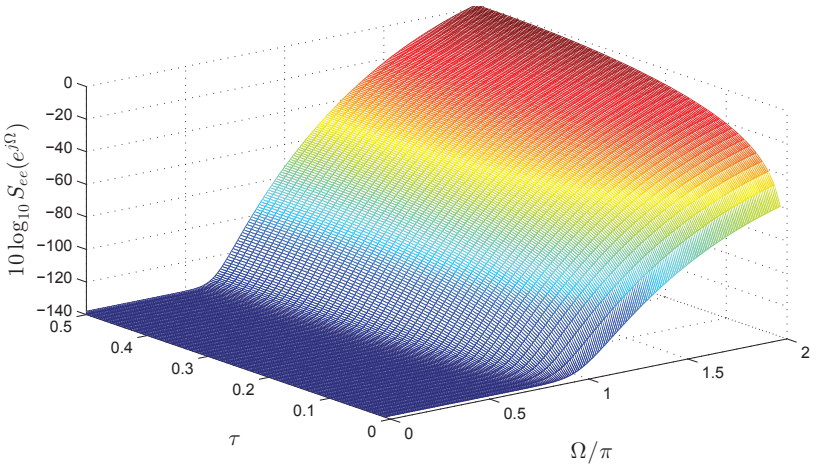

Figure 3.11: Approximation error for Farrow structure with polynomial order $P = 9$.

across all frequencies Ω and over all fractional delays τ . Here, $S_{ee}(e^{j\Omega})$ consists of two contributions — (i) an error due to inaccuracies on the Farrow structure, and (ii) a reconstruction error within the filter bank. Here, with a reconstruction error of -55dB [83], the latter dominates. This is underlined by the same error of -55dB that is obtained in combination with a Hann windowed sinc function, and a Farrow structure of order $P = 9$, as illustrated in Fig. 3.13 and Fig. 3.14 respectively. In contrast, embedding the sinc function characterised in Fig. 3.7 into the subbands yields an approximation error of approximately - 37.7dB; i.e. for this case, the fractional delay filter is sufficiently crude to dominate the overall error of the system. This is also supported by the approximation error σ^2_{full} in (3.26), which is summarised for the various fractional delay filter methods in Tab. 3.1. The fractional delay filter methods using the rectangularly truncated sinc has a length such that the system exhibits equivalent complexity to the displayed filter bank based methods.

Since the undecimated filter bank approach is costly in terms of computations,

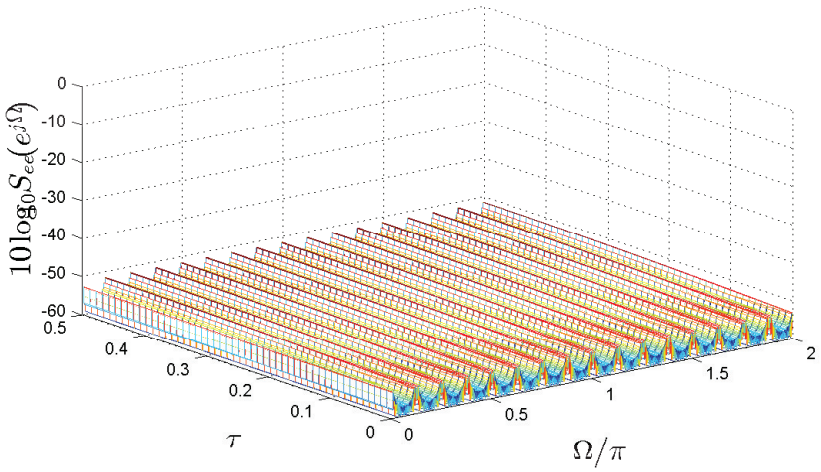

Figure 3.12: Approximation error for filter bank approach with $J = 16$, $L_p = 448$ and an $W = 3$ order Farrow filter as subband fractional delay $f[n]$.

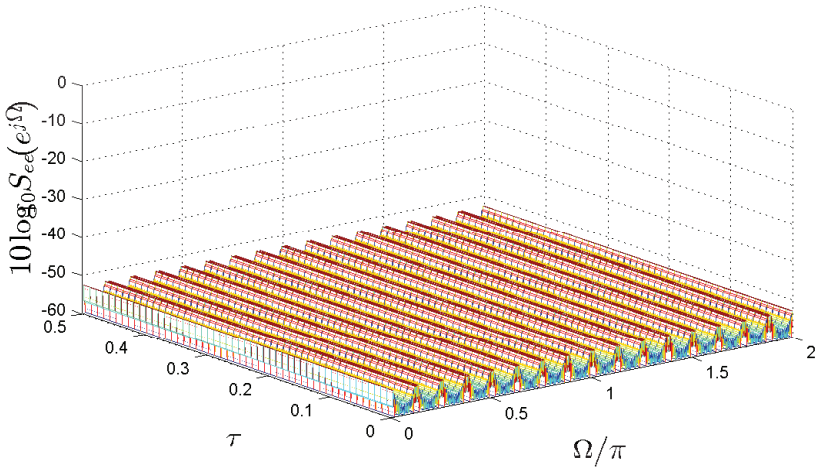

Figure 3.13: Approximation error for filter bank approach with $J = 16$, $L_p = 448$ and an Hann windowed sinc function with $N = 41$ as subband fractional delay $f[n]$.

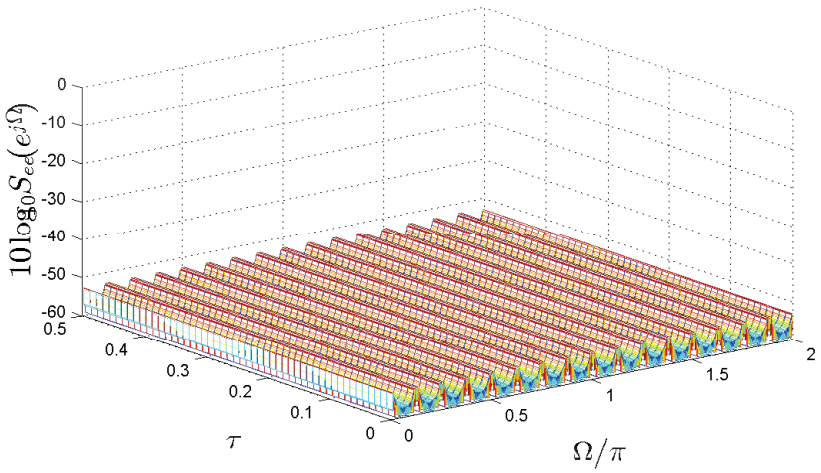

Figure 3.14: Approximation error for filter bank approach with $J = 16$, $L_p = 448$ and an $W = 9$ order Farrow filter as subband fractional delay $f[n]$.

FDF implementation	$\sigma^2_{\text{full}}/[\text{dB}]$
sinc	-21.1
Farrow, $P = 9$	-0.5
fiba & sinc	-38.0
fiba & Hann	-55.3
fiba & Farrow, $P = 3$	-55.5
fiba & Farrow, $P = 9$	-55.8

Table 3.1: Table of average errors over entire Nyquist band for different fractional delay filter implementations. The filter bank (fiba) methods use a $J = 16$ channel filter bank with a reconstruction error of approx. -55dB.

the filter bank should be designed such that it is just sufficiently good to match the desired approximation error for the FDF $f[n]$. This ensures that the system is not over-designed, and that the cost of the filter bank can be kept as low as possible.

3.5.2 Error Analysis and Complexity for Various Fractional Delay Filter Approaches

To quantitatively assess the performance of the proposed filter bank based fractional delay filters, two approximation errors are defined. A first error represents the average deviation from an ideal delay over the entire band,

$$\sigma^2_{\text{full}} = \frac{1}{\pi}\int_0^{\pi} S_{ee}(e^{j\Omega})\, d\Omega \quad . \tag{3.26}$$

A second error metric removes the highest octave, where the approximation is least accurate, therefore only integrating over the lower half of the spectrum

$$\sigma^2_{\text{half}} = \frac{2}{\pi}\int_0^{\pi/2} S_{ee}(e^{j\Omega})\, d\Omega \quad . \tag{3.27}$$

According to (3.26) and (3.27), the resulting measure for the windowed sinc function and the Farrow structure are shown in Fig. 3.15. This provides a clear indication that a restriction to lowpass signals provides accurate results, particularly for the Hann window, while state-of-the-art methods are unsuitable when applied over the entire Nyquist band.

3.6 Conclusion

The need for accurate broadband steering vectors for applications such as broadband angle of arrival estimation has motivated the implementation of fractional delay filters that can approach the ideal fractional delay over a large bandwidth. Since state-of-the-art fractional delays such as windowed sinc and Farrow filters perform best at low frequencies, this chapter has proposed high accuracy fractional delay filter based on a filter bank approach. Simulation results indicate

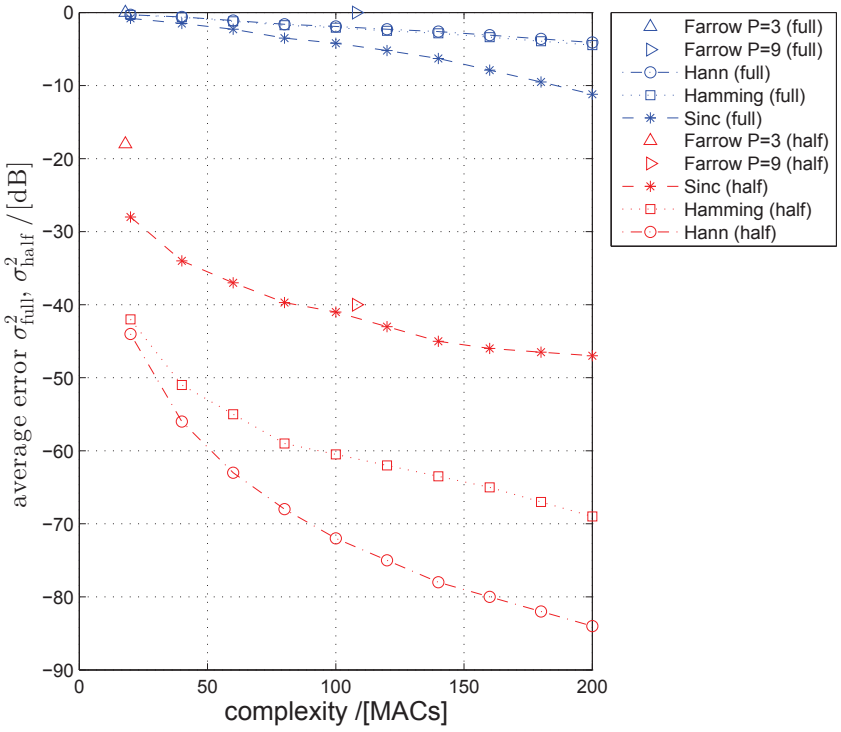

Figure 3.15: Error performance versus complexity for various fractional delay filter approaches.

that accuracy can be achieved across the entire bandwidth, and that the approximation error w.r.t. an ideal delay is either limited by the FDF inaccuracy or the reconstruction error of the filter bank, whichever is greater.

The next chapter will apply the broadband steering vectors introduced here to broadband AoA problems, to be addressed by polynomial MUSIC algorithm.

Chapter 4

Broadband MUSIC Algorithm

This chapter proposes a new method for broadband angle of arrival estimation, which is a generalisation of the narrowband multiple signal classification (MUSIC) algorithm to the broadband case. Based on the formulation of polynomial space-time covariance matrices, a polynomial eigenvalue decomposition is used to determine the noise-only subspace of this matrix, which can be scanned by appropriately defined broadband steering vectors as illustrated previously in Chapter 3, leading to the definition of a polynomial MUSIC (P-MUSIC) approach. Moreover, two broadband P-MUSIC algorithm versions are presented, which can resolve either angle of arrival alone or additionally the frequency range over which sources are active.

The chapter is organised as follows. Sec. 4.1 motivates the work within this chapter. In Sec. 4.2, the broadband subspace decomposition afforded by a polynomial eigenvalue decomposition (PEVD) for broadband signals is presented. We show how it can be implemented using two different iterative techniques: the second order sequential best rotation (SBR2) algorithm and the sequential matrix diagonalisation (SMD) algorithm. The proposed approach for AoA estimation for broadband sources, the polynomial MUSIC algorithm, is introduced in Sec. 4.3.

Two broadband P-MUSIC algorithm versions are presented, which resolve either the AoA alone or the AoA in combination with the frequency range over which sources are active. The performance and sensitivity of the proposed algorithms are analysed in Sec. 4.4 and Sec. 4.5 respectively, before conclusions are drawn in Sec. 4.6.

4.1 Introduction

As reviewed in Chapter 2, the original MUSIC algorithm [10] has been defined for the narrowband AoA scenario, and is not directly applicable to broadband cases. The reason is that the angle of incident in the broadband scenario has to be modelled by explicit time delays rather than phase shifts. Therefore, the lag value has to be taken into account when calculating the space-time covariance matrix for the sensor outputs, which leads to the elements of the space-time covariance matrix containing the complete auto- or cross correlation sequences rather than just a single correlation coefficient. This results in its corresponding cross-spectral density (CSD) matrix forming a polynomial matrix. In this case, the EVD cannot be used to diagonalise such a polynomial matrix at more than one time lag, and hence is not able to identify and separate the broadband signal subspaces, which are the core of the MUSIC algorithm.

In the past a number of efforts to derive broadband algorithms for AoA estimation have been pursued. As has been mentioned in Chapter 2, most broadband AoA techniques cleverly bypass the broadband problem in favour of narrowband processing, where first the broadband array data is decomposed into multiple narrowband signals of various frequencies by means of a discrete Fourier transform (DFT). Based on this decomposition, several algorithms have been proposed that vary by processing the different narrowband signals independently or coherently to get accurate AoA estimates. The incoherent methods in [11, 12] apply a nar-

rowband AoA technique separately for each frequency bin; thereafter a strategy is used for combining these independent estimates to obtain the final AoA estimate. The performance of this approach degrades when the sources are correlated or the frequencies of the signal of interest do not coincide with frequency bins [34]. The coherent approaches in [14, 15, 41] by contrast are based on the idea of cohering the different frequencies into a single "common" frequency for which narrowband high resolution AoA based method can then be used to estimate the source angles. However, the CSS approach [14] requires approximate knowledge of the AoA for pre-steering of the data in order to provide a good AoA estimation [41]. The novel method proposed in this chapter is free of such assumptions and implements a generalisation of the well known MUSIC algorithm directly to the broadband array data**.** The proposed polynomial MUSIC algorithm [34] offers the functionality of broadband AoA estimation, as well as the detection of the frequency range over which broadband sources are active**,** which differ from the previous methods that estimate the AoAs only.

4.2 Broadband Subspace Decomposition

Different from the narrowband case, in a broadband sensor array time delays rather than phase shifts bear information on the direction of a source. Therefore, the lag component has to be taken into account when calculating the space-time covariance matrix of the sensor outputs, which results in each element of this broadband covariance matrix to consist of the complete auto- or cross-correlation sequence between the various sensors, rather than just a single correlation coefficient. The z transform of this space-time covariance matrix is the cross-spectral density (CSD) matrix which includes Laurent polynomial elements and forms a polynomial matrix [28]. Since the EVD can only measure and remove instantaneous spatial correlations, it cannot sufficiently diagonalise the polynomial covari-

ance matrix. Instead, a polynomial matrix decomposition technique is required to factorise such a polynomial matrix at more than one lag value. A recently proposed polynomial matrix EVD (PEVD) [27] technique can be used to achieve this decomposition. PEVD is considered as a generalisation of the EVD to polynomial matrices, which transforms a polynomial (space-time) covariance matrix into a diagonal polynomial matrix using paraunitary matrices [27], and allows for the identification of the broadband (polynomial) signal and noise subspaces.

Therefore, this section will focus on a PEVD technique, whereby the idea of a polynomial EVD is introduced in Sec. 4.2.1. This is followed by a brief description of two iterative methods: the sequential best rotation (SBR2) algorithm [27] and the multiple shift maximum element sequential matrix diagonalisation (MSME-SMD) algorithm [29] which can be used to compute an approximation of the PEVD. The SBR2 algorithm is illustrated by a numerical example to demonstrate its ability for achieving strong decorrelation for a set of broadband signals, for identifying the broadband subspaces and then separating the signal-plus-noise and the noise-only subspaces, such that the polynomial space-time covariance matrix $\mathbf{R}[\tau]$ will be diagonalised for all lag values.

4.2.1 Polynomial Eigenvalue Decomposition (PEVD)

The main idea of the PEVD is to extend the conventional EVD for Hermitian matrices to the polynomial parahermitian matrices. The PEVD aims to factorise a parahermitian matrix $\mathbf{R}(z)$ by means of a paraunitary, i.e., lossless matrix $\mathbf{Q}(z)$. Therefore this section starts with a number of definitions to explain some extended properties for a polynomial matrix before stating the PEVD and its approximation by iterative methods such as SBR2 and MSME-SMD algorithms.

4.2.1.1 Parahermitian and Paraunitary Matrices

For scalar matrices, the Hermitian operator $\{\cdot\}^{\mathrm{H}}$ performs a transposition and complex conjugation, e.g., for any matrix $\mathbf{Q}^{\mathrm{H}} = (\mathbf{Q}^{\mathrm{T}})^* = (\mathbf{Q}^*)^{\mathrm{T}}$. For the polynomial case, the parahermitian operator $\tilde{\{\cdot\}}$ implies

$$\tilde{\mathbf{Q}}(z) = \mathbf{Q}^{\mathrm{H}}(1/z) \quad , \tag{4.1}$$

i.e. Hermitian transposing all matrix-valued coefficients, while z is replaced by $z^* = (1/z)$ and thus time-reversing the time domain matrix $\mathbf{Q}[\tau]$.

A Hermitian matrix is defined as the complex valued generalisation of a symmetric matrix such as $\mathbf{Q}^{\mathrm{H}} = \mathbf{Q}$. A polynomial matrix $\mathbf{Q}(z)$ is parahermitian if $\tilde{\mathbf{Q}}(z) = \mathbf{Q}(z)$ [84], where all coefficients associated with the polynomial elements have to satisfy $q_{ij}[t] = q^*_{ji}[-t] \quad \forall t \in \mathbb{Z}$.

Paraunitarity is a generalisation of the unitary characteristic for a complex matrix, where $\mathbf{Q}$ is a unitary matrix if it fulfils $\mathbf{Q}\mathbf{Q}^{\mathrm{H}} = \mathbf{Q}^{\mathrm{H}}\mathbf{Q} = \mathbf{I}$. Particularly, a unitary matrix $\mathbf{Q}$ is a transformation matrix which only performs a rotation of a vector but does not change its Euclidean norm, $||\mathbf{Q}\mathbf{w}||_2 = ||\mathbf{w}||_2$, with $\mathbf{w}$ arbitrary, i.e. the total power of the input vector is preserved [23, 63].

For the polynomial scenario, paraunitarity of a polynomial matrix $\mathbf{Q}(z)$ means that

$$\mathbf{Q}(z)\tilde{\mathbf{Q}}(z) = \tilde{\mathbf{Q}}(z)\mathbf{Q}(z) = \mathbf{I} \quad . \tag{4.2}$$

A paraunitary matrix $\mathbf{Q}(z)$ can be interpreted as the polyphase matrix of a lossless filter bank.

4.2.1.2 Idealistic PEVD

The Hermitian matrix $\mathbf{R}$ can be decomposed using the EVD, and the factorisation yields $\mathbf{R} = \mathbf{Q}\mathbf{\Lambda}\mathbf{Q}^{\mathrm{H}}$, with a unitary matrix $\mathbf{Q}$ and a diagonal matrix $\mathbf{\Lambda}$

containing real value eigenvalues. If we extend the narrowband EVD to a polynomial EVD (PEVD) of a parahermitian matrix $\mathbf{R}(z)$, then the decomposition becomes $\mathbf{R}(z) \approx \mathbf{Q}(z)\mathbf{\Lambda}(z)\tilde{\mathbf{Q}}(z)$, with $\mathbf{Q}(z)$ is a paraunitary matrix, and $\mathbf{\Lambda}(z)$ is a polynomial diagonal matrix whose entries have the properties of PSDs. This factorisation can be accurate for FIR paraunitary matrices with sufficiently high order [85].

For a given polynomial parahermitian matrix $\mathbf{R}(z)$, the aim of the ideal polynomial EVD for a broadband scenario is to find a paraunitary matrix $\mathbf{Q}(z)$ such that

$$\mathbf{\Lambda}(z) = \tilde{\mathbf{Q}}(z)\mathbf{R}(z)\mathbf{Q}(z) \quad , \tag{4.3}$$

where $\mathbf{\Lambda}(z)$ is a diagonal matrix containing the polynomial eigenvalues, such that the diagonal elements

$$\mathbf{\Lambda}(z) = \mathrm{diag}\{\Lambda_0(z), \Lambda_1(z), \Lambda_2(z), \ldots, \Lambda_{M-1}(z)\} \quad . \tag{4.4}$$

In addition, $\mathbf{\Lambda}(z)$ is spectrally majorised such that power spectral densities (PSDs) $\Lambda_m(e^{j\Omega}) = \Lambda_m(z)|_{z=e^{j\Omega}}$ fulfil

$$\Lambda_m(e^{j\Omega}) \geq \Lambda_{m+1}(e^{j\Omega}) \quad \forall\Omega, \quad m = 0 \ldots (M-2) \quad . \tag{4.5}$$

In (4.5), the PSDs are ordered in descending fashion, similar to the ranking of the eigenvalues in an ordered EVD. The matrix $\mathbf{Q}(z)$ is a paraunitary polynomial matrix as illustrated in (4.2).

So far, no algorithms exist to compute the factorisation of a parahermitian polynomial matrix $\mathbf{R}(z)$ as illustrated in (4.3). Hence the PEVD exists in approximation only, i.e., $\mathbf{R}(z) \approx \mathbf{Q}(z)\mathbf{\Lambda}(z)\tilde{\mathbf{Q}}(z)$, and can be calculated using iterative methods.

4.2.1.3 Iterative PEVD algorithms

In order to achieve the decomposition according to (4.3) currently two main families of algorithms exist: SBR2 and SMD. Below, we will detail SBR2 [27] and the MSME-SMD [29] as a member of the SMD family [28].

Second Order Sequential Best Rotation Algorithm. The SBR2 algorithm is an extension of the classical Jacobi algorithm [86] to parahermitian matrices [27]. At each step SBR2 finds the maximum off-diagonal element in the parahermitian matrix and transfers its energy onto the diagonal using an elementary paraunitary transformation. The paraunitary transformation includes two operations: first the maximum element is brought onto the zero lag $\mathbf{R}[0]$ with a delay matrix, next the energy of this maximum element is transferred to the diagonal using a Jacobi rotation.

With $\mathbf{S}^{(0)}(z) = \mathbf{R}(z)$, the ith iteration begins by finding the maximum off-diagonal element of $\mathbf{S}^{(i-1)}(z)$. This maximum is found by inspecting a set of modified column vectors $\hat{\mathrm{s}}_k^{(i)}[\tau] \in \mathbb{C}^{M-1}$, that contain all elements of the kth column of $\mathbf{S}^{(i-1)}[\tau]$ excluding the element on the diagonal. The lag, $\tau^{(i)}$, and column index, $k^{(i)}$, of the maximum off-diagonal element are found using

$$\{k^{(i)}, \tau^{(i)}\} = \arg\max_{k,\tau} \|\hat{\mathrm{s}}_k^{(i-1)}[\tau]\|_\infty \quad . \tag{4.6}$$

Based on $\tau^{(i)}$ and $k^{(i)}$ the maximum element is then delayed onto the zero lag using

$$\mathbf{S}^{(i)\prime}(z) = \tilde{\mathbf{\Lambda}}^{(i)}(z)\mathbf{S}^{(i-1)}(z)\mathbf{\Lambda}^{(i)}(z) \;, \quad i = 1 \ldots I \;, \tag{4.7}$$

where

$$\mathbf{\Lambda}^{(i)} = \mathrm{diag}\{\underbrace{1 \;\ldots\; 1}_{k^{(i)}-1} \; z^{-\tau^{(i)}} \; \underbrace{1 \;\ldots\; 1}_{M-k^{(i)}}\} \quad , \tag{4.8}$$

modifies the $k^{(i)}$th column of $\mathbf{S}^{(i-1)}(z)$, shifting it by $\tau^{(i)}$ samples. The matrix

$\tilde{\mathbf{\Lambda}}^{(i)}$ brings the corresponding $k^{(i)}$th row onto the zero lag by shifting it by $-\tau^{(i)}$ in the opposite direction.

A Jacobi rotation is then used to eliminate the maximum off-diagonal element. The unitary matrix $\mathbf{Q}^{(i)}$ is used to apply the Jacobi rotation,

$$\mathbf{S}^{(i)}(z) = \mathbf{Q}^{(i)\mathrm{H}}\mathbf{S}^{(i)\prime}(z)\mathbf{Q}^{(i)} \quad . \tag{4.9}$$

The Jacobi rotation affects only two rows and columns of the parahermitian matrix $\mathbf{S}^{(i)\prime}(z)$ based on the column and row indices obtained from the maximum off-diagonal element search, (4.6). The energy of the maximum element found using (4.6) is transferred onto the diagonal with the majority of the energy going to the element which is higher on the diagonal. Even though it does not guarantee it, this encourage spectral majorisation.

Convergence of the SBR2 algorithm has been proven in [27], as the paraunitary operations do not affect the overall energy in the parahermitian matrix and at each iteration more energy is transferred to the diagonal. The SBR2 algorithm continues until either a set number of iterations have passed or the maximum off-diagonal element falls below a pre-defined threshold. The delay and rotation matrices can be combined into a single paraunitary matrix,

$$\mathbf{Q}(z) = \prod_{i=1}^{I} \mathbf{Q}^{(i)}\mathbf{\Lambda}^{(i)}(z) \quad , \tag{4.10}$$

which performs the decomposition computed by SBR2.

Multiple Shift Maximum Element Sequential Matrix Diagonalisation. MSME-SMD algorithm [29] has two major differences compared to the SBR2 method. First, rather than using a simple Jacobi rotation to transfer energy from a single element on the zero lag, as is used in SBR2**,** MSME-SMD performs a

full EVD of the zero lag which clears the energy from all elements in the zero lag matrix $\mathbf{S}^{(i)}[0]$ at each iteration. Also where SBR2 brings a single maximum onto the zero lag during each iteration MSME-SMD uses a set of reduced search spaces to bring a total of $(M-1)$ maxima onto the zero lag at each iteration.

In addition to the two major differences mentioned above, the MSME-SMD algorithm also has an initialisation EVD step which ensures that all instantaneous correlations in the parahermitian matrix are removed,

$$\mathbf{S}^{(0)}[0] = \mathbf{Q}^{(0)\mathrm{H}}\mathbf{R}[0]\mathbf{Q}^{(0)} \quad , \tag{4.11}$$

where $\mathbf{S}^{(0)}[0]$ is diagonal and the model matrix obtained by its EVD, $\mathbf{Q}^{(0)}$, is applied to all lags of the parahermitian matrix such that $\mathbf{S}^{(0)}(z) = \mathbf{Q}^{(0)\mathrm{H}}\mathbf{R}(z)\mathbf{Q}^{(0)}$.

The ith iteration of the MSME-SMD algorithm starts the same way as that of SBR2, using (4.6) to find the maximum element in the parahermitian matrix $\mathbf{S}^{(i-1)}(z)$. Rather than immediately shifting the energy onto the diagonal as in SBR2, MSME-SMD continues to bring energy onto the zero lag by shifting multiple (locally) maximum elements. Due to the parahermitian nature of the polynomial matrix, maximum elements occur in complex conjugate pairs, which are translated onto the zero lag. Once the first maximum element pair has been brought onto the zero lag the rows and columns are permuted so that the maximum pair appears in the upper left 2×2 sub-matrix as shown in Fig. 4.1(a). Next the search space in Fig. 4.1(b) is used to find the second maximum within a reduced search space, which when brought onto the zero lag will not affect the first maximum in the upper left corner. The second maximum pair is then permuted such that it appears in the upper left 3×3 sub-matrix. The process is repeated for the third and fourth maxima using the search spaces shown in Fig. 4.1(c) and (d).

The reduced search spaces shown in Fig. 4.1 are used to guarantee that a total

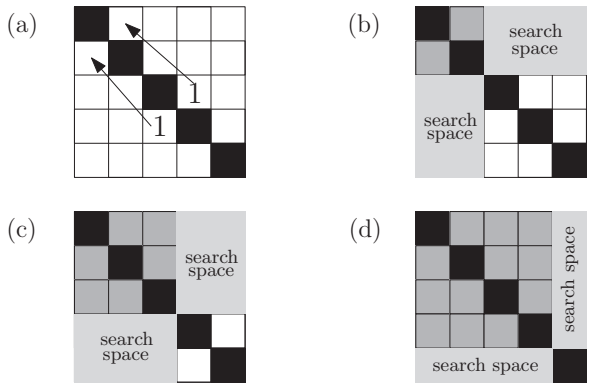

Figure 4.1: View of a 5×5 parahermitian matrix during the ith iteration, not showing the lag dimension: starting from the top 2×2 matrix containing the maximum off-diagonal element in (a), (b) shows an example of an element resistant to permutations, the third and fourth stages of the set of reduced search space strategy are shown in (c) and (d) [29].

of $(M-1)$ maxima are brought onto the zero lag at each iteration. In contrast, if we simply ignored the rows and columns in which previous maxima appear, we can only guarantee a total of $(M/2)$ maxima to be brought onto the zero lag. In MSME-SMD the delay matrix $\mathbf{\Lambda}^{(i)}$ combines the delay and permutation operations,

$$\mathbf{\Lambda}^{(i)} = \text{diag}\{1 \;\; z^{-\tau^{(i,1)}} \;\; \ldots \;\; z^{-\tau^{(i,M-1)}}\} \, \mathbf{P}^{(i)} \quad , \tag{4.12}$$

where the $\mathbf{P}^{(i)}$ combines the permutations used to send the maximum elements unto the upper left corner. The lag values used to find the maximum elements $\tau^{(i,m)}$, $m = 1 \ldots (M-1)$ form the delays for each column in (4.12).

The next step in the ith iteration of MSME-SMD is to diagonalise the zero lag matrix, $\mathbf{S}^{(i)\prime}[0]$, according to (4.7). In this case $\mathbf{Q}^{(i)}$ is the modal matrix of an EVD instead of the simple Jacobi rotation used in SBR2.

To finish an iteration of the MSME-SMD algorithm, the zero lag is ordered based on the diagonal entries to encourage spectral majorisation. The stopping criterion for MSME-SMD is either reached after a fixed number of iterations or when the maximum off-diagonal element falls below a given threshold, similar to

SBR2. The convergence of the MSME-SMD algorithm is given in [29] along with a more in-depth description of the algorithm and its performance with respect to other iterative PEVD algorithms.

Compared to SBR2 the major advantage of the MSME-SMD algorithm is the ability to diagonalise the parahermitian matrix in fewer iterations. In addition the MSME-SMD algorithm can achieve levels of diagonalisation that cannot be achieved using the SBR2 algorithm [87]. The main drawback of the MSME-SMD algorithm compared to SBR2 is extra computational cost of both the multiple element search and the application of the EVD modal matrix, $\mathbf{Q}^{(i)}$, to all lags.

4.2.1.4 Numerical Example

This section will demonstrate the operation of the SBR2 algorithm by a simple numerical example. The SBR2 algorithm is applied to a parahermitian matrix

$$\mathbf{R}(z) = \begin{bmatrix} 1 & -0.2z + 0.3z^2 & -0.2z^{-1} + 0.7z & 0.4z^{-1} \\ 0.3z^{-2} - 0.2z^{-1} & 1 & -0.5z^{-1} & 0.4z \\ 0.7z^{-1} - 0.2z & -0.5z & 1 & 0.3z^{-1} - 0.2z^2 \\ 0.4z & 0.4z^{-1} & -0.2z^{-2} + 0.3z & 1 \end{bmatrix},$$

where the largest off-diagonal element is $\xi_0 = 0.7$. After 50 iterations of SBR2, the largest off-diagonal value is now $\xi_{50} = 0.0328$. The polynomial matrices obtained through this decomposition, $\mathbf{Q}(z)$ and$\mathbf{\Lambda}(z)$, are shown in Figs. 4.2 and 4.3 respectively. Fig. 4.2 shows the paraunitary matrix $\mathbf{Q}(z)$ that diagonalises $\mathbf{R}(z)$.

From Fig. 4.3 it is clear that SBR2 has approximately diagonalised the parahermitian matrix $\mathbf{R}(z)$, which indicates that a strong decorrelation can be achieved

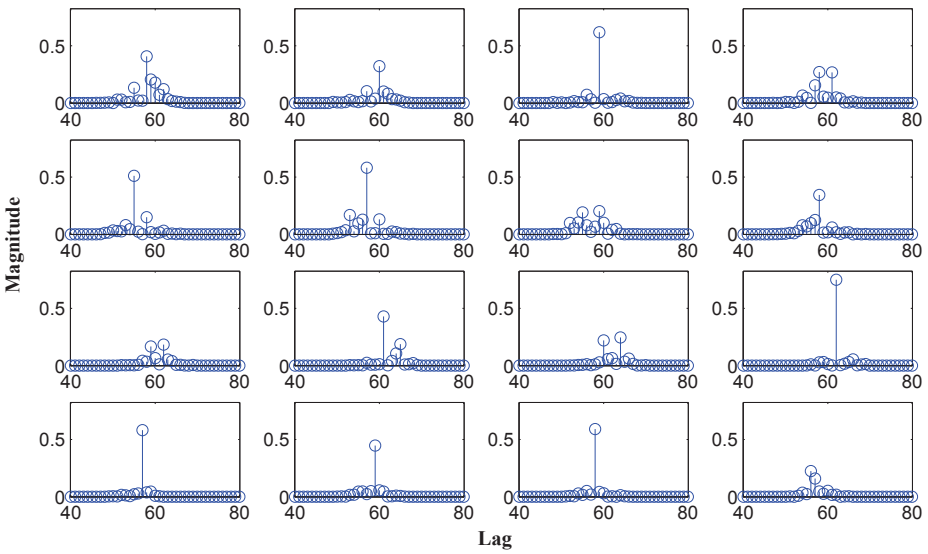

Figure 4.2: Paraunitary matrix $\mathbf{Q}(z)$ obtained from SBR2.

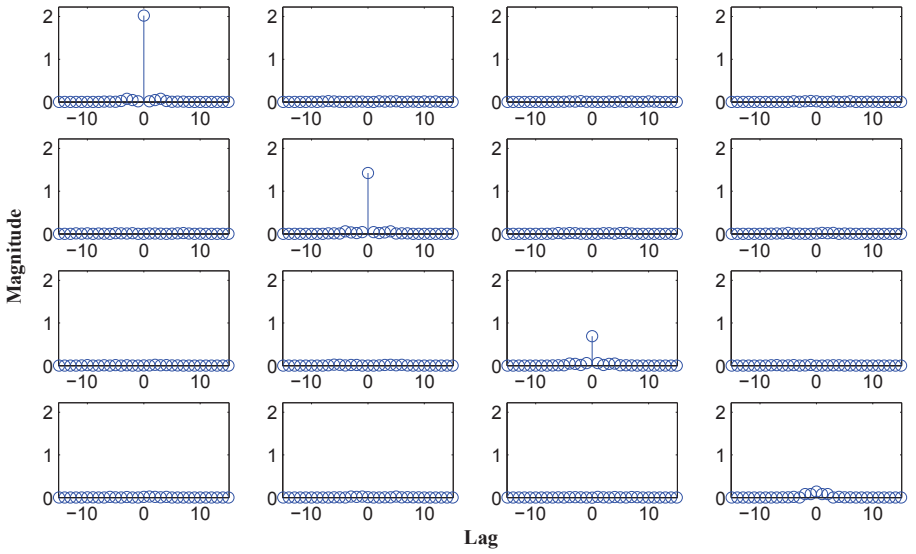

Figure 4.3: Diagonalised polynomial matrix $\mathbf{\Lambda}(z)$ obtained from SBR2.

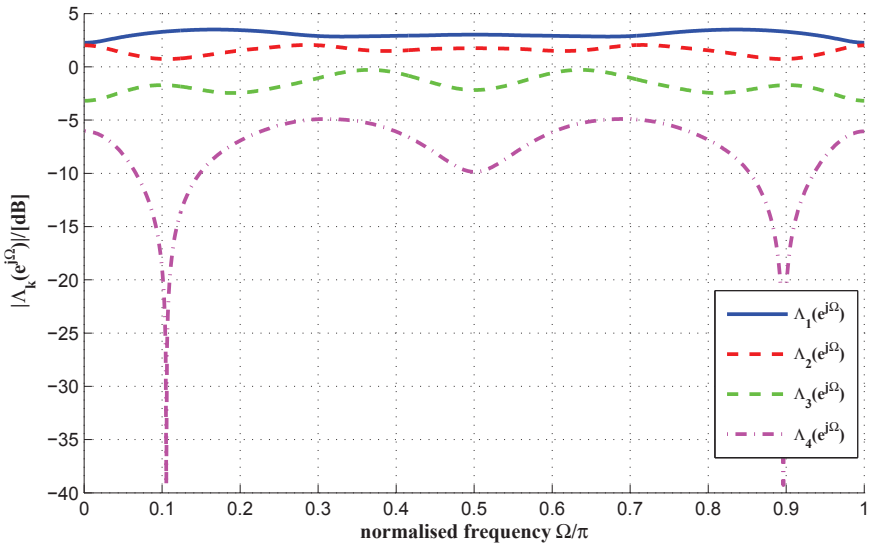

Figure 4.4: PSDs along the diagonal of $\mathbf{\Lambda}(z)$.

through the use of the SBR2 algorithm for parahermitian matrices. In addition, the SBR2 algorithm aims to achieve spectral majorisation by ordering the polynomial eigenvalues in descending fashion. The effect of the spectral majorisation is depicted in Fig. 4.4, which shows the power spectral densities along the diagonalised CSD matrix $\mathbf{\Lambda}(z)$. From Fig. 4.4, it can be seen that spectral majorisation has been achieved.

4.3 Proposed Polynomial MUSIC Algorithm

Based on the previous discussion of MUSIC, we propose to estimate the broadband AoAs using the same idea of a high resolution subspace based method. As a generalisation of narrowband MUSIC, this section will introduce the proposed polynomial MUSIC algorithm [34] for broadband AoA problems. The system model for the proposed method is illustrated in Fig. 4.5. In this technique, we

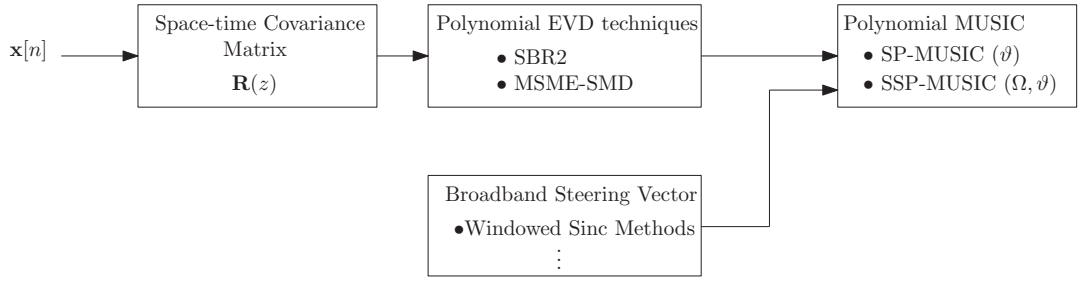

Figure 4.5: System model of the proposed polynomial MUSIC algorithm.

utilise a polynomial form of the space-time covariance matrix in combination with PEVD algorithms discussed in [23, 25] to determine its noise-only and signal-plus-noise polynomial subspaces. Thereafter, similar to narrowband MUSIC, the polynomial noise-only subspace is scanned by a broadband steering vector which has been presented in Chapter 3. The proposed algorithm as depicted in Fig. 4.5 will be described in detail below.

In Sec. 4.3.1, the definition of the space-time covariance matrix of the received sensor outputs is presented. SBR2 and MSME-SMD algorithms are used to calculate an approximate PEVD in order to identify polynomial noise-only subspace. A broadband steering vector is defined in Sec 4.3.2, which is required to emulate the time delay for broadband array signal processing. Sec 4.3.3 details the proposed polynomial MUSIC algorithms.

4.3.1 Space-Time Covariance Matrix and Polynomial EVD

An M-element array of omnidirectional sensors located at positions $\mathbf{r}_m, m = 1...M$ collects K broadband signals that contribute to a data vector $\mathbf{x}[n] \in \mathbb{C}^M$, in

addition to isotropic white noise $\mathbf{v}[n]$,

$$\mathbf{x}[n] = \sum_{k=1}^{K} \mathbf{a}_k[n] * s_k[n] + \mathbf{v}[n] \quad , \tag{4.13}$$

where $s_k[n]$ is the kth source signal, $\mathbf{a}_k[n]$ the corresponding broadband steering vector, and $*$ the convolution operator. The space-time covariance matrix of the data vector $\mathbf{x}[n]$ can be calculated as

$$\mathbf{R}[\tau] = \mathcal{E}\left\{\mathbf{x}[n]\mathbf{x}^{\mathrm{H}}[n-\tau]\right\} \quad , \tag{4.14}$$

where $\mathcal{E}\{\cdot\}$ denotes expectations and $\{\cdot\}^{\mathrm{H}}$ is the Hermitian transpose operator, and includes a time delay in form of the lag value τ. Its z transform $\mathbf{R}(z) \bullet\!\!-\!\!\circ \mathbf{R}[\tau]$,

$$\mathbf{R}(z) = \sum_{\tau} \mathbf{R}[\tau]\, z^{-\tau} \quad , \tag{4.15}$$

is the cross spectral density (CSD) matrix, which is parahermitian, i.e. $\mathbf{R}(z) = \tilde{\mathbf{R}}(z) = \mathbf{R}^{\mathrm{H}}(z^{-1})$. In practise, this polynomial space time covariance matrix $\mathbf{R}[\tau]$ needs to be estimated over a data window of N samples, and for a finite length of lag values L as well, and can therefore be calculated as.

$$\mathbf{R}(z) = \sum_{\tau=-L}^{L} \mathbf{R}[\tau]\, z^{-\tau} \quad , \tag{4.16}$$

where

$$\mathbf{R}[\tau] = \sum_{n=0}^{N-1} \frac{\mathbf{x}[n]\mathbf{x}^{\mathrm{H}}[n-\tau]}{N} \quad . \tag{4.17}$$

The CSD matrix can be factorised into a PEVD [23, 25],

$$\mathbf{R}(z) \approx \mathbf{Q}(z)\mathbf{\Lambda}(z)\tilde{\mathbf{Q}}(z) \quad , \tag{4.18}$$

whereby $\mathbf{Q}(z)$ is a paraunitary matrix and $\mathbf{\Lambda}(z) \in \mathbb{C}^{M\times M}(z)$ is an approximately diagonal matrix such that

$$\mathbf{\Lambda}(z) = \mathrm{diag}\{\Lambda_0(z)\ \Lambda_1(z)\ \ldots\ \Lambda_{M-1}(z)\} \quad , \tag{4.19}$$

which contains the polynomial eigenvalues $\Lambda_m(z)$. These are spectrally majorised such that the power spectral densities (PSDs) $\Lambda_m(e^{j\Omega}) = \Lambda_m(z)|_{z=e^{j\Omega}}$ fulfil

$$\Lambda_{m+1}(e^{j\Omega}) \geq \Lambda_m(e^{j\Omega}) \quad \forall\Omega, \quad m = 0\ldots(M-2) \quad . \tag{4.20}$$

The approximation in (4.18) holds for a sufficiently high order of an FIR $\mathbf{Q}(z)$ [61]. Thresholding the polynomial eigenvalues $\Lambda_m(z)$ reveals the number of independent broadband sources, K, contributing to $\mathbf{R}(z)$, and permits a distinction between signal-plus-noise and noise only subspaces, such that

$$\mathbf{R}(z) = \begin{bmatrix} \mathbf{Q}_s(z) & \mathbf{Q}_n(z) \end{bmatrix} \begin{bmatrix} \mathbf{\Lambda}_s(z) & \mathbf{0} \\ \mathbf{0} & \mathbf{\Lambda}_n(z) \end{bmatrix} \begin{bmatrix} \tilde{\mathbf{Q}}_s(z) \\ \tilde{\mathbf{Q}}_n(z) \end{bmatrix} \quad , \tag{4.21}$$

where $\mathbf{Q}_s(z) \in \mathbb{C}^{M\times K}$ holds the first K columns of the paraunitary matrix $\mathbf{Q}(z)$ which define the broadband (polynomial) signal-plus-noise subspace. The remaining $M-K$ columns of $\mathbf{Q}(z)$ contained in $\mathbf{Q}_n(z) \in \mathbb{C}^{M\times(M-K)}$ form a basis for the null space, and is also referred to as the polynomial noise-only subspace. Similar to narrowband MUSIC, the proposed P-MUSIC probes the noise-only subspace spanned by the columns of $\mathbf{Q}_n(z)$,

$$\mathbf{Q}_n(z) = \begin{bmatrix} \mathbf{q}_K(z) & \ldots & \mathbf{q}_{M-1}(z) \end{bmatrix} \quad , \tag{4.22}$$

The probing requires the definition and implementation of the broadband steering vector which will be briefly revisited in the next section.

4.3.2 Broadband Steering Vector (BSV)

Based on the definition of the broadband steering vector outlined in Chapter 3, here, in order to accurately reflect the time delays required to describe the received broadband sensor array data, a polynomial vector containing fractional delay transfer functions is required [34]. One possibility to implement these fractional delays is by means of an appropriately sampled sinc function, such that

$$a_l[n] = \mathrm{sinc}(nT_s - \Delta\tau_l) \quad . \tag{4.23}$$

With $A_l(z) \bullet\!\!-\!\!\circ a_l[n]$, a broadband steering vector in the z-domain can be defined as

$$\mathbf{a}_\vartheta(z) = \begin{bmatrix} A_0(z) \\ \vdots \\ A_{M-1}(z) \end{bmatrix} \quad . \tag{4.24}$$

The parameter ϑ on the l.h.s. of (4.24) indicates the dependency of $\Delta\tau_i$ on the angle of arrivals of the sources. For the implementation of fractional delays in (4.23), a truncation has to be introduced, leading to an approximation error. More accurate implementations for the broadband steering vector than a truncated sinc function have been discussed previously in Secs. 3.2 and 3.3.

4.3.3 Polynomial MUSIC

Similar to the narrowband MUSIC as described in Chapter 2, the null (polynomial noise-only) space in (4.22) is scanned by broadband steering vectors in (4.24) and leading to the generalised quantity

$$\mathbf{\Gamma}_\vartheta(z) = \tilde{\mathbf{a}}_\vartheta(z)\mathbf{Q}_n(z)\tilde{\mathbf{Q}}_n(z)\mathbf{a}_\vartheta(z) \quad . \tag{4.25}$$

This is no longer a norm measuring the vicinity of a broadband steering vector $\mathbf{a}_\vartheta(z)$ to the null-space of $\tilde{\mathbf{Q}}_n(z)$ as in narrowband MUSIC, but instead will compute a power spectral density (PSD). This motivates two versions of the P-MUSIC algorithm [34], which are presented in the following.

4.3.3.1 Spatial P-MUSIC (SP-MUSIC)

In order to measure the energy contained in the signal vector $\tilde{\mathbf{Q}}(z)\mathbf{a}_\vartheta(z)$, which is related to the zero lag term $\gamma_\vartheta[0]$ of the autocorrelation type sequence $\gamma_\vartheta[\tau] \circ\!\!-\!\!\bullet\, \Gamma_\vartheta(z)$, we integrate the PSD in (4.25) and provide a power term

$$\gamma_\vartheta[0] = \frac{1}{2\pi} \oint \Gamma_\vartheta(z)|_{z=e^{j\Omega}}\, d\Omega \quad . \tag{4.26}$$

This measure only depends on the angle of arrival ϑ, and collects all energy across the spectrum. Instead of explicity searching for the steering vectors that provide minimum energy, the SP-MUSIC spectrum is given by the reciprocal of (4.26)

$$P_{\text{SP-MUSIC}}(\vartheta) = \frac{1}{\gamma_\vartheta[0]} \quad , \tag{4.27}$$

which is maximised by the true angle of arrival ϑ of the signal sources.

4.3.3.2 Spatio-Spectral P-MUSIC (SSP-MUSIC)

With (4.25) describing a PSD, spectral clues can be exploited in addition to the spatial information extracted by (4.27). The spatio-spectral polynomial SSP-MUSIC is based on inverting a PSD-type function, and can be defined as

$$P_{\text{SSP-MUSIC}}(\vartheta, e^{j\Omega}) = \frac{1}{\tilde{\mathbf{a}}_{\varphi,\vartheta}(z)\mathbf{Q}_s^\perp(z)\mathbf{Q}_s^\perp(z)\mathbf{a}_{\varphi,\vartheta}(z)}|_{z=e^{j\Omega}} \quad . \tag{4.28}$$

Therefore in addition to localisation of sources with respect to ϑ , SSP-MUSIC can determine over which frequency range sources in the direction defined by the steering vector $\mathbf{a}_{\vartheta}(z)$ are active.

4.4 Simulation and Results

This section will demonstrate the performance of the two proposed versions of P-MUSIC for AoA estimation defined in (4.27) and (4.28) respectively. First, some controlled scenarios with numerical examples are presented to highlight the ability for spatial discrimination of the spatial SP-MUSIC for both a single source and multiple sources scenarios. Thereafter, a more complex scenario is tested for the spatio-spectral SSP-MUSIC algorithm and benchmarked against the independent frequency bin (IFB-MUSIC) algorithm that was described in Chapter 2.

4.4.1 Simple Angle of Arrival Estimation Scenario

For simplicity, we will consider a simple problem where a linear array with $M = 4$ uniformly spaced sensors separated by distances $d = c/f_s$ is receiving one or two broadband source(s) in a noise-free environment.

4.4.1.1 Single Source

Case 1. The source of interest impinging onto a sensor array is located at broadside ($\vartheta = 0°$). In this case, the source wavefront will arrive at all sensors at the same time such that $\Delta\tau = 0$. Therefore, the broadband steering vector for this case is given by

$$\mathbf{a}_{\vartheta=0^0} = [1 \quad 1 \quad 1 \quad 1]^{\mathrm{T}} \quad . \tag{4.29}$$

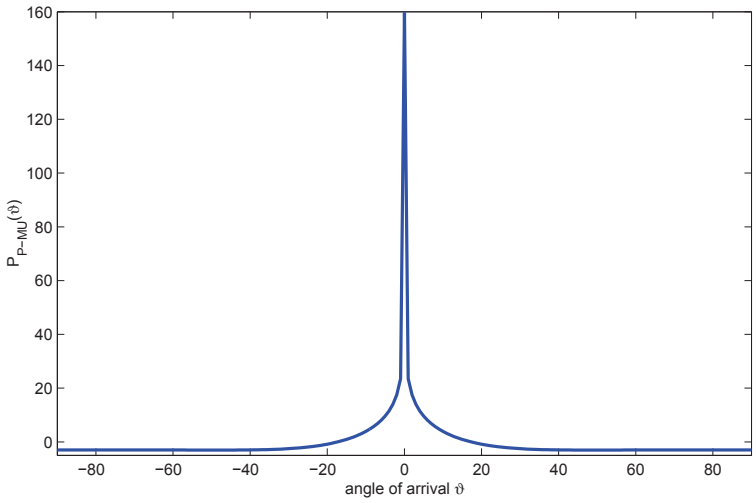

Figure 4.6: SP-MUSIC $P_{\text{SP-MUSIC}}(\vartheta)$ for a source located at broadside ($\vartheta = 0°$).

If the source emits an uncorrelated random signal with zero mean ($\mu = 0$) and unit variance ($\sigma_s^2 = 1$), then the resulting covariance matrix is

$$\mathbf{R}_1(z) = \mathbf{a}_{(\vartheta=0^o)}(z) \cdot \tilde{\mathbf{a}}_{(\vartheta=0^o)}(z) = \begin{bmatrix} 1 & 1 & 1 & 1 \\ 1 & 1 & 1 & 1 \\ 1 & 1 & 1 & 1 \\ 1 & 1 & 1 & 1 \end{bmatrix} . \tag{4.30}$$

This matrix $\mathbf{R}_1(z)$ has rank one, and the SP-MUSIC algorithm is identical to the narrowband MUSIC except for the use of broadband steering vectors in evaluating (4.27). The result in Fig. 4.6 shows that the proposed SP-MUSIC clearly identifies the source angle ($\vartheta = 0°$) with a sharp peak at the exact location.

Case 2. In this situation, the source now is located at the end-fire position ($\vartheta = -90°$), therefore the wavefront arriving at each sensor is delayed by exactly

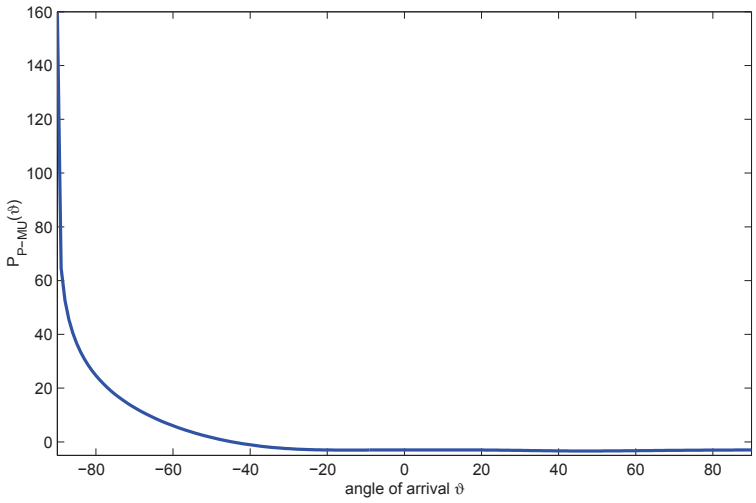

Figure 4.7: SP-MUSIC $P_{\text{SP-MUSIC}}(\vartheta)$ for a source located at end-fire ($\vartheta = -90°$).

one sampling period. The broadband steering vector can be calculated as

$$\mathbf{a}_{\vartheta=-90^o}(z) = \begin{bmatrix} 1 & z^{-1} & z^{-2} & z^{-3} \end{bmatrix}^{\mathrm{T}} \quad . \tag{4.31}$$

As a result, the spatio-temporal covariance matrix for the end-fire position is

$$\mathbf{R}_2(z) = \mathbf{a}_{(\vartheta=-90^o)}(z)\tilde{\mathbf{a}}_{(\vartheta=-90^o)}(z) = \begin{bmatrix} 1 & z^{1} & z^{2} & z^{3} \\ z^{-1} & 1 & z^{1} & z^{2} \\ z^{-2} & z^{-1} & 1 & z^{1} \\ z^{-3} & z^{-2} & z^{-1} & 1 \end{bmatrix} \quad . \tag{4.32}$$

The result for the spatial P-MUSIC algorithm is depicted in Fig. 4.7, which correctly identifies the angle of arrival ($\vartheta = -90°$) of the desired source.

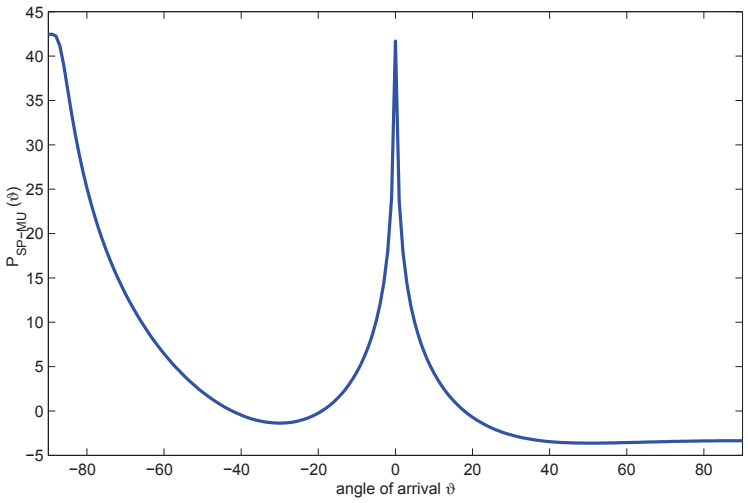

Figure 4.8: SP-MUSIC $P_{\text{SP-MUSIC}}(\vartheta)$ for a scenario with two independent sources of equal strength located at broadside and end-fire positions.

4.4.1.2 Multiple Sources

For this situation, we assume that two independent sources, one located at broadside and the other at the end-fire positions, are impinging upon the sensor array, hence the space-time covariance matrix is given by

$$\begin{aligned}\mathbf{R}(z) &= \mathbf{a}_{(\vartheta=0^o)}(z)\tilde{\mathbf{a}}_{(\vartheta=0^o)}(z) + \mathbf{a}_{(\vartheta=-90^o)}(z)\tilde{\mathbf{a}}_{(\vartheta=-90^o)}(z) \\ &= \begin{bmatrix} 2 & 1+z^1 & 1+z^2 & 1+z^3 \\ 1+z^{-1} & 2 & 1+z^1 & 1+z^2 \\ 1+z^{-2} & 1+z^{-1} & 2 & 1+z^1 \\ 1+z^{-3} & 1+z^{-2} & 1+z^{-1} & 2 \end{bmatrix} . \end{aligned} \tag{4.33}$$

The proposed spatial P-MUSIC algorithm identifies two large polynomial eigenvalues, and from the noise-only subspace, the spatial P-MUSIC algorithm derives the result in Fig. 4.8. It can be seen from the figure that the proposed SP-MUSIC can accurately identify the angles of arrival of both sources.

Number of sensors M	8
Number of broadband sources K	2
AoAs	$\vartheta_1 = 30°$,$\vartheta_2 = -20°$
Sources frequency ranges	$\Omega_1 \in [0.3125\pi, 0.7182\pi]$ $\Omega_2 \in [0.4688\pi, 0.9375\pi]$

Table 4.1: The specification of the simulation.

4.4.2 Spatio-Spectral Estimation

For a more realistic scenario, we consider an $M = 8$ element array illuminated by two uncorrelated broadband sources, with the characteristic as indicated in Table 4.1. The array signals are corrupted by uncorrelated independent and identically distributed complex Gaussian noise at SNR of 20dB. The source signals are simulated as a series of complex exponentials of different frequencies Ω_i with randomised phases. The delay with which the waveform propagates across the array is implemented in the frequency domain by separately implementing the steering vector as defined in Chapter 2 for every complex harmonic. The number of samples used to estimate the space time covariance matrix is chosen to be 64000, with the range of lags set to $|\tau| \leq 20$. Two different scenarios are considered, which are highlighted below.

Scenario 1. The exact frequency locations of the source components coincide with the bin frequencies of an independent frequency bin processor, i.e, at integer multiples of $\Omega = 2\pi/L$, where $L = 64$ is the number of frequency bins. For the DFT-based independent bin processing methods provides the inputs to independent MUSIC algorithms operating in every frequency bin. Results depicted in Fig. 4.9 indicate that the IFB provides very accurate retrieval of both sources in terms of angle of arrival as well as their spectral range.

Scenario 2. In this case, the source frequencies are located at frequencies which are not bin frequencies in the DFT. The IFB here is used to benchmark the

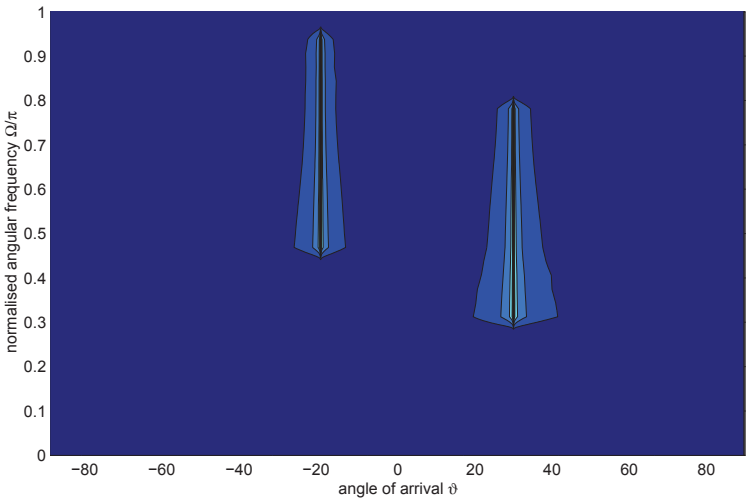

Figure 4.9: Narrowband MUSIC applied to independent frequency bins, for an $M = 8$ element array and bin frequencies coinciding with those of the sources.

proposed SSP-MUSIC method. The IFB approach is known to yield a very poor worst-case performance [88]. As can be seen in Fig. 4.10, the result exhibits a large number of spurious components in the lower frequency range. In addition the IFB approach is not able to extract the source at $\vartheta = 30°$ as well as in scenario 1.

The proposed spatio-spectral P-MUSIC algorithm (**??**) is applied to the same data as the IFB processor in Fig. 4.10. The estimated polynomial covariance matrix $\mathbf{R}(z)$ from this data is illustrated in Fig. 4.11, from which the SBR2 algorithm generates a paraunitary matrix $\mathbf{Q}(z)$ and a diagonal polynomial matrix $\mathbf{\Lambda}(z)$ as depicted in Fig. 4.12 and Fig. 4.13, respectively.

The result in Fig. 4.13 shows that $\mathbf{R}(z)$ is approximately diagonalised, while the output signal power is concentrated in the first and the second elements of the polynomial diagonal matrix $\mathbf{\Lambda}(z)$ which allows to identify the polynomial noise only subspace $\mathbf{Q}_n(z)$ contained in the paraunitary matrix $\mathbf{Q}(z)$ as depicted in Fig. 4.12. Fig. 4.14, shows the PSDs along the diagonalised CSD matrix $\mathbf{\Lambda}(z)$ in Fig. 4.13. It can be seen from Fig. 4.14, that spectral majorisation has been achieved and that the polynomial signal subspace is defined by the first two

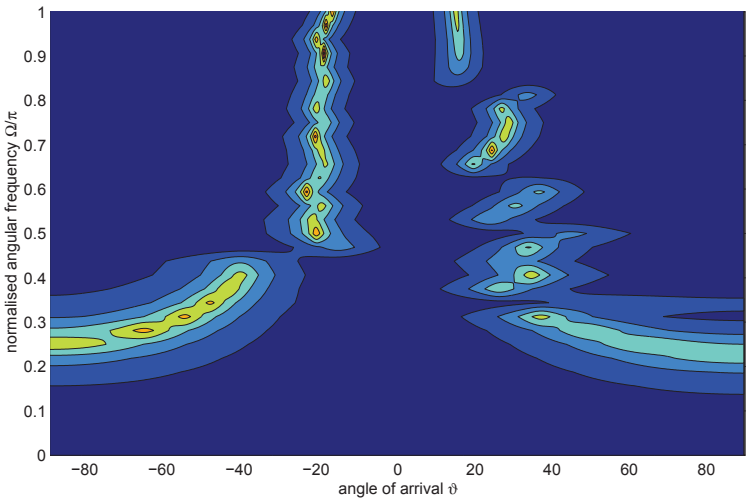

Figure 4.10: Narrowband MUSIC applied to independent frequency bins, for an $M = 8$ element array and bin frequencies not coinciding with those of the sources.

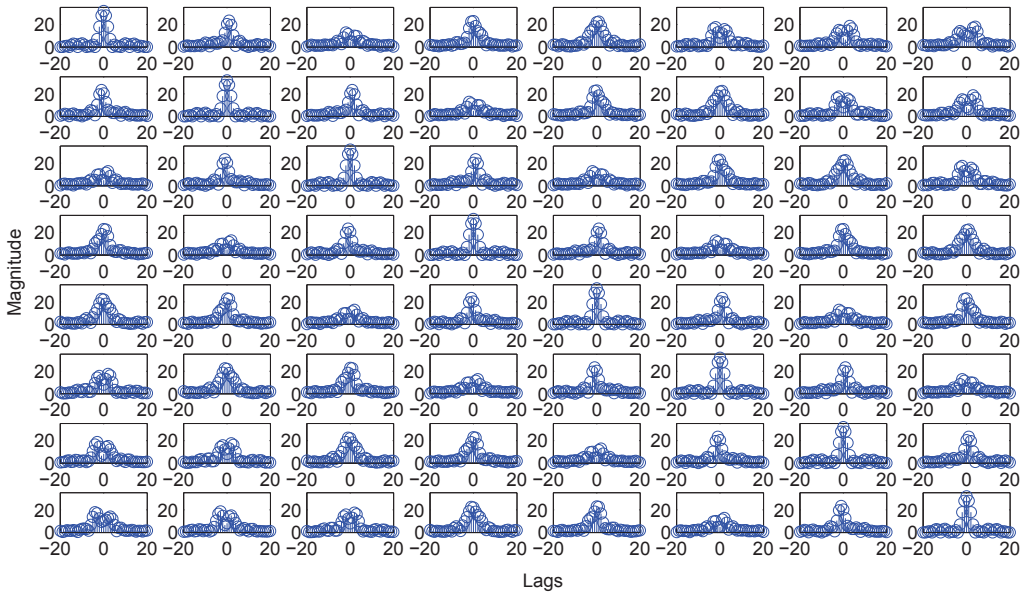

Figure 4.11: Estimated polynomial covariance matrix $\mathbf{R}(z)$.

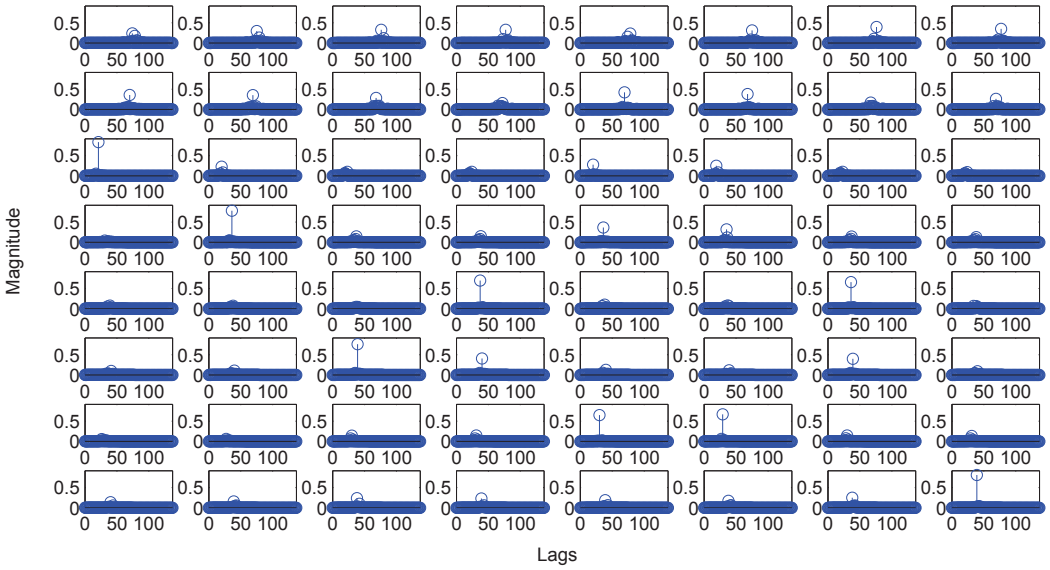

Figure 4.12: A paraunitary matrix $\mathbf{Q}(z)$ obtained when the SBR2 is applied to $\mathbf{R}(z)$ shown in Fig. 4.11.

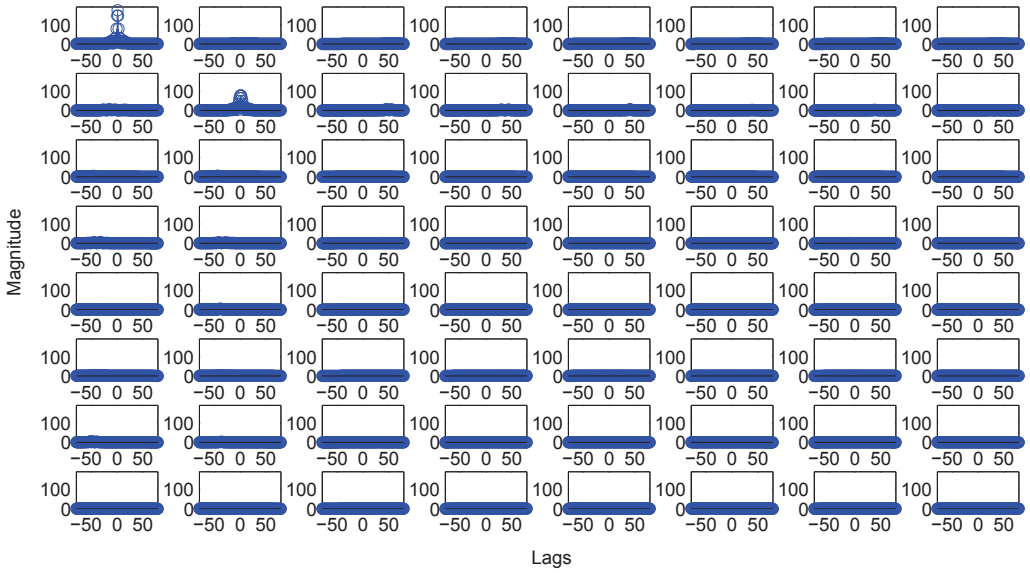

Figure 4.13: The diagonal polynomial matrix $\mathbf{\Lambda}(z)$ produced by applying the SBR2 algorithm to the polynomial space-time covariance matrix $\mathbf{R}(z)$ demonstrated in Fig. 4.11.

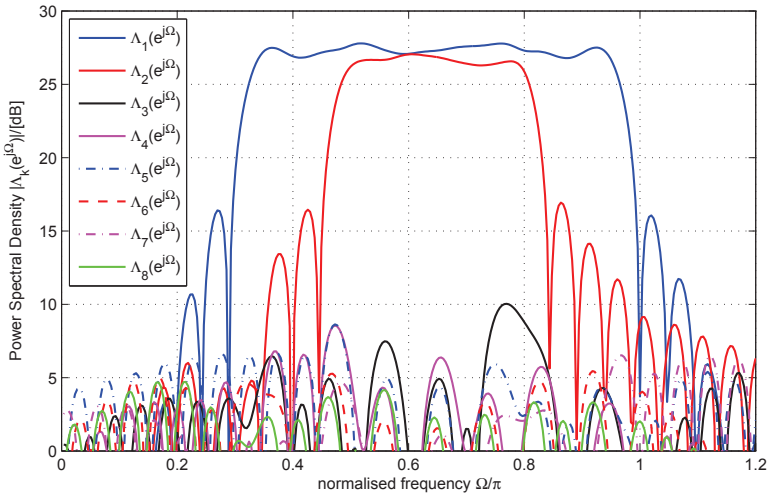

Figure 4.14: Power spectral densities of diagonal elements of $\mathbf{\Lambda}(z)$ demonstrating spectral majorisation.

polynomial eigenvalues $\Lambda_1(\mathrm{e}^{j\Omega}), \Lambda_2(\mathrm{e}^{j\Omega})$ which have the highest spectra, while the noise only subspace is identified by the polynomial eigenvalues with the lowest spectra i.e., $\Lambda_3(\mathrm{e}^{j\Omega}), \ldots, \Lambda_8(\mathrm{e}^{j\Omega})$. As a result the broadband (polynomial) subspaces have been identified.

With broadband steering vectors computed according to (4.24), the results of the proposed spatio-spectral P-MUSIC approach (**??**) is shown in Fig. 4.15. Different from Fig. 4.10, SSP-MUSIC allows to accurately extract both angles of arrival and the frequency ranges of the two contained broadband sources, the resolution is not as sharp as the IFB processor with coinciding frequency bins as in Fig. 4.9 (scenario 1). This is due to the constructed nature of the IFB setup, as well as the fact that the fractional delay filters implementing the time delays associated with different angles ϑ are not accurate across the entire frequency range [43]. Also the accuracy of the polynomial matrix decomposition algorithms leading to the identification of the polynomial noise-only subspace [37] is limited. However, it is important to note that while the IFB processor is extremely sensitive to the location of the sinusoidal components, the proposed SSP-MUSIC

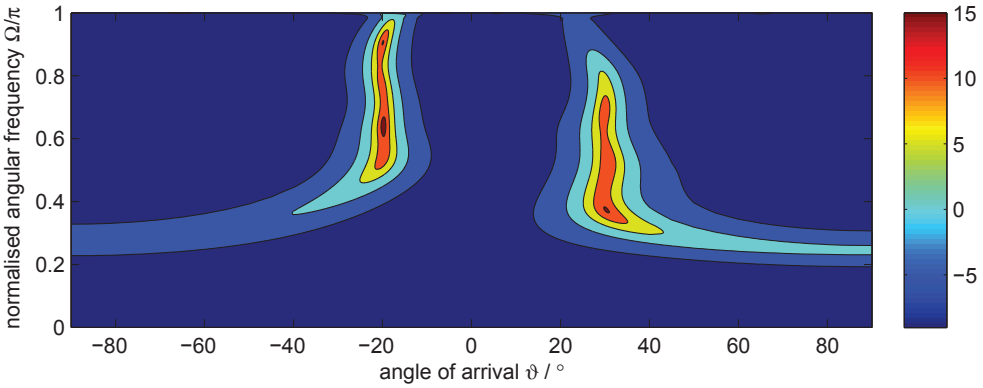

Figure 4.15: Performance of Spatio-Spectral SSP-MUSIC.

algorithm has been found very robust.

4.5 Sensitivity Analysis

In this section, we present simulation results to demonstrate the impact of the accuracy of both the broadband steering vector (BSV) implementation techniques as discussed in Chapter 3 as well as the PEVD techniques on the performance of the proposed P-MUSIC algorithms. In Sec. 4.5.1, we compare the performance of the SP-MUSIC algorithm based on four different BSV implementation methods such as a windowed sinc function (rectangular and Hann) windows, the Farrow structure with polynomial order 9 and a novel proposed method based on the filter bank approach [36]. In Sec.4.5.2, two polynomial matrix decomposition approaches are applied to diagonalise the space-time covariance matrix of the array broadband signals. Iterative PEVD approaches based on both the SBR2 and the recently proposed MSME-SMD algorithms are shown with impact on the accuracy for both versions of the P-MUSIC algorithm.

4.5.1 Performance of P-MUSIC Based on the Broadband Steering Vector Implementation

In the following simulations, the impact of the broadband steering vector implementations on the performance of the proposed SP-MUSIC algorithm will be analysed. As has been described in Chapter 3, the broadband steering vector can be implemented using various methods based on the required accuracy for different applications. Four different implementation methods for the BSV are included to asses the performance of the SP-MUSIC. The simulation scenario has two broadband sources impinging onto an array with $M = 4$ sensors from broadside, $\vartheta_1 = 0°$, and end-fire, $\vartheta_2 = -90°$. Fig. 4.16 shows the simulation results for the SP-MUSIC algorithm based on various implementation of broadband steering vector. Results as depicted in Fig. 4.16 indicate that the implementation of the broadband steering vector based on the filter bank approach outperforms the other design methods in terms of high resolution of the SP-MUSIC algorithm, i.e. SP-MUSIC provides sharp peaks at both angle of arrivals, while the truncated sinc (rectangular) and Hann windowed with length $N = 100$, implementation methods perform approximately the same and provide slightly higher resolution than the Farrow structure-based implementation with order $P = 9$.

4.5.2 Performance of P-MUSIC Based on Different Iterative PEVD Algorithms

In this section we demonstrate and highlight the accuracy of SSP-MUSIC by exploring the impact of the performance of different iterative PEVD algorithms in [23], [25]. For this set of simulations, two broadband sources are impinging onto a $M = 8$ sensor array antenna from $\vartheta_1 = 20°$ and $\vartheta_2 = -30°$ directions. Further, independent and identically distributed white Gaussian noise is added

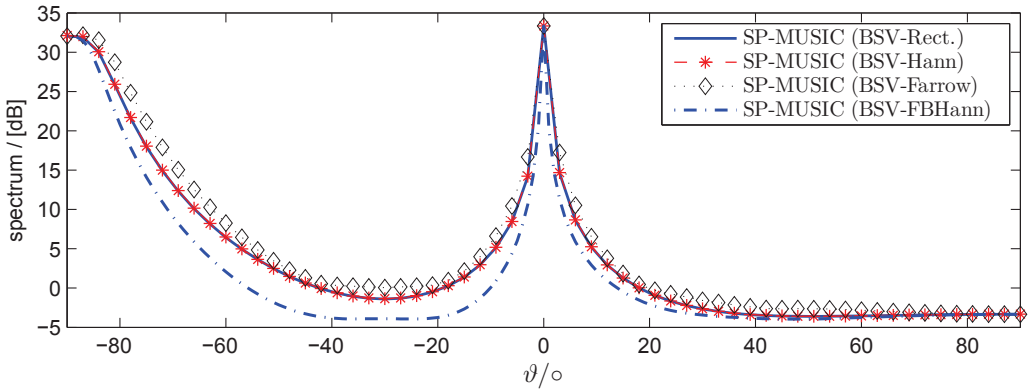

Figure 4.16: Comparison of the performance of SP-MUSIC algorithm for different BSV implementation methods.

to the sensors at an SNR of 20 dB. The two sources are active over the normalised angular frequency range of $\Omega_1 \in [0.3125\pi, 0.7182\pi]$, $\Omega_2 \in [0.4688\pi, 0.9375\pi]$ respectively. To exclude error sources other than inaccuracies in the subspace identification, we have modelled the data as a sum of closely spaced sinusoids with randomised phases, for whom the individual and highly accurate narrowband steering vectors can be used to simulate the data. Two different polynomial matrix decomposition techniques, i.e. SBR2 and MSME-SMD, are used for diagonalising the estimated space-time covariance matrix $\mathbf{R}[\tau]$ of the sensor output data, in order to identify the noise only subspace. In the simulation below, the number of iterations are chosen to be 50 for both algorithms and the energy of the polynomial matrices is calculated using the squared Frobenius norm of a polynomial matrix $\mathbf{A}(z) \in \mathbb{C}^{n\times m}$ [27] defined as

$$||\mathbf{A}(z)||_F^2 = \sum_{\tau}\sum_{n=1}^{N}\sum_{m=1}^{M}|a_{nm}[\tau]|^2 \quad , \tag{4.34}$$

where $a_{nm}[\tau]$ is the element in the nth row and mth column of $A[\tau] \circ\!\!-\!\!\bullet A(z)$.

The space-time covariance matrix $\mathbf{R}(z)$ for this scenario is calculated according to (4.16) whereby the correlation lag value is set to $\tau = 20$. Fig. 4.17 shows the

polynomial covariance matrix $\mathbf{R}(z)$ estimated from the received signals. Thereafter, both the SBR2 and the MSME-SMD algorithms are applied to factorise this matrix according to (4.18). For the SBR2 algorithm, the obtained diagonal matrix $\mathbf{\Lambda}(z)$ can be seen in Fig. 4.18, whereby the order of $\mathbf{\Lambda}(z)$ after 50 iterations is 175. The input estimated polynomial space time covariance matrix $\mathbf{R}(z)$ has a squared Frobenius norm of 1.3078e+05, with 2.7439e+04 positioned in the main diagonal elements. This is approximately 20.98 % of the total energy of the matrix.

Following the application of the SBR2 algorithm, the energy on the off-diagonal elements in $\Lambda(z)$ is decreased to 2.6577e+03, amounting 2.03 % (-16.9204 dB) of the total energy of the matrix. On the other hand, applying MSME-SMD to $\mathbf{R}(z)$, produces a decomposition similar to (4.18). The resulting polynomial diagonal matrix $\mathbf{\Lambda}(z)$ is depicted in Fig. 4.19. The order of $\mathbf{\Lambda}(z)$ in this case is 735, with the squared Frobenius norm of the off-diagonal elements being 429.807 which amounts 0.3286 % (-24.8327 dB) of the total energy of the matrix. Therefore, a higher level of diagonalisation can be achieved via MSME-SMD algorithm compared to the SBR2 algorithm, by transferring more energy onto the main diagonal. Thus a better identification of the signal-plus-noise and the noise-only subspaces is achieved.

The performance of the SSP-MUSIC algorithm based on SBR2 and MSME-SMD approaches is illustrated in Figs. 4.20 and 4.21 respectively. It can be seen that SSP-MUSIC based on MSME-SMD decomposition outperforms the one using SBR2, whereby a cleaner estimate for both angles and frequency of the estimated sources is extracted.

Finally, we study the impact of PEVD approaches on the performance of the spatial P-MUSIC algorithm. Fig. 4.22 compares the performance of the SP-

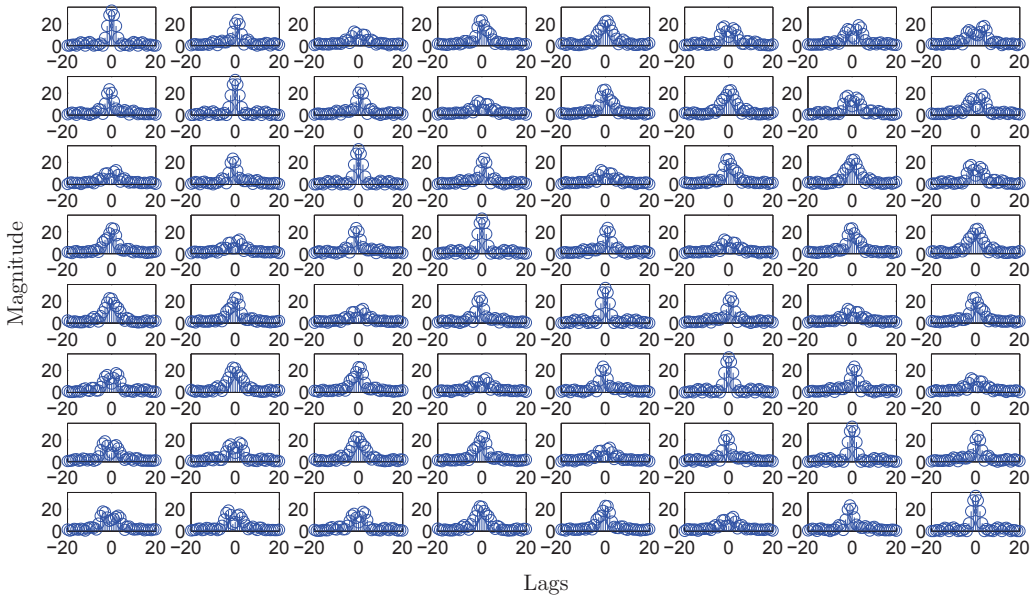

Figure 4.17: The polynomial space-time covariance matrix $\mathbf{R}(z)$.

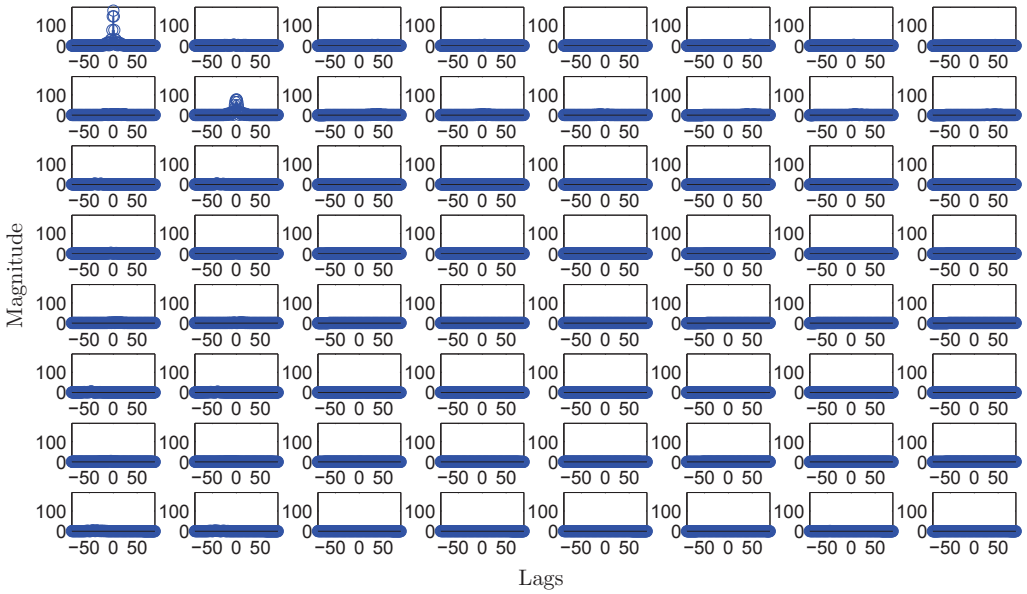

Figure 4.18: The diagonalised polynomial matrix $\Lambda(z)$ obtained when the SBR2 algorithm is applied to the polynomial covariance matrix $\mathbf{R}(z)$ shown in Fig. 4.17.

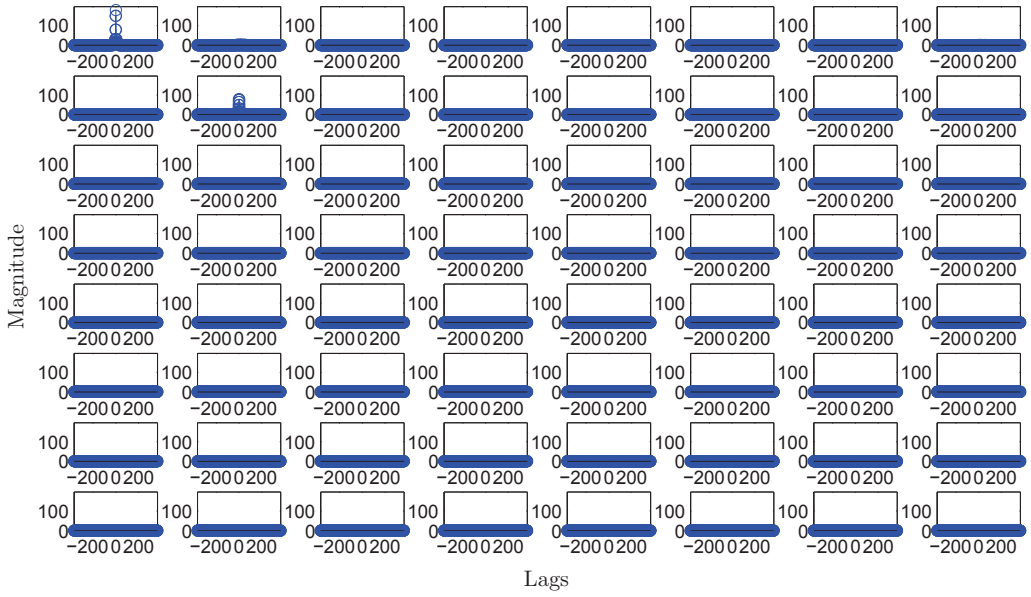

Figure 4.19: The diagonalised polynomial matrix $\Lambda(z)$ obtained when the MSME-SMD algorithm is applied to the polynomial covariance matrix $\mathbf{R}(z)$ depicted in Fig. 4.17.

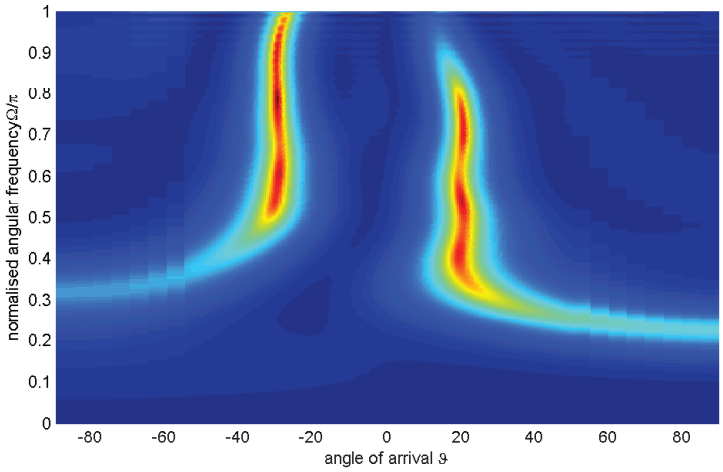

Figure 4.20: Performance of SSP-MUSIC based on SBR2 for PEVD for a scenario with two independent broadband sources located at $\vartheta_1 = 20°$ and $\vartheta_2 = -30°$.

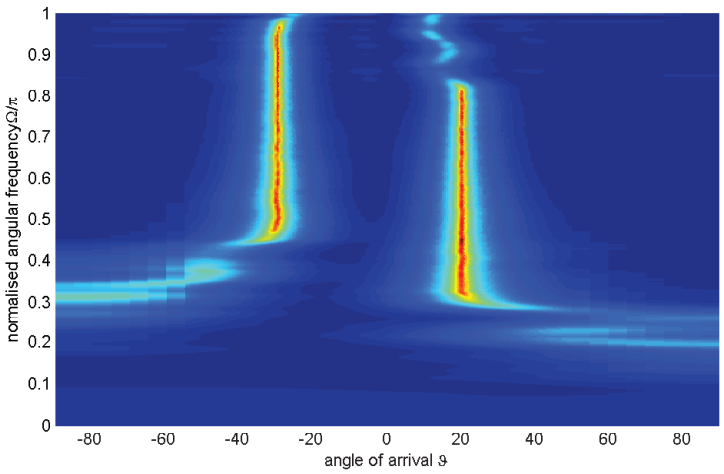

Figure 4.21: Performance of SSP-MUSIC based on MSME-SMD for PEVD for a scenario with two independent broadband sources located at $\vartheta_1 = 20°$ and $\vartheta_2 = -30°$.

MUSIC based on the SBR2 and the MSME-SMD decomposition techniques, where the simulation results are normalised to a spectrum peak value of one. It can be seen that the SP-MUSIC based on the MSME-SMD provides superior resolution than the one using the SBR2 algorithm, which demonstrates that the accuracy of the PEVD is crucial to the performance of any subsequent polynomial subspace based techniques.

4.6 Conclusion

Motivated by the desire for high resolution AoA estimation for broadband signal processing applications, this chapter has proposed a novel algorithm known a polynomial MUSIC (P-MUSIC). The new algorithm is a generalisation of the well-known narrowband MUSIC to broadband AoA problems. The derived P-MUSIC approach offers two variations, either estimating the angle of arrival alone (SP-MUSIC), or providing both spatial and spectral information for the broadband sources that contributing to the space-time covariance matrix (SSP-

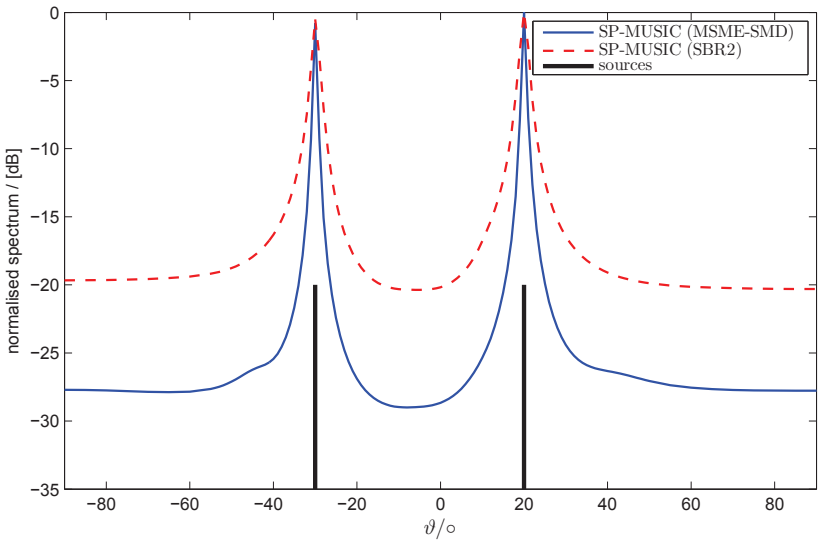

Figure 4.22: Performance of the SP-MUSIC based on the polynomial matrix decomposition techniques,i.e. the SBR2 and the MSME-SMD algorithms for a scenario with two broadband sources located at $\vartheta_1 = 20°$ and $\vartheta_2 = -30°$.

MUSIC). Both versions of P-MUSIC require the identification of the polynomial noise-only subspace from the estimated covariance matrix as well as the definition of a broadband steering vector.

Since the broadband covariance matrix is a polynomial matrix, a recently proposed novel PEVD technique has been applied to diagonalise this polynomial matrix. PEVD algorithms such as SBR2 and MSME-SMD can acheive approximate diagonalisation and allow for the identification and separation of the broadband (polynomial) subspaces, i.e. signal-plus-noise and noise only subspaces.

Simulation results have highlighted the ability of the proposed P-MUSIC algorithms based on SBR2 to accurately estimate the directions and the spectrum clues for broadband sources. Moreover, we have demonstrated that the proposed P-MUSIC outperforms the IFB approach if signal frequencies do not coincide with frequency bins [28], where the latter was found to be very sensitive to the exact location of frequency components within the array data. In contrast, the

proposed P-MUSIC algorithms have shown to be very robust.

Further enhancement in the performance for the proposed algorithm can be achieved by using the recently proposed MSME-SMD algorithm [25], which provides a better diagonalisation compared to SBR2 [23]. The simulation results show that SSP-MUSIC based on the MSME-SMD decomposition outperforms the one using SBR2. Therefore, we have demonstrated that a higher level of diagonalisation leads to a better identification of the relevant signal subspaces, such that the proposed P-MUSIC can extract a more accurate estimate w.r.t. both angles and frequency of the estimated sources.

In the next chapter, a link between the proposed P-MUSIC algorithm with the recently proposed auto-focusing method for broadband AoA estimation will be addressed.

Chapter 5

Analysis and Comparison of Broadband AoA Techniques

In Chapter 4, the P-MUSIC algorithm was introduced as a generalisation of narrowband MUSIC to broadband AoA estimation, based on polynomial matrix decomposition techniques. In this chapter we express the link between P-MUSIC and the recently proposed auto-focussing MUSIC (AF-MUSIC) method.

This chapter is divided into two parts: firstly, a connection between the P-MUSIC algorithm and the AF-MUSIC approach is presented. We analyse the AF technique in the framework of polynomial covariance matrix decompositions, leading to insight into similarities and differences with P-MUSIC. Secondly, the chapter contains an extensive comparison between P-MUSIC algorithms and other broadband AoA estimation methods presented in Chapter 2, including AF-MUSIC, PSCM and broadband beamforming techniques, where different scenarios are considered. This aim is to demonstrate the ability of these techniques in resolving sources' AoAs. We show that compared to other techniques, P-MUSIC robustly estimates the AoAs and the frequency spectrum of broadband signals for different scenarios.

This chapter is organised as follows. Sec. 5.1 motivates the work within this chapter. In Sec. 5.2 we begin by reviewing the AF broadband AoA estimation approach and the formulation of MUSIC based on the AF method is then related to the two P-MUSIC algorithms. Simulation results to verify the relation between these algorithms are found in Sec. 5.3. A comparison between the two versions of P-MUSIC and other broadband AoA approachers for different scenarios is performed through simulations in Sec. 5.4. The chapter ends with conclusion in Sec. 5.5.

5.1 Introduction

As mentioned Chapter 2, most of the existing broadband AoA methods are based on transforming the broadband AoA problem into one or several narrowband problems. Then, narrowband direction finding techniques such as subspace-based methods can be applied to each bin-frequency individually or coherently. Different from broadband coherent AoA estimation methods in [14, 15], where the broadband approach is cleverly bypassed in favour of narrowband processing, an EVD algorithm for polynomial space-time covariance matrices [27, 29] has recently led to the P-MUSIC algorithm [34]. P-MUSIC exploits the idea of subspace decomposition created by the polynomial EVD and is applicable directly to broadband array data. While this approach seems quite distinct from AF-MUSIC [41], the purpose of the first part of this chapter is to express the auto-focussing approach in the framework of polynomial matrix notations to highlight similarities and differences to P-MUSIC. The second part of this chapter provides a comparison between different broadband AoA estimation techniques with the P-MUSIC method proposed in this thesis.

5.2 Coherent Covariance and Focussing Matrices

A large family of broadband angle of arrival estimation algorithms are based on the idea of the coherent signal subspace (CSS) method, whereby focussing matrices appropriately align covariance matrices across narrowband frequency bins. The recently proposed AF approach, claiming to belong to this family. The AF approach has reviewed in Sec. 2.5.3, and will be expressed in the framework of a polynomial matrix decomposition and also will be compared to P-MUSIC next.

5.2.1 Auto-Focussing Approach via CSD Matrix and PEVD

Based on a L-point DFT of the space-time covariance matrix,

$$\mathbf{R}(e^{j\Omega_l}) = \sum_{\tau=0}^{L-1} \mathbf{R}[\tau] e^{-j\Omega_l \tau} \quad , \tag{5.1}$$

with $\Omega_l = \frac{2\pi}{L} l, l = 0 \ldots (L-1)$, the auto-focussing method [40] is based on a autofocussing covariance matrix

$$\mathbf{R}_{\mathrm{AF}} = \sum_{l=0}^{L-1} \mathbf{T}(e^{j\Omega_l}) \mathbf{R}(e^{j\Omega_l}) \mathbf{T}^{\mathrm{H}}(e^{j\Omega_l}) \quad , \tag{5.2}$$

obtained by coherently combining across frequency bins through unitary and frequency-dependent focussing matrices $\mathbf{T}(e^{j\Omega_l})$.

With the modal matrix $\mathbf{Q}_0$ obtained at the reference frequency Ω_0 via EVD of (5.1), the focussing matrix can be formulated as a paraunitary matrix $\mathbf{T}(z)|_{z=e^{j\Omega}} = \mathbf{Q}_0 \mathbf{Q}^{\mathrm{H}}(e^{j\Omega})$. Replacing the summation over frequency bins in (5.2) by the integ-

ration over the Fourier transform (i.e. $L \to \infty$) will lead to

$$\begin{aligned} \mathbf{R}_{AF} &\approx \frac{1}{2\pi} \oint \{ \left\{ \mathbf{T}(z)\mathbf{R}(z)\tilde{\mathbf{T}}(z) \right\}_{z=e^{j\Omega}} d\Omega \\ &= \mathbf{Q}_0 \frac{1}{2\pi} \oint \left\{ \tilde{\mathbf{Q}}(z)\mathbf{R}(z)\mathbf{Q}(z) \right\}_{z=e^{j\Omega}} d\Omega \, \mathbf{Q}_0^{\mathrm{H}} \quad . \end{aligned} \tag{5.3}$$

Since the paraunitary matrix $\mathbf{Q}(z)$ diagonalises $\mathbf{R}(z)$, the argument under the integral is the polynomial EVD of (4.3), resulting in a diagonal matrix of power spectral densities, $\frac{1}{2\pi} \oint \mathbf{\Gamma}(e^{j\Omega}) d\Omega = \mathbf{\Gamma}[0]$, where $\mathbf{\Gamma}[0]$ is the evaluation of $\mathbf{\Gamma}[\tau] \circ\!\!-\!\!\bullet \mathbf{\Gamma}(z)$ for zero lag. Therefore

$$\mathbf{R}_{\mathrm{AF}} \approx \mathbf{Q}_0 \mathbf{\Gamma}[0] \mathbf{Q}_0^{\mathrm{H}} = \mathbf{Q}_0 \begin{bmatrix} \sigma_1^2 & & \\ & \ddots & \\ & & \sigma_M^2 \end{bmatrix} \mathbf{Q}_0^{\mathrm{H}} \quad , \tag{5.4}$$

represents the coherent covariance matrix in terms of the polynomial EVD of the CSD matrix.

Further, the PEVD of the CSD matrix provides a paraunitary $\mathbf{Q}(z)$ leading to an auto-focussing matrix $\mathbf{Q}_0 \tilde{\mathbf{Q}}(z)$ that is continuous in frequency.

5.2.2 Polynomial MUSIC algorithms and Auto-Focussing Approach

For the P-MUSIC algorithm [34], a spatial (SP-MUSIC) and a spatio-spectral version (SSP-MUSIC) have been presented in Secs. 4.3.3.1 and 4.3.3.2 respectively.

From the spectrum of AF-MUSIC in (2.42) and SSP-MUSIC in (4.28), then with $\mathbf{Q}_0$ being the evaluation of the paraunitary $\mathbf{Q}(z)$ at the reference frequency Ω_0, such as $\mathbf{Q}_0 = \mathbf{Q}(z)|_{z=e^{j\Omega_0}}$, it can be noticed that the former is equivalent to evaluating the spatio-spectral polynomial MUSIC spectrum at a reference fre-

quency Ω_0, and can be expressed by

$$S_{\mathrm{AF}}(\varphi,\vartheta) = S_{\mathrm{SSP}}(\varphi,\vartheta,e^{j\Omega})|_{\Omega=\Omega_0} \quad . \tag{5.5}$$

In addition, to obtain the same spatio-spectral characterisation of the array data as provided by SSP-MUSIC with the auto-focussing approach, a sequence of different modal matrices $\mathbf{Q}_0$ at different reference frequencies Ω_0 could be calculated, for all of which the AF spectrum in (2.42) is then evaluated.

The SP-MUSIC integrates the power spectral density (PSD) in the denominator of (4.28), and provides a power term

$$\gamma = \frac{1}{2\pi}\oint \left(\tilde{\mathbf{a}}_{\varphi,\vartheta}(z)\mathbf{Q}_s^{\perp}(z)\tilde{\mathbf{Q}}_s^{\perp}(z)\mathbf{a}_{\varphi,\vartheta}(z)\right)|_{z=e^{j\Omega}}\, d\Omega \quad . \tag{5.6}$$

Therefore the SP-MUSIC spectrum can be calculated by the reciprocal of (5.6).

If the integral in (5.6) is approximated by a sum over L discrete frequency bins, i.e.

$$\gamma \approx \frac{1}{L}\sum_{l=0}^{L-1}\mathbf{a}_{\varphi,\vartheta}^{\mathrm{H}}(e^{j\Omega_l})\mathbf{Q}_s^{\perp}(e^{j\Omega_l})\mathbf{Q}_s^{\perp,\mathrm{H}}(e^{j\Omega_l})\mathbf{a}_{\varphi,\vartheta}(e^{j\Omega_l}) \quad , \tag{5.7}$$

then (5.7) is the summation over the denominator terms of (4.28) for all possible reference frequencies Ω_l with $\Omega_l = \frac{2\pi}{L}l$, $l = 0\ldots(L-1)$. The paraunitary matrix $\mathbf{Q}(z)$ that feeds into (5.7) has been demonstrated in (5.4) to cohere the spatio-temporal covariance matrix in the auto-focussing sense.

5.3 Numerical Simulations

In this section, we present simulation results to demonstrate the connection between the P-MUSIC algorithm and the AF approach.

5.3.1 Implementation Aspects

It has been shown in [85] that the polynomial EVD in (4.3) fulfilling spectral majorisation can be approximated very closely by FIR paraunitary matrices even if an exact decomposition by FIR filter banks may not exist. Therefore, here we rely on the PEVD based on both the SBR2 and SMD algorithms [27, 28, 29], which iteratively approximates the decomposition in (4.3), and has been proven to converge, whereby the number of iterations will determine the accuracy with which diagonalisation and spectral majorisation are approximated. Broadband steering vectors are based on fractional delay filters as presented in Chapter 3..

5.3.2 Idealistic Example with Exact PEVD

In this scenario, a single source emits an uncorrelated Gaussian signal. In an otherwise noise-free scenario, this signal is received by a spatially and temporally critically sampled array with $M = 4$ sensors from end-fire position $\vartheta = 90°$. Therefore, the broadband steering vector of the source is given by

$$\begin{aligned} \mathbf{a}_{\vartheta=90}(z) &= \frac{1}{\sqrt{M}} \left[1\ z^{-1}\ \dots\ z^{-M+1}\right]^{\mathrm{T}} \\ &= \frac{1}{2} \left[1\ z^{-1}\ z^{-2}\ z^{-3}\right]^{\mathrm{T}} \quad , \end{aligned} \tag{5.8}$$

and the space-time covariance matrix can be calculated as

$$\mathbf{R}(z) = \begin{bmatrix} 1 & z^{1} & \dots & z^{M-1} \\ z^{-1} & 1 & & \vdots \\ \vdots & & \ddots & \vdots \\ z^{-M+1} & \dots & \dots & 1 \end{bmatrix} \quad . \tag{5.9}$$

Because $\mathbf{R}(z)$ is rank one, a manifold of diagonalising decompositions exists, with one possibility

$$\mathbf{Q}(z) = \operatorname{diag}\left\{1 \; z^{-1} \; \ldots \; z^{-M+1}\right\} \mathbf{T}_{\mathrm{DFT}} \quad , \tag{5.10}$$

where $\mathbf{T}_{\mathrm{DFT}}$ is a normalised, unitary L-point DFT matrix. For SSP-MUSIC in (4.28), the spectrum is shown in Fig. 5.1(a), the AoA of the end-fire source is clearly identified. In line with broadband arrays, at lower frequencies the fixed aperture degrades the spatial resolution, with no ability to discern sources at DC.

However, for the AF technique, at a given reference frequency Ω_0, it can be shown that $\mathbf{R}_{\mathrm{coh},\Omega_0} = \mathbf{R}(z)|_{z=e^{j\Omega_0}}$ and $\mathbf{\Lambda}_{\mathrm{coh},\Omega_0} = \operatorname{diag}\{1, 0, \ldots, 0\}$. Using the null space $\mathbf{Q}_s^{\perp}(e^{j\Omega_0})$ obtained from the EVD of $\mathbf{R}_{\mathrm{coh},\Omega_0}$, the MUSIC spectrum is evaluated for a range of $N = 64$ reference frequencies Ω_0. This leads to a spectrum very closely related to SSP-MUSIC, with the difference, $S_{\mathrm{diff}}(\vartheta, e^{j\Omega}) = |S_{\mathrm{SSP}}(\vartheta, e^{j\Omega}) - S_{\mathrm{AF}}(\vartheta, \Omega)|$, plotted in Fig. 5.1(c). It can be seen that the error reaches a maximum of 10dB where the SSP-MUSIC spectrum is numerically most sensitive, i.e. towards the source at the end-fire $\vartheta = 90°$, and for the DC component, $\Omega = 0$, which can be attributed to the inaccuracies in implementing broadband steering vectors. Note the trivial broadband steering vector towards broadside $\vartheta = 0°$, $\mathbf{a}_{0°}(z) = \frac{1}{\sqrt{4}}[1\,1\,\ldots\,1]^{\mathrm{T}}$, for which the error in Fig. 5.1(c) is negligible.

Due to the trivial space-time covariance matrix, SBR2 converges instantly to the exact PEVD, yielding exact results for SP-MUSIC in Fig. 5.2. AF-MUSIC is shown both for a single reference frequency, and integrated over a range of reference frequencies, with results somewhat degraded compared to SP-MUSIC.

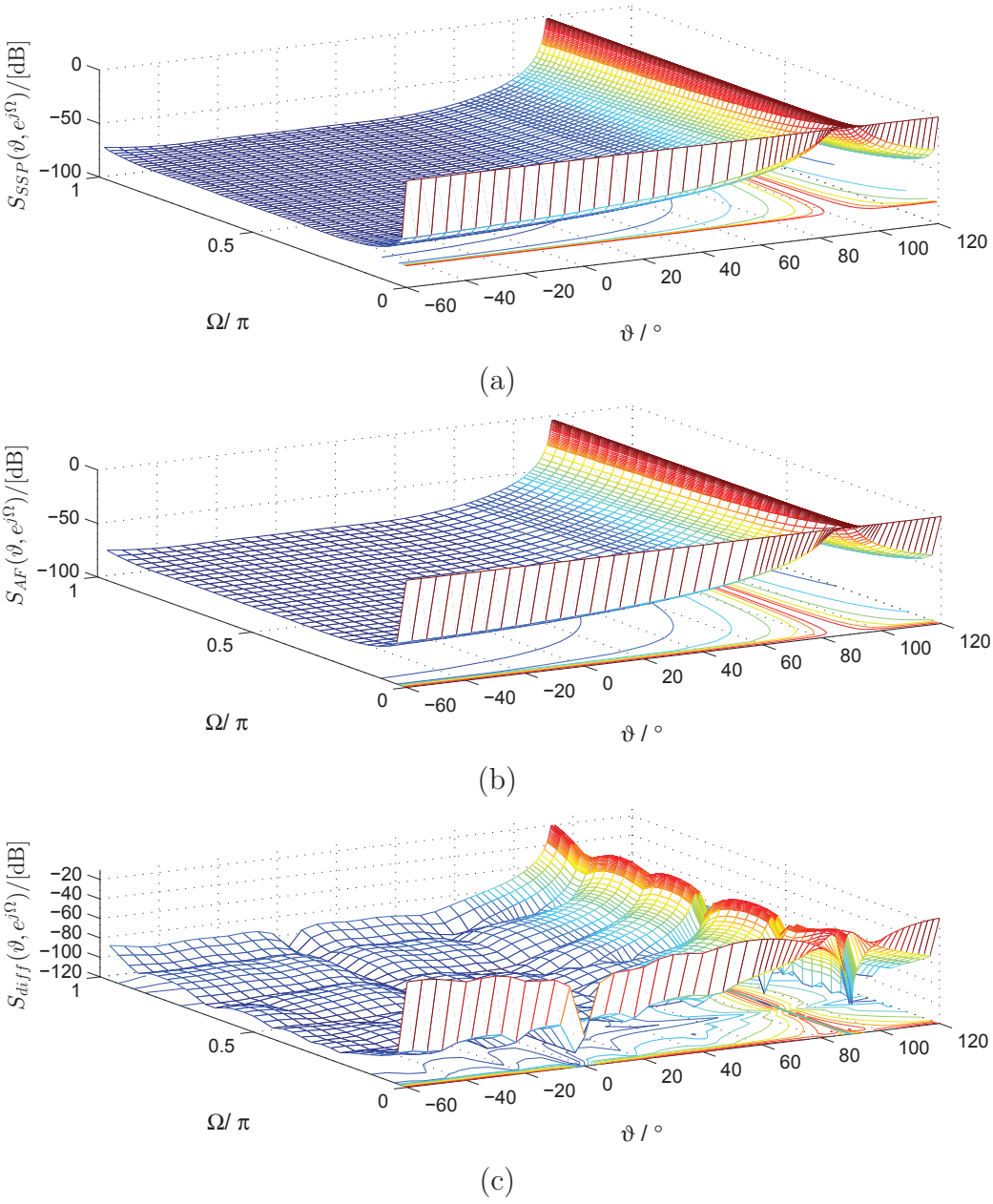

Figure 5.1: (a) SSP-MUSIC spectrum, (b) AF-MUSIC spectrum and (c) difference between SSP-MUSIC and AF-MUSIC for a single source at $\vartheta = 90°$.

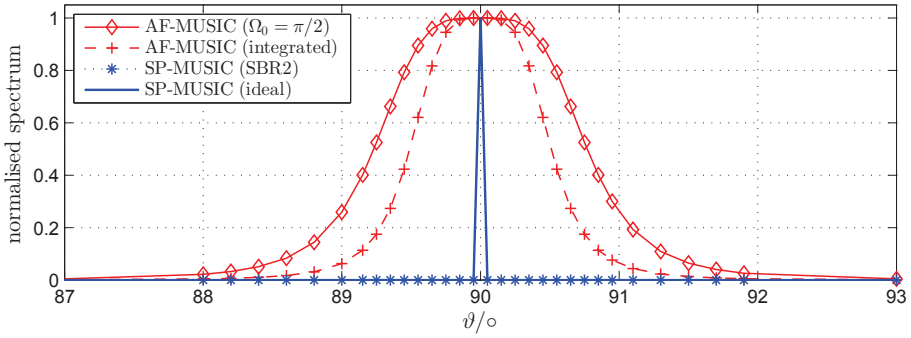

Figure 5.2: Comparison between AF-MUSIC (i) at $\Omega_0 = \frac{\pi}{2}$, (ii) integrated according to (5.7), and SP-MUSIC (iii) with estimated and (iv) ideal PEVD.

5.4 Comparison of P-MUSIC with Other AoA Methods

In this section, the benefit of the proposed P-MUSIC algorithms is demonstrated and compared with other broadband AoA estimation techniques introduced in Chapter 2, which includes the auto-focussing (AF), parametric spatial-covariance matrix (PSCM) and the broadband beamforming approaches for different simulation scenarios. Performance measures employed for this assessment include the accuracy of AoA estimates and their ability to resolve closely spaced sources, and estimating the frequency spectrum of the broadband sources.

A uniform linear array with $M = 8$ sensors is selected for all simulation scenarios. The sensors are separated by distances equal to half of the smallest wavelength $d = \lambda_{\min}/2$ of the incoming broadband signals to guarantee that there is no spatial aliasing. The number of broadband sources K is changed in each scenario to demonstrate the resolution of the different methods, i.e, the ability for distinguishing between multiple sources with close AoAs. All simulations below assume that the number of sources K is known or correctly estimated from the covariance matrices, and consequently the (polynomial) subspaces, i.e.

	sources frequency ranges	sources AoAs (ϑ_k)
source 1	$\Omega \in \left[\frac{2}{8}\pi;\ \frac{6}{8}\pi\right]$	$20°$
source 2	$\Omega \in \left[\frac{3\pi}{8};\ \frac{7}{8}\pi\right]$	$-10°$

Table 5.1: Specification for scenario with two sources.

the noise only and the signal-plus-noise subspaces, have the correct dimensions. Furthermore, for the P-MUSIC algorithm the order of the space-time covariance matrices (number of lags) used in the algorithm is $|\tau| \leq 50$, and the PEVD is calculated based on two iterative algorithms, i.e., SBR2 and MSME-SMD. Both algorithms were allowed to run for 100 iterations and the number of bin frequencies used for implementing the AF approach is fixed to $L = 256$ and is the same for all simulation scenarios.

The broadband data model discussed in Sec. 2.2.1 and given by (2.5) is used throughout all the simulations, whereby the broadband sources are modelled as a white Gaussian signal with unit variance. Sensor signal are generated from the sources using the broadband steering vectors discussed in Chapter 3.

5.4.1 Realistic Scenario with Two Sources

In the first set of simulations, the sensor array with $M = 8$ elements is illuminated by two overlapping uncorrelated broadband sources of equal power with specifications as indicated in Tab. 5.1.. The sources are active over two different frequency ranges as shown in Fig. 5.3. Further, independent and identically distributed white Gaussian noise with zero mean and unit variance is added to the sensor signals at an SNR of 20 dB. Fig. 5.4 compares the performance of SSP-MUSIC based on both SBR2 and MSME-SMD approaches, AF-MUSIC and the broadband beamformer techniques, whereby the sources' AoAs and the frequency spectrum contained in the broadband sources can be extracted from this figure. From Fig. 5.4, we can see that both versions of SSP-MUSIC and AF-MUSIC

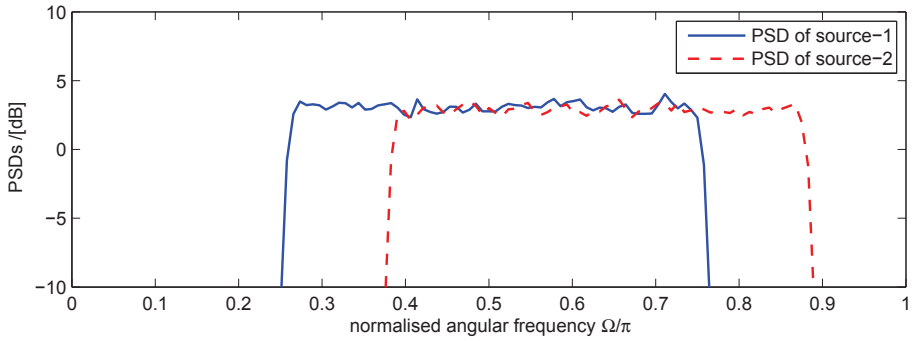

Figure 5.3: PSDs of the two broadband signals of interest.

provide good estimates for both sources' AoAs and frequency ranges, while the broadband beamformer has poor resolution due to its resolution limit, also known as the beamwidth as defined in [50, 89]

$$\Delta\vartheta \approx \frac{\lambda}{L_N} \quad , \tag{5.11}$$

where λ is the wavelength of the incoming source signals, L_N is the length of the sensor array equal to $L_N = (M-1)\cdot d$, with d the spacing between neighbouring sensors. The beamwidth decreases with an increase in the number of sensors, the spacing between adjacent sensors, and the source signal frequency.

Fig. 5.5 demonstrates the performance of SP-MUSIC with the other algorithms for extracting only AoA information. In this figure, the simulation results are normalised to a spectrum peak value of one. Furthermore, we add the PSCM approach [19,20] for this comparison to test its ability to resolve multiple sources. From Fig. 5.5 it can be seen that SP-MUSIC based on MSME-SMD extracts the two sources well: they look equal in power and offers a slightly higher resolution than AF-MUSIC, especially for the source located at 20°. In addition, in spectral ranges where all sources are active, AF-MUSIC outperforms SP-MUSIC based on SBR2 and retains the equality of the powers. Note that both versions of SP-

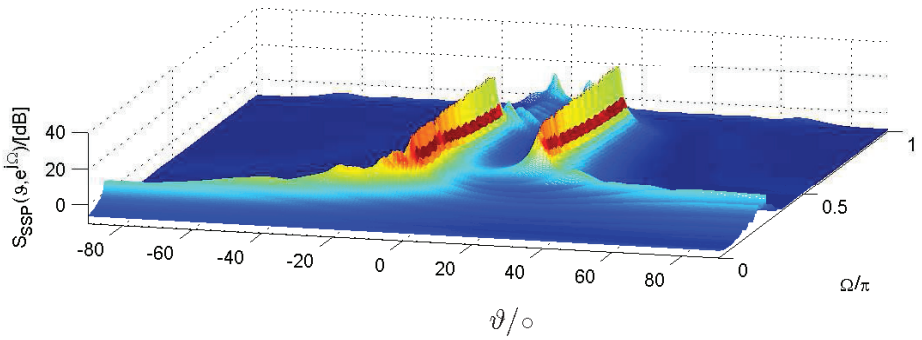

(a)

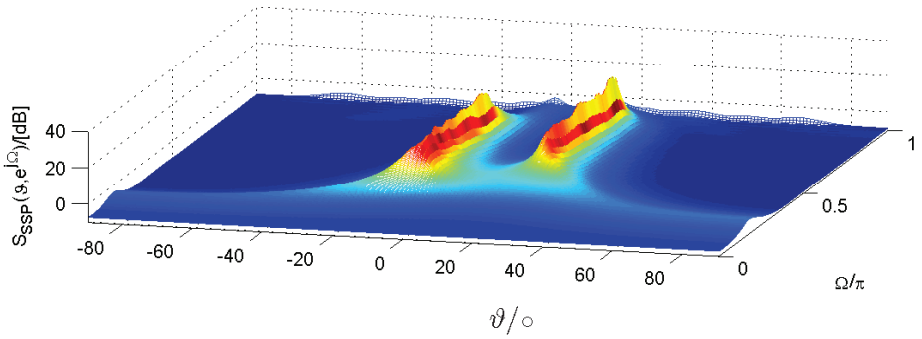

(b)

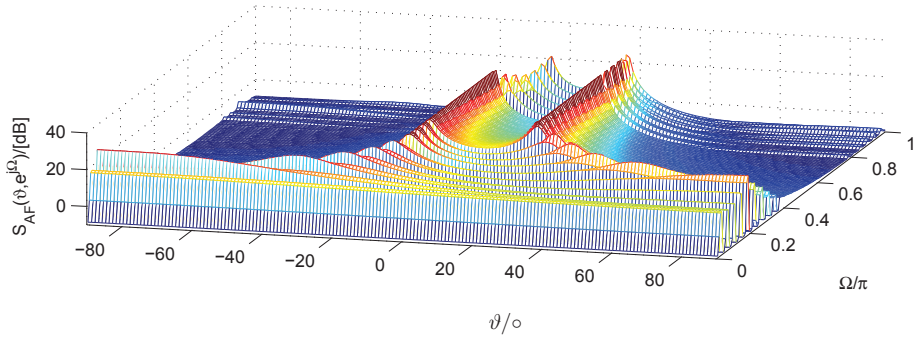

(c)

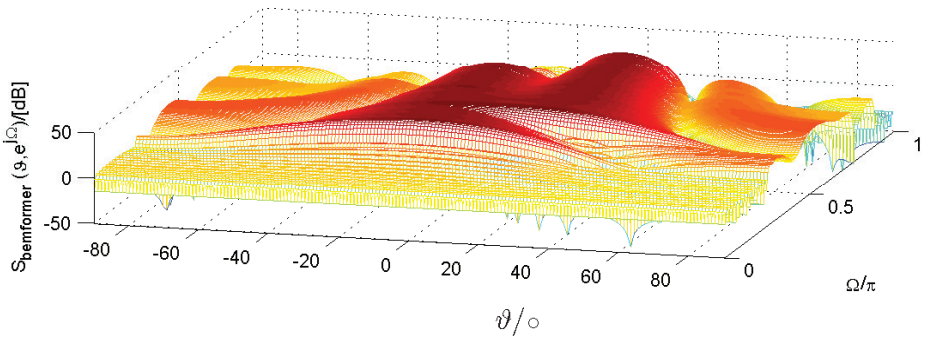

(d)

Figure 5.4: Spectra comparison; (a) SSP-MUSIC (MSME-SMD) (b) SSP-MUSIC (SBR2) (c) AF-MUSIC and (d) Broadband beamformer for 2 overlapping sources.

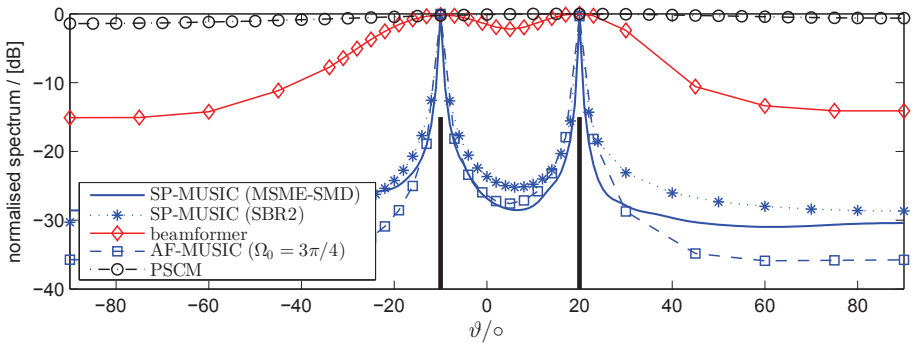

Figure 5.5: Comparison between SP-MUSIC based on (i) MSME-SMD (ii) SBR2 PEVD, (iii) broadband beamformer, (iv) AF-MUSIC and (v) PSCM approaches for a scenario with two broadband sources arriving from $-10°$ and $20°$.

MUSIC in Fig. 5.5 are evaluated over the entire spectrum, hence not requiring any prior spectral knowledge, while AF-MUSIC is required to be within the overlap spectral ranges of the sources in order to provide accurate result, as indicated by a snapshot for $\Omega = \frac{3}{4}\pi$ in Fig. 5.5; outside the overlap region, the performance is degraded.

The simulation results in Figs. 5.4 and 5.5 also indicate that the broadband beamformer is able to distinguish the sources but with lower resolution compared with both SP-MUSIC and AF-MUSIC algorithms, while the PSCM technique fares worst and fails to identify more than one source while only providing a very poor estimate for the source at $20°$.

5.4.2 Realistic Scenario with Three Sources

A second realistic simulation scenario contains a mixture of three broadband overlapping uncorrelated sources of equal power impinging onto the array from different directions with specifications as shown in Tab. 5.2. The sources are active over different frequency ranges as highlighted by the PSDs of these sources depicted in Fig. 5.6. Additive white Gaussian noise corrupts the sensor signals at

sources	sources frequency ranges	AoA (ϑ_k)
source-1	$\Omega \in [\frac{2\pi}{8}; \frac{7\pi}{8}]$	$-30°$
source-2	$\Omega \in [\frac{\pi}{2}; \pi]$	$20°$
source-3	$\Omega \in [\frac{3\pi}{8}; \pi]$	$40°$

Table 5.2: Specification for scenario with three sources

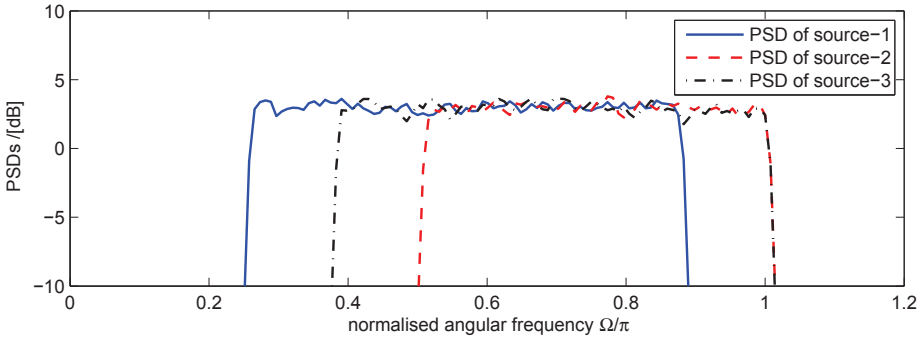

Figure 5.6: PSDs of the three overlapping broadband sources.

a signal-to-noise ratio (SNR) of 20dB.

The PSCM approach is left out here since it does not provide comparable performance as demonstrated in the previous section. Results for the remaining methods are depicted in Fig. 5.7. As with the previous section, these figures aim to reveal both the true AoAs of the sources and their frequency spectra. From Fig. 5.7, it can be seen that SSP-MUSIC based on the MSME-SMD outperforms all methods: it offers high resolution and the extracted sources appear to be approximately equal in power over the entire spectrum and for all AoAs.

Moreover, the results indicate that the two versions of P-MUSIC and AF-MUSIC provide a robust estimation by correctly extracting the sources' AoAs and their frequency ranges, while the broadband beamformer performs worst, with its beamwidth imposing a resolution limit.

Similarly to the previous section, the spectra in Fig. 5.8 are normalised such

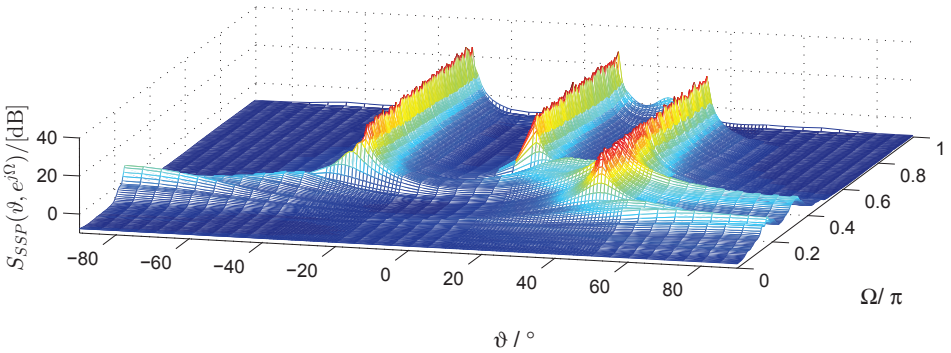

(a)

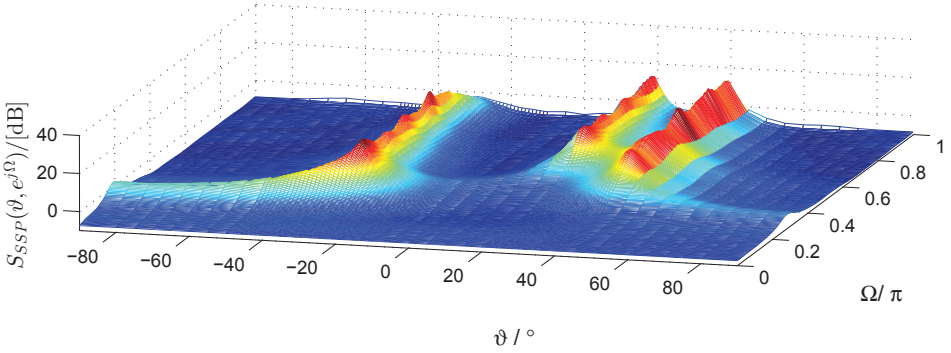

(b)

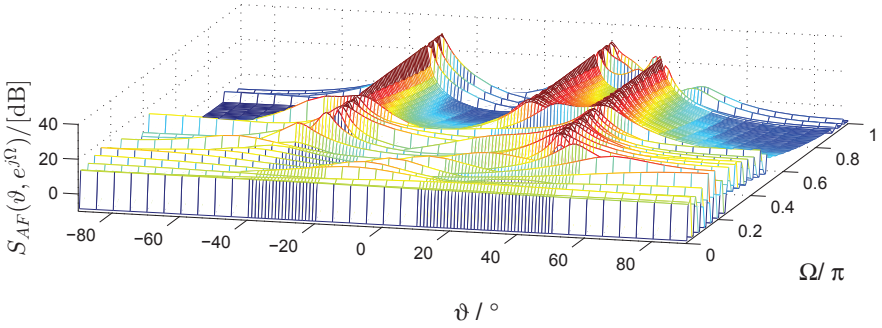

(c)

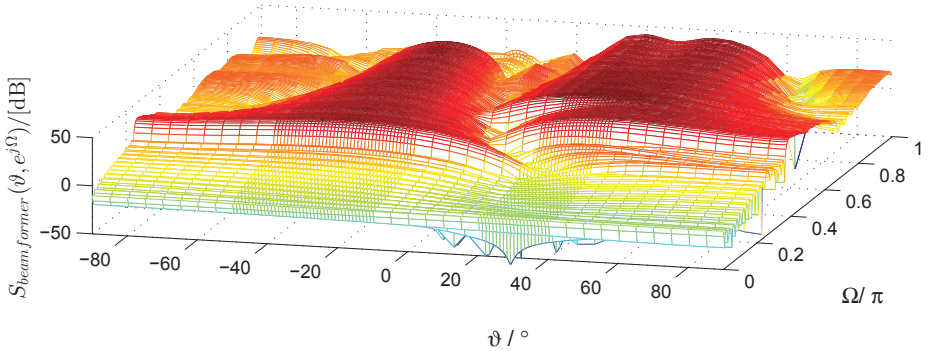

(d)

Figure 5.7: (a) SSP-MUSIC (MSME-SMD) (b) SSP-MUSIC (SBR2) (c) AF-MUSIC and (d) beamformer spectra for 3 overlapping sources.

that their maxima are unity. The results can be interpreted such that the SP-MUSIC based on MSME-SMD and AF-MUSIC algorithms have similar performance, whereby the three peaks in Fig. 5.8 are corresponding to the correct directions of the sources. The width of the spectrum peaks especially at the source locations $\vartheta \in [20°, 40°]$ are sharper than those achieved by SP-MUSIC based on the SBR2 and the broadband beamformer. SP-MUSIC based on the SMD family of decompositions provides superior resolution compared to SP-MUSIC with SBR2. This result can be attributed to the higher level of diagonalisation obtained by the MSME-SMD decomposition algorithm, which leads to accurate estimation of the broadband noise-only subspace. Similar to the previous section, in spectral ranges where all sources are active, AF-MUSIC provides better resolution than SP-MUSIC based on the SBR2 algorithm. However, both versions of SP-MUSIC in Fig. 5.8 are calculated over the entire spectrum, hence not requiring any prior spectral knowledge, while the AF-MUSIC is required to be within the overlap spectral ranges of the sources in order to provide accurate results, as indicated by a snapshot for $\Omega = \frac{3}{4}\pi$ in Fig. 5.8; outside the overlap region, the performance is degraded. Moreover, in both situations, SP-MUSIC based on SBR2 is much better than the broadband beamformer which cannot correctly detect the sources at 20° or 40°. The next section investigates how closely spaced sources affect the AoA estimates.

5.4.3 Resolution of Closely Spaced Sources

We further study the ability of these algorithms to resolve closely spaced source signals. In this case we only change the location of the third source from 40° to 25° to be close to the source located at 20° with angle separation $\Delta\vartheta = 5°$. The simulation parameters otherwise remain as before. It is clearly seen from

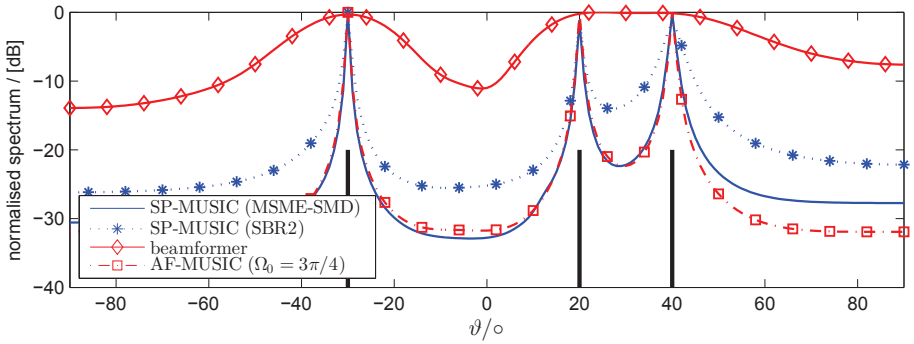

Figure 5.8: Comparison between SP-MUSIC based on (i) MSME-SMD (ii) SBR2 PEVD and (iii) broadband beamforming and AF-MUSIC for a scenario with three sources.

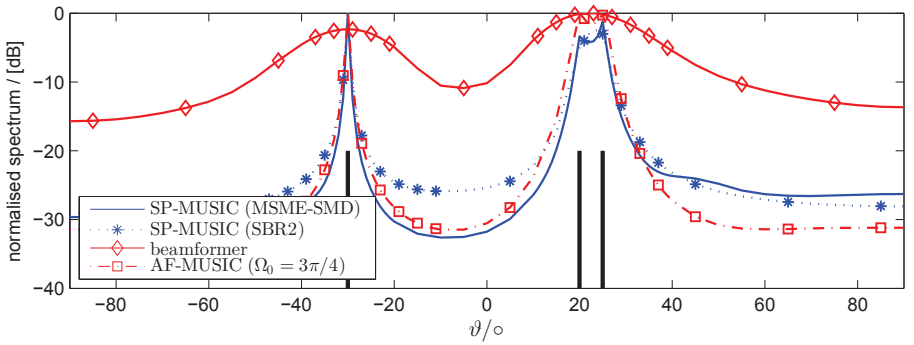

Figure 5.9: Scenario with 3 sources and close angular spacing.

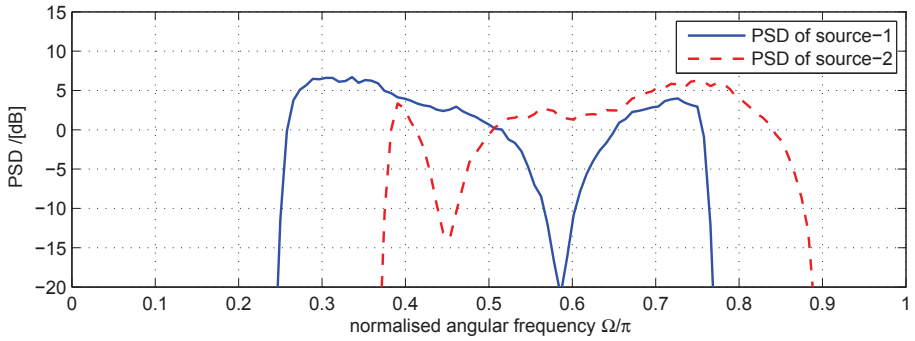

Figure 5.10: PSDs of the two broadband sources with unequal power.

Fig. 5.9 that the performance of all methods degrades as the angle separation is decreased. However, SP-MUSIC with MSME-SMD and AF-MUSIC have reliable performance and closely spaced sources can be resolved, while SP-MUSIC based on SBR2 and the beamformer fail to differentiate between the two adjacent sources. The other source located at $\vartheta = -30$ is detected by all methods, whereby SP-MUSIC with MSME-SMD and AF-MUSIC are almost identical and outperform the others. In the next section we will investigate how a difference in PSDs between the sources affects the AoA estimates.

5.4.4 Sources with Unequal Power Spectral Densities

In the following, we study the impact of varying power between sources on the performance of AoA algorithms. Fig. 5.10 shows the PSDs of two overlapping broadband sources that arriving on the sensor array from angles of $\vartheta \in [-10°, 20°]$, and active over the frequency ranges $\Omega \in [\frac{2}{8}\pi,\ \frac{6}{8}\pi]$ and $\Omega \in [\frac{3}{8}\pi,\ \frac{7}{8}\pi]$. In addition, the sensor signals are corrupted by spatially and temporally uncorrelated noise at 20 dB SNR. It can be seen from Fig. 5.10 that the sources are not spectrally majorised. The effect of spectral majorisation during a PEVD factorisation is highlighted in Fig. 5.11, where the PSDs along the diagonal of $\mathbf{\Lambda}(z)$ are obtained

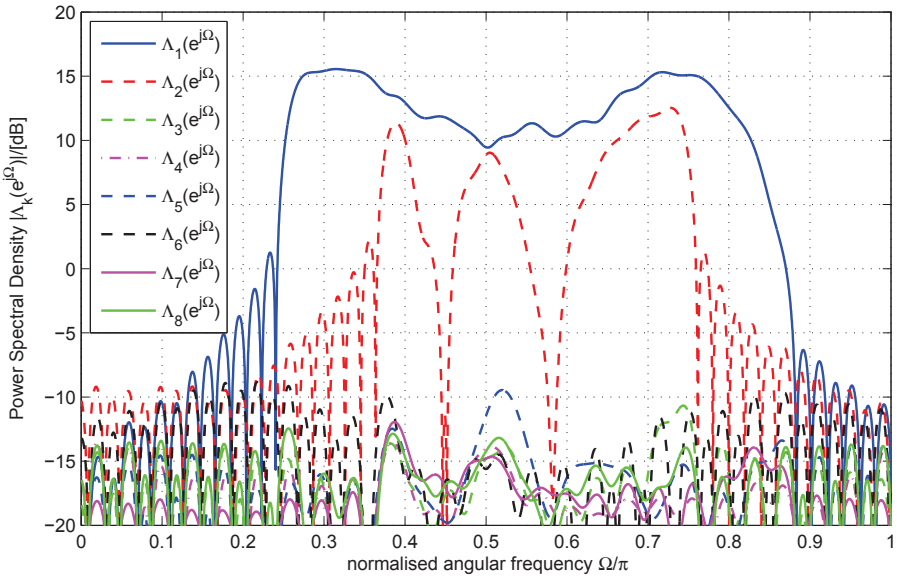

Figure 5.11: The majorised output spectra obtained using SBR2 for the given input signals spectra in Fig. 5.10

using the SBR2 algorithm. Although not shown here, the MSME-SMD algorithm produces majorised spectra similar to those obtained via SBR2 in Fig. 5.11. The MUSIC spectra for SP-MUSIC based on both SBR2 and MSME-SMD, AF-MUSIC and broadband beamforming methods are depicted in Fig. 5.12. Here, AF-MUSIC is evaluated at different reference frequencies, while the other methods are evaluated similar to the previous simulation scenarios; their graphs are simply repeated for Fig. 5.11(a)-(c) for a more straightforward comparison to AF-MUSIC. It is clear from Figs. 5.12(b) and (c) that once the source power is lower than some level in a specific frequency range, the performance of AF-MUSIC is degraded, whereby the second source cannot be detected. They also show that both SP-MUSIC versions work quite well with unequal and frequency-dependent PSDs, and they produce estimates that are nearly as accurate as the estimates produced for equally powered sources.

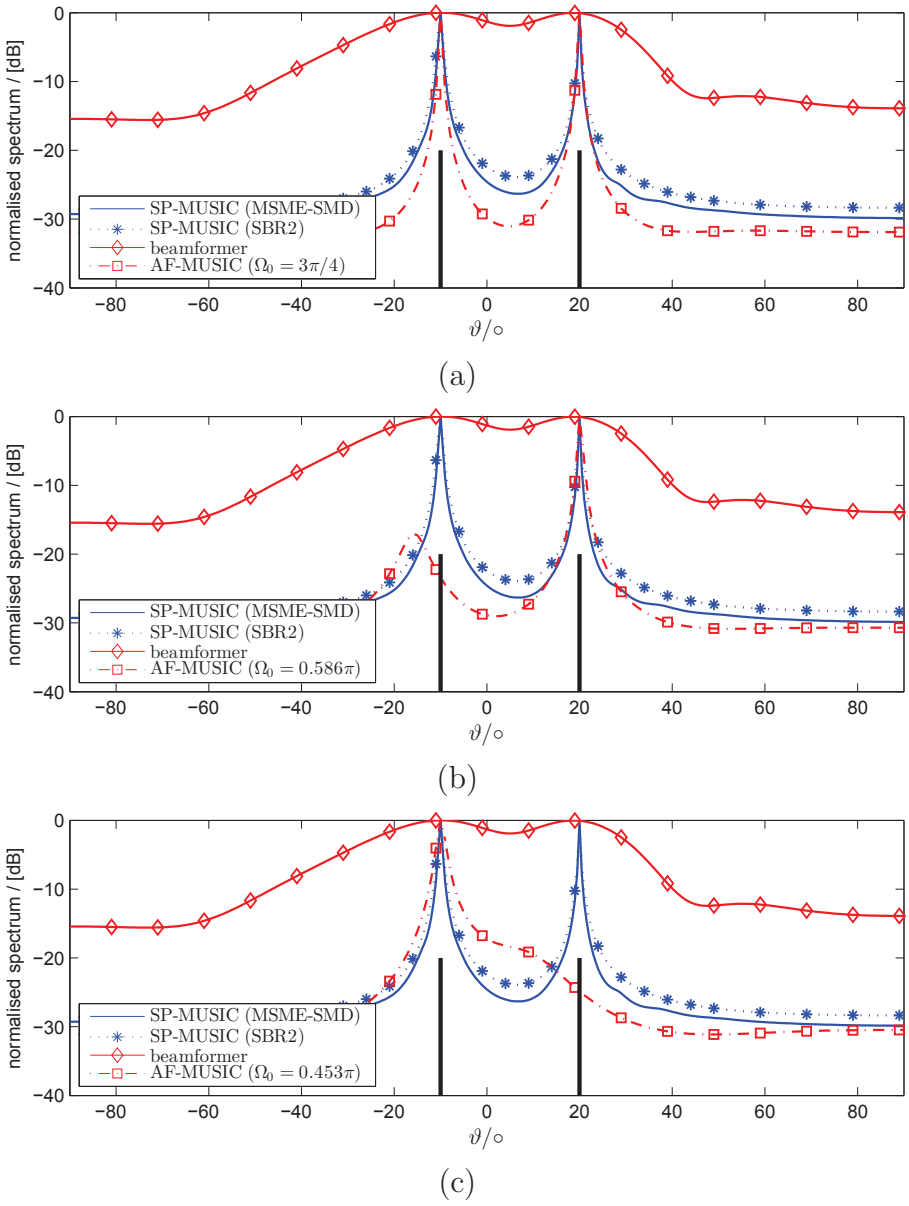

Figure 5.12: AoA estimates for different methods applied to a scenario with two sources having unequal power and frequency-dependent PSDs.

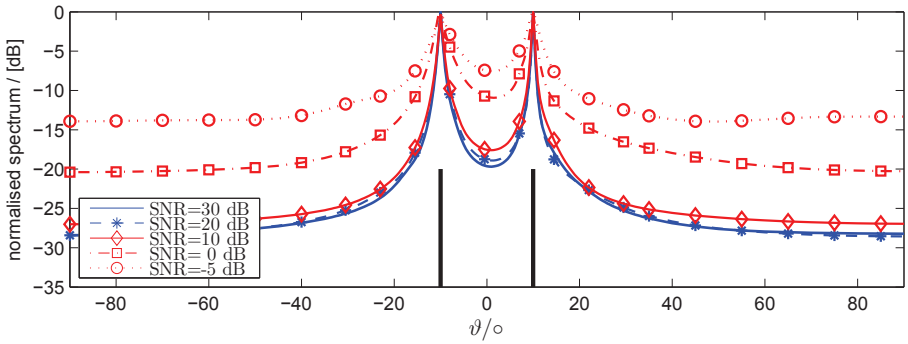

Figure 5.13: Resolution performance of SP-MUSIC based on MSME-SMD for different SNR.

5.4.5 Statistical evaluation of resolution

Finally, we study the impact of varying SNR on the accuracy of the polynomial MUSIC algorithm. This simulation demonstrate the resolution performance of SP-MUSIC based on the MSME-SMD technique under different SNR. The simulation scenario consists of two independent broadband source signals arriving from $-10°$and $10°$ directions. The source signals are white noise with equal power. Th e simulation process is repeated for several values of SNR, namely $-5, 0, 10, 20, 30$ dB. The simulation results are depicted in Fig. 5.13

As can be seen from Fig. 5.13, with the increase in the SNR, the beam width of SP-MUSIC spectrum becomes narrow and the direction of the signals become clearer. The resolution accuracy of SP-MUSIC algorithm is increased and the two signals are clearly identifiable. It can be concluded that the value of the SNR can affect the performance of high resolution AoA estimation algorithm directly, whereas at low SNR the estimation error increases and the performance of SP-MUSIC algorithm will sharply decline.

5.5 Conclusion

In this chapter, we have linked the proposed polynomial MUSIC algorithms with the auto-focussing approach for broadband AoA estimation. The AF approach has been expressed in the framework of polynomial space-time covariance matrices and their polynomial eigenvalue decomposition obtained from the iterative SBR2 and SMD algorithms, and under the assumption of the DFT sufficiently well approximating the Fourier transform. Simulation results have shown that the polynomial spatio-spectral SSP-MUSIC algorithm is able to equate to the AF approach when evaluated at the reference frequency, while the polynomial spatial MUSIC algorithm has been illustrated to relate to a summation of AF terms for a set of reference frequencies. Numerical simulations have indicated that the polynomial MUSIC methods perform similar to the AF-approach where the exact PEVD is known or easily determined. For more realistic scenarios, restricting AF to sensible fractional bandwidths will provide superior resolution over P-MUSIC; however, the latter does not rely on a-priori spectral information and can be calculated over the entire bandwidth with appealing results.

In addition, in this chapter we have compared the performance of the proposed P-MUSIC algorithms with other broadband AoA estimation methods such as AF-MUSIC, PSCM and broadband beamforming algorithms for different simulation scenarios. Different from other broadband techniques, P-MUSIC works directly on the broadband sensor array data, and is designed to retrieve both AoA information and the frequency spectrum of the sources. Simulation results have highlighted that P-MUSIC algorithms are robust and can provide reliable performance, and that closely spaced broadband sources can be resolved. P-MUSIC based on SMD algorithms can outperform P-MUSIC with SBR2 and provide reliable performance for closely spaced sources. The MSME-SMD tends to achieve a better diagonalisation than the SBR2 algorithm, which allows for a better iden-

tification of the polynomial subspaces, making MSME-SMD an attractive PEVD algorithm in the context of broadband AoA estimation.

Chapter 6

Conclusion and Future Work

In this chapter, a summary and some concluding remarks are given, and several directions for future work are discussed.

6.1 Summary

The main aim of the research presented in this thesis has been to design and implement high resolution AoA estimation for broadband sensor array applications. This aim was accomplished by presenting a novel high resolution polynomial MUSIC algorithm. P-MUSIC differs from most AoA estimation methods which are designed to only retrieve the AoA information of sources, while the P-MUSIC algorithms can be used to estimate the sources' AoAs alone or in combination with their frequency content. In this thesis, the proposed algorithms were shown to be robust when compared to other broadband AoA estimation algorithms.

The fundamental concept of AoA estimation and its classification based on the signal bandwidth was introduced in Chapter 2. In addition, it also highlighted the differences between the broadband and narrowband array cases, and also reviewed narrowband and broadband AoA estimation approaches.The concept of

a broadband steering vector was formally introduced in Chapter 3, together with its implementation based on fractional delay filters. To attain high accuracy over a large bandwidth, a new design of fractional delay filter (FDF) based on undecimated filter banks was proposed. We have demonstrated that very accurate group delays across the entire spectrum can be achieved using the proposed new design. This differs from standard FDFs such as the windowed sinc functions and Farrow structures, which break down at frequencies close to half of the sampling rate. In addition, if high accuracy is required, the filter bank approach can also offer computational advantages. Although the complexity of the proposed FDF is slightly higher than the standard FDFs, it has been shown that such a deployment yields significant improvements in terms of error performance.

In Chapter 4, the P-MUSIC algorithm for broadband AoA estimation was presented. P-MUSIC is based on the broadband (polynomial) subspace decomposition afforded by the PEVD. Moreover, P-MUSIC algorithm was originally implemented using the SBR2 algorithm for a PEVD decomposition. The performance of two versions of P-MUSIC algorithms, the polynomial spatial (PS-MUSIC) and the polynomial spatio-spectral (PSS-MUSIC), was compared with an IFB approach. Simulation results have shown the robustness of P-MUSIC compared with the IFB approach, especially if the signal frequencies do not coincide with the bin frequencies of the IFB processor. For further enhancement of the proposed P-MUSIC, the recently proposed SMD approach has been adopted, which offers a better diagonalisation compared with the SBR2 approach. We have demonstrated that a higher level of diagonalisation leads to a better identification of the relevant signal subspaces, such that the new version of P-MUSIC can extract a cleaner estimate w.r.t. both angle and frequency of the estimated sources.

In Chapter 5, we have addressed the link between the P-MUSIC algorithms

and the recently proposed AF approach for broadband AoA estimation. For this, the latter is expressed in the framework of polynomial space-time covariance matrices and their polynomial eigenvalue decomposition, and under the assumption that the DFT sufficiently well approximates the Fourier transform. Simulation results have shown that the polynomial spatio-spectral MUSIC algorithm equates to the AF method when evaluated at the reference frequency, while the polynomial spatial MUSIC algorithm has been shown to relate to a summation of auto-focussing terms for a set of reference frequencies. While for the AF method, this requires side- or a priori information on the sources' PSDs, no prior knowledge is required for the P-MUSIC algorithms. In the last part of this chapter, an extensive comparison of different broadband AoA estimation algorithms by means of simulations was included. Simulation results have illustrated that the proposed P-MUSIC has been found very robust and shown that it can effectively work for scenarios with multiple sources, closely spaced sources and frequency variant source signals.

6.2 Future Work

There are several possibilities for future work based on the research presented throughout this thesis. In the following, some further directions are outlined.

Throughout Chapter 4, it has been assumed that the broadband sources are independent or uncorrelated which follows the assumption made for narrowband MUSIC. It will be interesting to investigate the estimation of sources' AoAs when there is a correlation between the broadband signals which arises e.g. through multipath propagation in the medium. Most AoA estimation techniques are degraded in this scenario while a broadband steering vector could be made to incorporate multiple directions.

The current design of the P-MUSIC algorithm is based on linear arrays, but

could be extended to other array geometries, e.g. circular, planar or arbitrary array structures. This could be achieved by applying suitable changes to the design of the broadband steering vectors, thereafter extending it to both azimuth and elevation angles. Challenges can also be found in the design of P-MUSIC to deal with more complicated propagation models whereby the ideal far-field assumption no longer holds for sources, such as in the case of near-field propagation whereby wavefronts impinging onto the array are no longer planar but spherical.

The proposed P-MUSIC algorithm is based on the iterative PEVD algorithms such as SBR2 and MSME-SMD algorithms. These algorithms have been used to diagonalise the space-time covariance matrix of the sensor signals, yielding polynomial matrices of high orders. In other contexts, such as for broadband communications, ideas have been pursue to shorten these systems in order to reduce the effort in both design and implementation [90, 91]. In order to reduce the P-MUSIC complexity, the reduction of the PEVD computation complexity with no or little loss in performance might be possible and very worthwhile.

Finally, the algorithms proposed in this thesis could be applied to real, measured, experimental data in order to verify the results obtained with both ideal and realistic multi-source data.

References

[1]. M. I. Skolnik, Radar Handbook-Third edition: McGraw-Hill, Inc., 2008.

[2]. A.J. Paulraj, R. Nabar and D. Gore. Introduction to Space-Time Wireless Communications. Cambridge University Press, 2003.

[3]. D. Udgeon and R. Mersereau, Multidimensional Digital Signal Processing, Prentice-Hall, 1983.

[4]. W. Kellermann, "Analysis and design of multirate systems for cancellation of acoustical echoes," in Proc. *IEEE International Conference on Acoustics, Speech, and Signal Processing*, New York, USA, vol. 5, pp. 2570 – 2573, April 1988.

[5]. W. Kellermann, "Analysis and design of multirate systems for cancellation of acoustical echoes," in *Proc. IEEE International Conference on Acoustics, Speech, and Signal Processing*, New York, USA, vol. 5, pp. 2570 – 2573, April 1988.

[6]. W. Herbordt and W. Kellermann, "Limits for generalized sidelobe cancellers with embedded acoustic echo cancellation," in *Proc. IEEE International Conference on Acoustics, Speech, and Signal Processing*, Salt Lake City, Utah, vol. 5, pp. 3241 – 3244, May 2001.

[7]. M. S. Brandstein and S. M. Griebel, "Nonlinear, model-based microphone array speech enhancement," *Acoustic Signal Processing for Telecommunications*, ed. S. L. Gay and J. Benesty, Kluwer Academic Publishers, 2000.

[8]. M. Wax and I. Ziskind. "On unique localization of multiple sources by passive sensor arrays." in *IEEE Transactions on Acoustics, Speech, and Signal Processing*. vol. 37, no. 7, pp. 996 – 1000, July 1989.

[9]. S. Bellofiore, J. Foutz, C. Balanis and A. Spanias. "Smart-antenna system for mobile communication networks. Part 2. Beamforming and network throughput." In *IEEE Antennas and Propagation Magazine*. Vol. 44, issue 4, pp. 106 – 114, August 2002.

[10]. R. O. Schmidt, "Multiple emitter location and signal parameter estimation," in *IEEE Transactions on Antennas and Propagation*, vol. 34, no. 3, pp. 276 - 280, March 1986.

[11]. M. Wax and T. Kailath. "Spatio-temporal spectral analysis by eigenstructure methods," in *IEEE Transactions Acoustic, Speech, Signal Processing*, vol. 32, issue 4, pp. 817 - 827, August 1984.

[12]. B. Ottersten and T. Kailath. "Wideband direction-of-arrival estimation using the ESPRIT algorithm," in *IEEE Transactions on Acoustic, Speech and, Signal Processing*, vol. 5, pp. 2666 - 2669, April 1988.

[13]. Y. Yoon, L. Kaplan, and J. McClellan, "TOPS: New DOA estimator for wideband signals," in *IEEE Transactions on Signal Processing*, vol. 54, no. 6, pp. 1977 - 1989, June 2006.

[14]. H. Wang and M. Kaveh, "Coherent signal-subspace processing for the detection and estimation of angles of arrival of multiple wideband sources," in *IEEE Transactions on Acoustics, Speech and Signal Processing*, vol. 33, no. 4, pp. 823 - 831, August 1985.

[15]. H. Wang and M. Kaveh, S "On the performance of signal-subspace processing–part ii: Coherent wide-band systems," in *IEEE Transactions on Acoustics, Speech and Signal Processing*, vol. 35, no. 11, pp. 1583 - 1591, November 1987.

[16]. E. DiClaudio and R. Parisi, "WAVES: Weighted average of signal subspaces for robust wideband direction finding," in *IEEE Transactions on Signal Processing*, vol. 49, no. 10, pp. 2179 - 2191, October 2001.

[17]. Lee, T.-S., "Efficient wide-band source localization using beamforming invariance technique." In *IEEE Transactions Signal Processing*, vol. 42, no. 6, pp. 1376 - 1387, June 1994.

[18]. T. Do-Hong and P. Russer. "An analysis of wideband direction-of-arrival estimation for closely-spaced sources in the presence of array model errors." In *IEEE Microwave and Wireless Components Letters*, vol. 13, no. 8, pp. 314 - 316, August 2003.

[19]. W. Ng, J. Reilly, T. Kirubarajan, and J.-R. Larocque, "Wideband array signal processing using MCMC methods." In *IEEE Transactions on Signal Processing*, vol. 53, no. 2, pp. 411 - 426, February 2005.

[20]. J. Dmochowski, J. Benesty, and S. Affes. "Direction of arrival estimation using the parameterized spatial correlation matrix." In *IEEE Transactions on Audio, Speech, and Language Processing*, vol. 15, no. 4, pp.1327 - 1339, May 2007.

[21]. J. Dmochowski, J. Benesty, and S. Affes. "Direction of arrival estimation using eigenanalysis of the parameterized spatial correlation matrix." In *IEEE International Conference on Acoustics, Speech and Signal Processing*, vol. 1, pp. I-1 – I-4, April. 2007.

[22]. J. P. Dmochowski, J. Benesty, and S. Affes. "Broadband music: Opportunities and challenges for multiple source localization". In *IEEE Workshop on Applications of Signal Processing to Audio and Acoustics*, pp. 18–21, October 2007.

[23]. M. Souden, J. Benesty, and S. Affes. "Broadband source localization from an eigenanalysis perspective." In *IEEE Transactions on Audio, Speech, and Language Processing*, vol. 18, no. 6, pp. 1575 - 1587, August 2010.

[24]. M. Souden, J. Benesty, and S. Affes. "Eigenanalysis based broadband source localization." In *IEEE International Conference on Acoustics Speech and Signal Processing*, pp. 81 - 84, March 2010.

[25]. K. Mahata, "A Subspace Algorithm for WideBand Source Localization Without NarrowBand Filtering," in *IEEE Transactions on Signal Processing*, vol. 59, no. 7, pp. 3470–3475, July 2011.

[26]. H. Yu et al, "A New Method for Wideband DOA Estimation." In *International Conference on Wireless Communications, Networking, and Mobile Computing*, pp. 598-601, September 2007.

[27]. J. G. McWhirter, P. D. Baxter, T. Cooper, S. Redif, and J. Foster, "An EVD Algorithm for Para-Hermitian Polynomial Matrices," in *IEEE Transactions on Signal Processing*, vol. 55, no. 5, pp. 2158 - 2169, May 2007.

[28]. S. Redif, S. Weiss, and J. G. McWhirter. "An approximate polynomial matrix eigenvalue decomposition algorithm for para-Hermitian matrices." In *11th IEEE International. Symposium on Signal Processing and Information Technology*. Inf. Tech., pp. 421 - 425, Bilbao, Spain, December. 2011.

[29]. J. Corr, K. Thompson, S. Weiss, J. G. McWhirter, I. K. Proudler. "Multiple shift maximum element sequential matrix diagonalisation for parahermitian matrices." in *2014 IEEE Workshop on Statistical Signal Processing (SSP)*, pp. 312-315, June 2014.

[30]. C. H. Ta and S. Weiss. "A Design of Precoding and Equalisation for Broadband MIMO Systems." In *15th International. Conference. DSP*, pp. 571 - 574, Cardiff, UK, July 2007.

[31]. A. Sandmann, A. Ahrens and S. Lochmann. "Resource Allocation in SVD-Assisted Optical MIMO Systems using Polynomial Matrix Factorization." In *Proceedings of Photonic Networks 16, ITG Symposium*, pp. 1-7, Leipzig, Germany, May 2015.

[32]. S. Redif, J. McWhirter, and S. Weiss. "Design of FIR paraunitary filter banks for subband coding using a polynomial eigenvalue decomposition." In *IEEE Transactions on Signal Processing*, vol. 59, no. 11, pp. 5253 - 5264, November 2011.

[33]. S. Weiss, S. Redif, T. Cooper, C. Liu, P. D. Baxter, and J. G. McWhirter. "Paraunitary Oversampled Filter Bank Design for Channel Coding." *EURASIP Journal of Applied Signal Processing*, vol. 2006, pp. 1 – 10, 2006.

[34]. M. Alrmah, S. Weiss, and S. Lambotharan, "An extension of the music algorithm to broadband scenarios using polynomial eigenvalue decomposition," in *19th European Signal Processing Conference*, pp. 629 – 633, Barcelona, Spain, August 2011.

[35]. M. Alrmah, S. Weiss and JG McWhirter. "Implementation of Accurate Broadband Steering Vectors for Broadband Angle of Arrival Estimation." In *Intelligent Signal Processing (ISP) Conference*, pp. 1 – 6, London, UK, December 2013.

[36]. M. Alrmah and S. Weiss. "Filter Bank Based Fractional Delay Filter Implementation for Widely Accurate Broadband Steering Vectors." In *5th IEEE International Workshop on Computational Advances in Multi-Sensor Adaptive Processing (CAMSAP)*, pp. 332 - 335, Saint Martin, December 2013.

[37]. M. Alrmah, J. Corr, A. Alzin, K. Thompson, and S. Weiss. "Polynomial Subspace Decomposition for Broadband Angle of Arrival Estimation." In *Sensor Signal Processing for Defence (SSPD 2014)*, pp. 1 -5, Edinburgh, UK, September 2014.

[38]. M. Alrmah, M. N. Hussin, S. Weiss, and S. Lambotharan. "Comparison of Broadband Direction of Arrival Estimation Algorithms." In *9th IMA International Conference on Mathematics in Signal Processing*, Birmingham, UK, December 2012.

[39]. M. Alrmah, S. Weiss, S Redif, S. Lambotharan and JG McWhirter. "Angle of Arrival Estimation for Broadband Signals: A Comparison." In *Intelligent Signal Processing (ISP) Conference*, pp. 1 - 6, London, UK, December 2013.

[40]. S. Weiss, M. Alrmah, S. Lambotharan, JG. McWhirter and M. Kaveh. "Broadband Angle of Arrival Estimation Methods in a Polynomial Matrix Decomposition Framework." In *5th IEEE International Workshop on Computational Advances in Multi-Sensor Adaptive Processing (CAMSAP)*, pp. 109 - 112, Saint Martin, December 2013.

[41]. P. Pal and P. P. Vaidyanathan. "A novel autofocusing approach for estimating directions-of-arrival of wideband signals." In *43rd Asilomar Conference on Signals, Systems and Computers*, pp. 1663 - 1667, Pacific Grove, Canada, November 2009.

[42]. A. Yardim, G. Cain, and P. Henry, "Optimal two-term offset windowing for fractional delay," in *Electronics Letters*, vol. 32, no. 6, pp. 526 - 527, March 1996.

[43]. T. I. Laakso, V. V¨alim¨aki, M. Karjalainen, and U. K. Laine, "Splitting the Unit Delay," in *IEEE Signal Processing Magazine*, vol. 13, no. 1, pp. 30 - 60, January 1996.

[44]. C. W. Farrow, "A continuously variable digital delay element". In *IEEE International Symposium on Circuits and Systems*, vol. 3, pp. 2641 – 2645, Espoo, Finland, June 1988.

[45]. D.H. Johnson and D.E. Dudgeon, Array Signal Processing: Concepts and Techniques, Signal Processing Series. Prentice Hall, Englewood Cli®s, NJ, 1993.

[46]. D. K. Cheng, Field and Wave Electromagnetics. New York, Addison-Wesley Publishing Company, 2nd., 1989.

[47]. J.G. Proakis and Dimitris G. Manolakis, Digital Signal Processing: Principles Algorithms and Applications, Prentice Hall, 3rd edition, 1996.

[48]. Bartlett, M. An Introduction to Stochastic Process. New York: Cambridge University Press, 1956.

[49]. H. Krim and M. Viberg. "Two decades of array signal processing research: the parametric approach." In *IEEE Signal Processing Magazine*, vol. 13, no. 4, pp. 67 - 94, July 1996.

[50]. J. Capon. "High-resolution frequency-wave number spectrum analysis." *Proceedings of the IEEE*. vol. 57, no. 8, pp. 1408 – 1418, 1969.

[51]. R. Roy. And T. Kailath. “ESPRIT – Estimation of signal parameters via rotational invariance techniques.” In *IEEE Transactions on Acoustics, Speech, and Signal Processing*. vol. 37, no. 7, pp. 984 – 995, July 1989.

[52]. S. Valaee and P. Kabal, “Wideband array processing using a two-sided correlation transformation,” In *IEEE Transactions on Signal Processing*, vol. 43, no. 1, pp. 160 - 172, January 1995.

[53]. P. Stoica and R. Moses, Spectral analysis of signals. Prentice Hall, 2005.

[54]. A. Barabell, “Improving the resolution performance of eigenstructure-based direction-finding algorithms". In *Proc. IEEE Acoustics, Speech, and Signal Processing (ICASSP'83)*, vol. 8, pp. 336 – 339, May 1983.

[55]. M. Zoltowski, G. Kautz and S. Silverstein. “Beamspace Root-MUSIC". In *IEEE Transactions on Signal Processing*, vol. 41, no. 1, pp. 344 - 364, Jan. 1993.

[56]. O. A. Oumar, M. F. Siyau, and T. P. Sattar, “Comparison between music and esprit direction of arrival estimation algorithms for wireless communication systems,” in *Proc. IEEE Future Generation Communication Technology (FGCT)*, 2012 International Conference on, pp. 99–103, December 2012.

[57]. Li. Minghui , “Advanced Array Processing Techniques and Systems". In *International Journal of Computer Research*, vol. 17, no. 4, pp. 1-33, 2009.

[58]. S. S. Reddi and A. B. Gershman, “An alternative approach to coherent source location problem”. In Signal Processing, vol. 59, pp. 221-233, 1997.

[59]. P. Stoica, B. Ottersten, M. Viberg, R. L. Moses, “Maximum Likelihood Array Processing for Stochastic Coherent Sources,” In *IEEE Transactions on Signal Processing*, vol. 44, no. 1, pp. 96-105, Jan. 1996.

[60]. T. J. Shan, M. Wax and T. Kailath, “On spatial smoothing for direction-of-arrival estimation of coherent signals.” In *IEEE Transactions on Acoustic, Speech and Signal Processing,* vol. 33, no. 1, pp. 806-811, 1985.

[61]. S. U. Pillai, “Forward/Backward Spatial Smoothing Techniques for Coherent Signal Identification,” in *IEEE Transactions on Signal Processing*, vol. 37, no. 1, pp. 8-15, January 1989.

[62]. N. Yuen, B. Friedlander, “DOA Estimation in Multipath: An Approach Using Fourth-Order Cumulants.” In *IEEE Transactions on Signal Processing*, vol. 45, no. 5, pp. 1253-1263, May 1997.

[63]. H. Wang and M. Kaveh, S “On the performance of signal-subspace processing–part ii: Coherent wide-band systems,” In *IEEE Transactions on Acoustics, Speech and Signal Processing*, vol. 35, no. 11, pp. 1583 - 1591, Nov. 1987.

[64]. H. Hung and M. Kaveh, "Focussing matrices for coherent signal subspace processing," In *IEEE Transactions on Acoustics, Speech and Signal Processing*, vol. 36, no. 8, pp. 1272-1281, August 1988.

[65]. ZM Liu, ZT Huang, YY Zhou, "Direction-of-arrival estimation of wideband signals via covariance matrix sparse representation." In *IEEE Transactions on Signal Processing*. vol. 59, no. 9, pp. 4256-4270, September 2011.

[66]. L. GAN, X. WANG. " DOA estimation of wideband signals based on slice-sparse representation." In *EURASIP Journal on Advances in Signal Processing*, vol. 2013, no. 18, pp. 1-10, 2013.

[67]. S. Pejoski and V. Kafedziski, "Sparse Covariance Fitting Method for Direction of Arrival Estimation of Uncorrelated Wideband Signals." In *Telfor Journal*, vol. 6, no. 2, 2014.

[68]. S. Cotter, B. Rao, E. Kjersti, K. Delgado, "Sparse solutions to linear inverse problems with multiple measurement vectors." In *IEEE Transactions on Signal Processing*. Vol. 53, no. 7, pp.2477–2488, 2005.

[69]. P.Murphy, A. Krukowski, and A. Tarczynski, "An efficient fractional sample delayer for digital beam steering," in *IEEE International Conference on Acoustics, Speech, and Signal Processing*, vol. 3, pp. 2245 -2248, Munich, Germany, April 1997.

[70]. A. Yardim, G. Cain, and P. Henry, "Optimal two-term offset windowing for fractional delay," *Electronics Letters*, vol. 32, no. 6, pp. 526 - 527, March 1996.

[71]. A. Papoulis, Signal Analysis. New York: McGraw-Hill, 1984.

[72]. M. Sac and M. Blok, "Gain deficit effect in the fractional delay filter design by the window method," in *Proc. SPIE Photonics Applications in Astronomy, Communications, Industry, and High-Energy Physics Experiments*, vol. 75021G, pp. 1 – 6, August 2009.

[73]. J. Selva, "An efficient structure for the design of variable fractional delay filters based on the windowing method," in *IEEE Transactions on Signal Processing*, vol. 56, no. 8, pp. 3770 - 3775, August 2008.

[74]. Paul A. Lynn, Wolfgang Fuerst: Introductory Digital Signal Processing with Computer Applications, John Wiley & Sons, ISBN 0-471-97984-8.

[75]. A. Oppenheim. And R. Schafer., Discrete-time Signal Processing. Upper Saddle River, NJ: Prentice Hall, 1999.

[76]. J. Vesma and T. Saramaki, "Interpolation filters with arbitrary frequency response for all digital receivers." In *Proceedings of IEEE International Symposium on. Circuits System*, vol. 2, pp. 568-571, Georgia, USA, May 1996.

[77]. J. Vesma and T. Saramaki, "Polynomial-based interpolation filters—Part I: Filter synthesis." In *Circuits Systems Signal Process*, vol. 26, no. 2, pp. 115–146, April 2007.

[78]. A. Agarwal, L. Boppana and R. Kodali, “Lagrange's polynomial based farrow filter implementation for SDR.” In *2014 IEEE Region 10 Symposium*, Kuala Lumpur- Malysia, pp. 269 – 274, April 2014.

[79]. M. Unser, A. Aldroubi, and M. Eden, “Fast B-spline transforms for continuous image representation and interpolation,” in *IEEE Trans. Pattern Analysis and Machine Intelligence*, vol. 13, no. 3, pp. 277–285, March 1991.

[80]. F. harris, “Performance and design considerations of Farrow filter used for arbitrary resampling,” *in Proc. 13th Int. Conf. on Digital Signal Processing*, Santorini, Greece, pp. 595– 599, July 1997.

[81]. S.Weiss, S. R. Dooley, R.W. Stewart, and A. K. Nandi, “Adaptive Equalisation in Oversampled Subbands,” in *IEEE Electronics Letters*, vol. 34, no. 15, pp. 1452-1453, July 1998.

[82]. M. Harteneck, S.Weiss, and R. Stewart, “Design of near perfect reconstruction oversampled filter banks for subband adaptive filters,” in *IEEE Transactions on Circuits and Systems II: Analog and Digital Signal Processing*, vol. 46, no. 8, pp. 1081-1085, August 1999.

[83]. S. Weiss, L. Lampe, and R. W. Stewart, “Efficient implementations of complex and real valued filter banks for comparative subband processing with an application to adaptive filtering,” in *Proc. Int. Symp. Communication Systems & Digital Signal Processing*, Sheffield, U.K., vol. 1, pp. 32 – 35, April 1998.

[84]. P.P. Vaidyanathan. Multirate Systems and Filter Banks. Prentice Hall, 1993.

[85]. S. Icart and P. Comon. “Some properties of Laurent polynomial matrices.” In *9th IMA Conf. Mathematics in Signal Processing*, pp. 4, Birmingham, UK, December 2012.

[86]. G. H. Golub and C. F. Van Loan. Matrix Computations. John Hopkins University Press, 3rd ed., 1996.

[87]. J. Corr, K. Thompson, S. Weiss, J.G. McWhirter, and I.K. Proudler, Causality constrained multiple shift sequential matrix diagonalisation for parahermitian matrices,” in *22th European Signal Processing Conference*, pp. 1277-1281, Lisbon, Portugal, September 2014

[88]. S. Weiss and I. K. Proudler. Comparing Efficient Broadband Beamforming Architectures and Their Performance Trade-Offs. In *14th International Conference on Digital Signal Processing*, vol. 1, pp. 417 - 422, Santorin, Greece, July 2002.

[89]. J. Benesty, J. Chen and Y. Huang, Microphone Array Signal Processing. 2008 Springer-Verlag Berlin Heidelberg

[90]. J. A. Foster, J. G. McWhirter and J. Chambers, “Limiting the order of polynomial matrices within the SBR2 algorithm," in *IMA Conference on Mathematics in Signal Processing*, Cirencester, UK, 2006.

[91]. Chi Hieu Ta and S. Weiss, ”Shortening the order of paraunitary matrices in SBR2 algorithm," in *International Conference on Information, Communications & Signal Processing*, pp. 1- 5, Singapore, December 2007.